System Energy Optimisation Strategies for DC Railway Traction Power Networks

by

Zhongbei Tian

A thesis submitted to
the University of Birmingham
for the degree of
DOCTOR OF PHILOSOPHY

Department of Electronic, Electrical and Systems Engineering
College of Engineering and Physical Sciences
University of Birmingham, UK
June 2017

Abstract

As a result of rapid global urbanisation, energy and environmental sustainability are becoming increasingly significant. According to the Rail Transport and Environment Report published by International Union of Railways in 2015, energy used in the transportation sector accounts for approximately 32% of final energy consumption in the EU. Railway, representing over 8.5% of the total traffic in volume, shares less than 2% of the transport energy consumption. Railway plays an important role in reducing energy usage and CO_2 emissions, compared with other transport modes such as road transport. However, despite the inherent efficiency, the energy used by the rail industry is still high, making the study of railway energy efficiency of global importance. Previous studies have investigated train driving strategies for traction energy saving. However, few of them consider the overall system energy optimisation, which depends on various factors including driving styles and timetables. This thesis aims to find a system energy optimisation solution for urban railways.

This thesis begins with a review of the main arrangement of the railway systems and literature on energy optimisation studies in railways. The development of the energy evaluation simulation software for DC-fed railway systems is demonstrated. The train movement model and railway power network model are integrated into the simulator. This energy simulator is able to calculate the energy flow of the whole system according to multiple-train driving controls and timetables.

This thesis further analyses the energy consumption of urban systems with regenerating trains, including the energy supplied by substations, used in power transmission networks, consumed by monitoring trains, and regenerated by braking trains. The results indicate that, for urban transit systems where trains are monitoring and braking frequently, the efficient use of regenerated braking energy is important in reducing net energy consumption. Based on a case study of Beijing Yizhuang Subway Line, it has been found that the available regenerative braking energy and total substation energy consumption vary with timetables. The difference in energy consumption between the best and worst headways is 35%, suggesting the importance of the study of timetable optimisation.

Under fixed route infrastructure constraints, train traction energy consumption is determined by the driving controls. This thesis proposes an approach to searching energy-efficient driving strategies with coasting controls. The simulation results show that the optimal driving style reduces traction energy consumption by 28%, compared with existing driving controls. A Driver Advisory System (DAS) is designed and implemented in a field test on Beijing Yizhuang Subway Line. The driver guided by the DAS achieves 16% of traction energy savings, compared with driving without the DAS.

The global system energy consumption, which is the energy supplied by the substations, is further studied in this thesis. A Monte Carlo Algorithm is employed to evaluate the factors of system energy consumption. An ‘energy factor’ is defined and used to estimate the system energy consumption. The driving controls and dwell times are optimised jointly. The case study indicates that the substation energy is reduced by around 38.6% with the system optimised operations. The efficiency of using regenerative braking energy is improved to from 80.6 to 95.5%.

Acknowledgement

I would like to give my sincere appreciation to my supervisors Dr Stuart Hillmansen and Prof. Clive Roberts for their consistent encouragement, patience as well as invaluable guidance during my PhD study. Their enthusiasm for research and teaching, care and kindness to students, and a wide range of knowledge inspired me to pursue a research career.

I am extremely grateful to Dr Paul Weston and Dr Ning Zhao who always offered me invaluable knowledge, thoughtful guidance, great inspiration, and critical comments. I am also grateful to Dr Lei Chen, Dr Robert Ellis, Dr Shuai Su and Dr Minwu Chen for sharing their invaluable knowledge, advice and experience to support my research and projects. In addition, I would like to thank all the members of the Birmingham Centre for Railway Research and Education (BCRRE) for their kind help.

Finally, I would like to express my gratitude to my families and friends for their encouragement and patience. In particular, I would like to thank my wife Xinyu Yu for her love, understanding and support.

Table of Contents

List of Figures

List of Tables

List of Acronyms

Term	Explanation / Meaning / Definition
ACO	Ant Colony Optimisation
ATO	Automatic Train Operation
BYSL	Beijing Yizhuang Subway Line
BF	Brute Force
CBTC	Communications Based Train Control
DE	Differential Evolution
DAS	Driver Advisory System
DP	Dynamical Programming
ESS	Energy Storage Systems
EBF	Enhanced Brute Force
GTO	Gate Turn Off Thyristor
GA	Genetic Algorithm
ICCG	Incomplete Cholesky Conjugate Gradient
IGBT	Insulated Gate Bipolar Transistor
MTES	Multi-Train Energy Simulator
PMSM	Permanent Magnet Synchronous Motors
PWM	Pulse Width Modulation
STMS	Single Train Motion Simulator
TIMS	Train Information Measurement System
TPS	Train Performance Simulation
VVVF	Variable Voltage Variable Frequency

Note: International System of Units is used throughout this thesis without statement.

Chapter 1

Introduction

1.1 Background

Energy and environmental sustainability in transportation have received a great deal of attention in recent decades. The Intergovernmental Panel on Climate Change's Synthesis Report, stated that the transport sector was responsible for about 23% of total energy-related CO_2 emissions worldwide in 2014 [1]. In the EU, the energy consumed by transportation accounts for approximately 32% of final end use of energy in 2015 [2]. Railway contributes less than 2% of the EU transport sector's total energy consumption even though it has over 8.5% of total traffic in volume. Compared with other transport forms, railway plays an important role in reducing the environmental impact and improving energy efficiency. By offering efficient transport with low environmental impacts, railway helps create a more sustainable approach to transport.

Urban rail systems have been increasing rapidly during recent decades [3]. Urban rail transit, in general, refers to a railway system providing passenger services within metropolitan areas. Metros, light rails, tramways, and commuter rails are all different forms of urban rail transportation. The aim of urban rail is to transport passengers in a city quickly and easily. Hong Kong metro regularly transports 80,000 passengers per hour

during peak time, which is four times higher than by bus [3]. Urban rail transit is also characterised by short headway and dwell time, and a high number of stations with short interstation distances. Urban rail systems can effectively satisfy high transportation demand and reduce air pollution in metropolitan areas.

Although the railway system is arguably one of the most efficient forms of land based transport, how to operate trains more efficiently is still of global importance. To improve sustainability, members of the International Union of Railways and Community of European Railway and Infrastructure Companies proposed a unified approach to environmental and sustainability topics in the European rail sector in 2010 [4]. They addressed four targets for the rail sector to improve performance in terms of the environment, including climate protection, energy efficiency, exhaust emissions and noise. European railway companies agreed to reduce specific average CO_2 emissions from train operation by 50% in 2030, compared to the emissions in 1990. In addition, it was agreed that by 2030 the energy consumption from train operation will be reduced by 30%, compared to the consumption in 1990.

Several European projects have been carried out to improve the energy efficiency in railway systems. The Railenergy project co-funded by the European Commission, started from 2006 to address energy efficiency of the integrated railway system [5]. Recommendations included innovative traction technologies, components and layouts to the development of rolling stock, operation and infrastructure management strategies. In 2012, 17 project partners collaborated on the OSIRIS project, including public transport operators, railway manufacturers and research centres [6]. The OSIRIS project aimed to reduce the energy consumption within European urban rail systems with emphasis on

developing and testing technological and operational solutions and tools. The MERLIN project was conducted to investigate and demonstrate the viability of an integrated management system to achieve a more sustainable and optimised energy usage in European electric mainline railway systems [7]. RSSB, a non-profit company supported by major rail industry stakeholders, delivered guidance to improve railway energy consumption in 2014 [8]. The research in the railway energy area covers traction energy sources, electrification safety, electrification systems, fixed interface equipment, and vehicle-mounted interface equipment. This guide communicates the outputs of the research in the area of rail energy to ensure the work is accessible. Longer term research has been carried out to support the implementation of the railway technical strategies.

The study of innovative strategies and technologies to reduce railway energy consumption also attracts researchers across the world. Comprehensive energy-related indicators for urban rail systems have been developed to analyse the actual energy performance of the system, assess energy optimisation strategies and monitor the progress of the implemented measures [9]. The current practices, strategies and technologies to reduce energy consumption are assessed by a holistic approach [10]. The energy consumption in existing urban rail systems could be reduced by approximately 25–35% by optimising driving controls, timetables, operation strategies and energy storage devices.

Due to the significance of rail energy and the high potential to reduce the energy consumption in urban rail systems, this thesis further investigates the energy optimisation solutions for urban rail systems. Although a number of studies have been carried out to reduce energy consumption, a system wide approach to optimising global energy consumption of an urban rail system has not been fully identified. The performance when

implementing the energy-efficient strategies has not been validated. In order to fill the gap in existing studies of rail energy, this thesis aims to investigate system energy optimisation strategies to improve the efficiency of the whole urban rail system. In addition, the thesis aims to provide solutions to a more sustainable electric urban railway system.

1.2 Objectives

To study a system approach to improving the energy efficiency of an urban rail system, the following objectives need to be addressed:

- A review of literature on railway energy systems is required initially. By comparing and analysing previous studies of energy-saving technologies in railways, the advantages and disadvantages of existing approaches can be fully assessed. A clear and detailed research plan should be identified after the literature analysis.
- Train movement and traction power supply network modelling is a crucial tool in understanding railway energy systems. Simulation software needs to be developed for evaluating the energy consumption of railway systems according to specific infrastructure data and operations. Several challenges including dynamic operation modelling, power flow analysis with regeneration and time-efficient computation should be considered in the development of the simulation software.
- Solutions to improving the energy efficiency of railway systems should be proposed. The constraints in railway operations should be considered in solving the optimisation problems. Various optimisation methods should be discussed and evaluated in producing the energy-efficient strategies. The performance in terms of energy reduction for different approaches needs to be demonstrated.

- The application of energy-efficient operations should be considered. Theoretical studies based on simulation could provide good results in terms of energy savings. However, applying the technology into the real world is also challenging and important. In this thesis, the feasibility of using the proposed strategies will be demonstrated.

1.3 Thesis Structure

In order to achieve the aim of energy optimisation, this thesis will address the aspects shown in Figure 1.1.

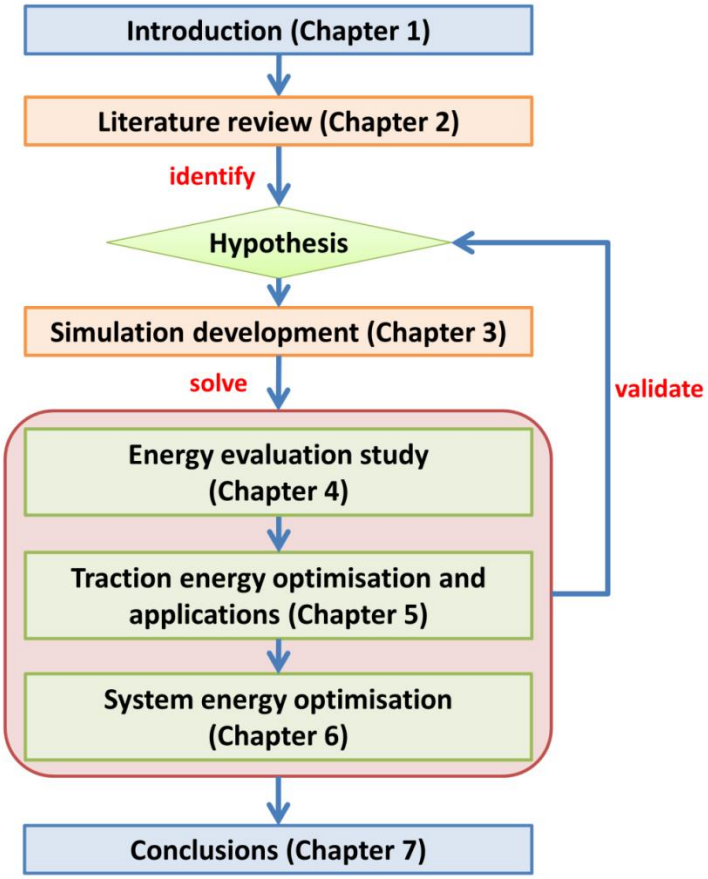

Figure 1.1 The structure of the thesis

Chapter 1 presents the background of the current situation in railway systems. The importance of railway energy is illustrated. The main research purpose of this thesis is proposed, which is to develop a system approach to improving the energy efficiency of a railway system.

Chapter 2 reviews the literature related to energy systems in railways. The existing methods to reduce energy consumption for railways are analysed and the gap of previous studies is identified. In order to fill the gap, the hypothesis of this thesis is proposed. The following chapters will investigate system-wide energy optimisation solutions which have not been fully studied.

Chapter 3 illustrates the development of simulation software for a railway integrated system. The train motion and traction power network simulation are integrated to calculate multi-train energy consumption according to the operation controls. The simulator is used as a crucial tool to evaluate the energy performance of railway systems.

Chapter 4 presents the evaluation of the energy consumption through the whole system, based on the energy simulator. The traction energy, regenerative energy and system energy consumption are fully analysed. The factors which influence the energy consumption in each sector are illustrated. The significance of studying traction and system energy optimisation is addressed.

Chapter 5 proposes an approach to reducing traction energy consumption. Two optimisation algorithms, Brute Force and a Genetic Algorithm, are used and compared in the optimisation. The application of traction energy optimisation is demonstrated and validated based on the case study of Beijing Yizhuang Subway Line.

Chapter 6 proposes a system approach to achieving global energy optimisation, by improving the optimisation method proposed in Chapter 5. The Monte Carlo Algorithm used for system energy optimisation is reliable and effective. The performance of system energy optimisation is demonstrated based on the case study of Beijing Yizhuang Subway Line.

In Chapter 7, the conclusions and contributions of this thesis are summarised. The hypothesis is validated according to the solutions defined in this thesis. The future work is also described.

Chapter 2

Literature Review of Rail Energy

2.1 Introduction

A railway traction power system provides energy for trains to transport passengers or loads to destinations. Due to the low rolling resistance between wheels and rails, the railway system is widely considered as one of the most efficient forms of land-based transport [11]. Since energy prices are rising and environmental concerns are growing, train energy-efficient operation techniques have been given increasing attention in recent years. Transportation is facing increasing pressure to optimise energy management strategies.

This chapter first presents an overview of the characteristics of a DC-fed railway traction power system. Various studies of railway energy reduction have been carried out during recent decades [12]. The literature on railway energy optimisation is reviewed and analysed in this chapter. By comparing and summarising prior literature, the hypothesis of this thesis is proposed. The detailed objectives of the energy optimisation study in this thesis are presented.

2.2 DC Railway Traction Power Systems

All electrical railway feeding networks transmit AC or DC energy through conductor systems along the track to supply electric vehicles. AC supplies are commonly used for main lines and high-speed railways, but metros, light railways, and suburban railways generally use DC supplies.

2.2.1 DC Power Supplies

In modern railways, the DC traction substations are normally equipped with transformers and rectifiers, drawing electricity from local distribution networks. Figure 2.1 presents a typical feeding network for a DC railway system [13]. The electrical supply fed to railways is typically at 132, 66 or 33 kV AC, depending on the size and demand of railway systems. A medium voltage distribution network is normally at 11 kV, fed by step down transformers. The medium voltage network provides energy for the whole railway system. The passenger station is supplied by 415 V 3-phase transformed from 11 kV for domestic usage. Traction substations use transformers and rectifiers to convert 11 kV AC into 600 to 3000 V DC. The economic distance between substations increases with a higher voltage level. It is recommended to be 4-6 km for 750 V, 8-13 km for 1500 V and 20-30 km for 3000 V [13]. The distance of substations is determined by the power and the number of trains in the network. To improve the efficiency of current transmission, the return rails are normally bonded together and the catenaries are connected at points midway between substations [14].

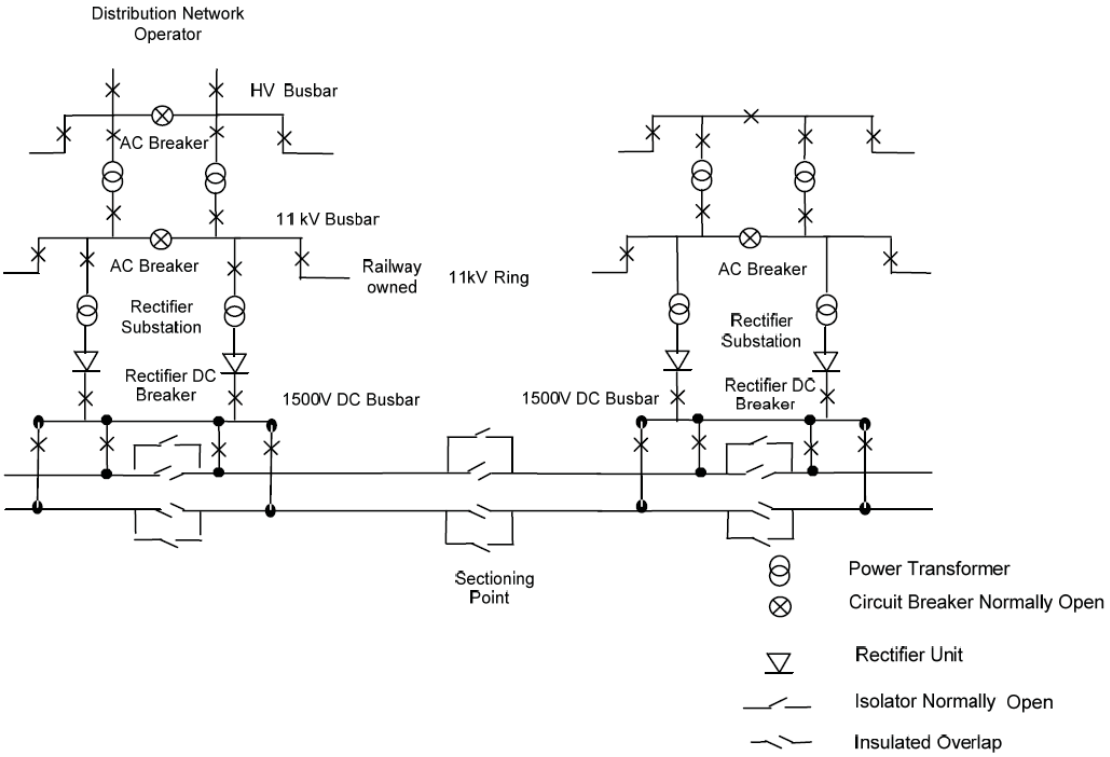

Figure 2.1 A typical DC feeding arrangement, produced by Dr. Roger White [13]

The rectifier substation is used to produce direct current by converting the 3-phase current. The rectifier for a 750 V network is usually composed of two 6-pulse paralleling bridge converters, as shown in Figure 2.2. As a result, an overall 12-pulse output ripple is produced. Vehicles collect current from the overhead line or third rails by pantographs or shoes. The current is usually returned by running rails. The benefit of using conductor rails is to reduce construction cost. However, a few systems, for example, the London underground, return current through an additional insulated conductor. In this way, the stray current passing through iron tube tunnels and other metallic structures could be prevented [15].

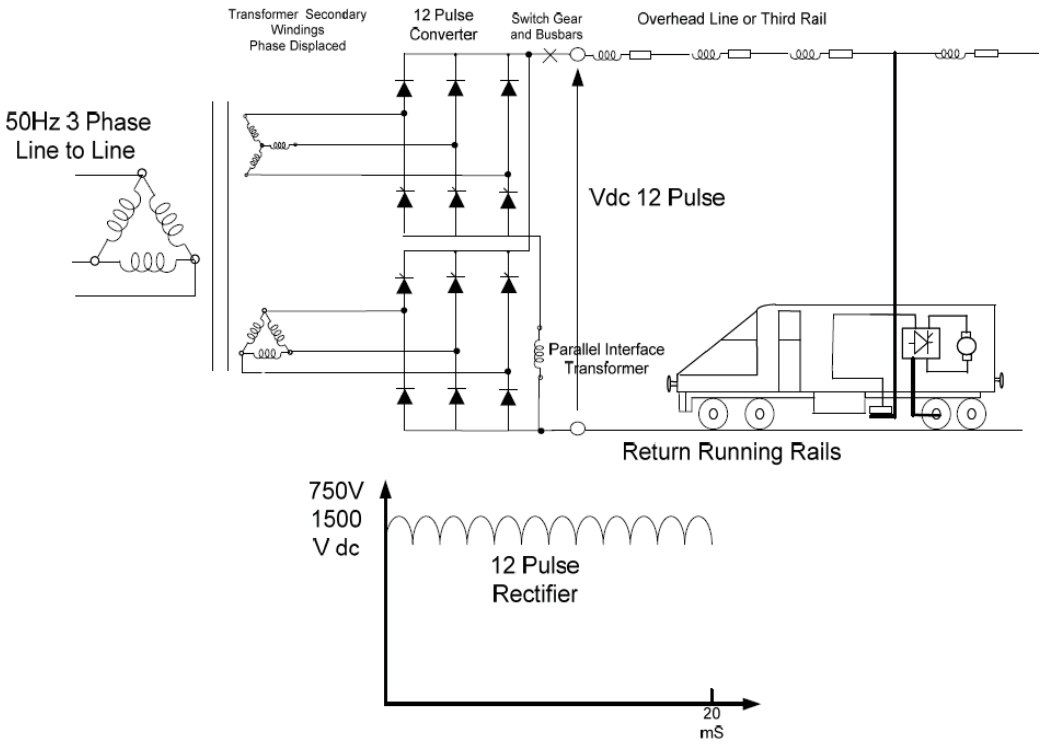

Figure 2.2 A typical 12-pulse bridge converter, produced by Dr. Roger White [13]

2.2.2 Traction Drives

DC and AC electric motors are commonly used in railways, regardless of DC or AC traction supplies [16]. Modern power electronic devices provide suitable smooth power flow to different types of traction motors. In this section, the operation principles of DC and AC motor drives with DC supplies are reviewed. More detailed discussion of traction drives can be found in [17, 18].

2.2.2.1 DC Motor Drives

A DC motor is controlled by various voltage supplies. The motor terminal voltage was originally increased by shorting out resistances in series or reduced by recombining

resistances. This device is called camshaft controller, and it is still in operation in some metros or tram systems [14]. In modern control schemes, a DC-DC chopper converter is used to convert a fixed DC voltage into various voltages. The overall drive efficiency is significantly improved. A typical chopper circuit for DC motor drives is shown in Figure 2.3. A closed loop control is adopted to obtain the required armature or field current subject to the demand of driving speed. Figure 2.4 describes the voltage waveforms with various duty cycle ratios by chopper controllers. A PWM (Pulse Width Modulation) is used to change the average output voltage by duty-cycle controls. Bi-directional operation makes it feasible to combine step up and step down converters, which realises the return of regenerative braking energy back to the supply to be used by nearby rolling stock [19].

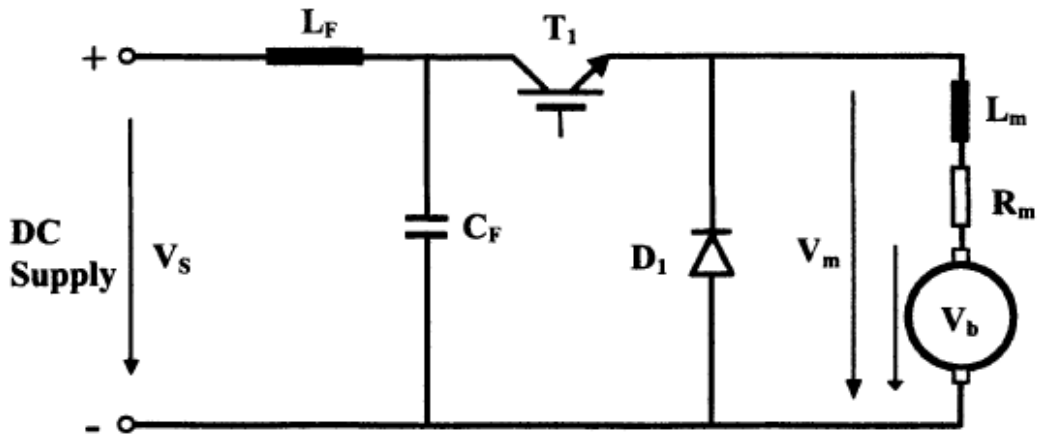

Figure 2.3 Chopper circuit for DC motor drives, produced from University of Birmingham traction system course notes [14]

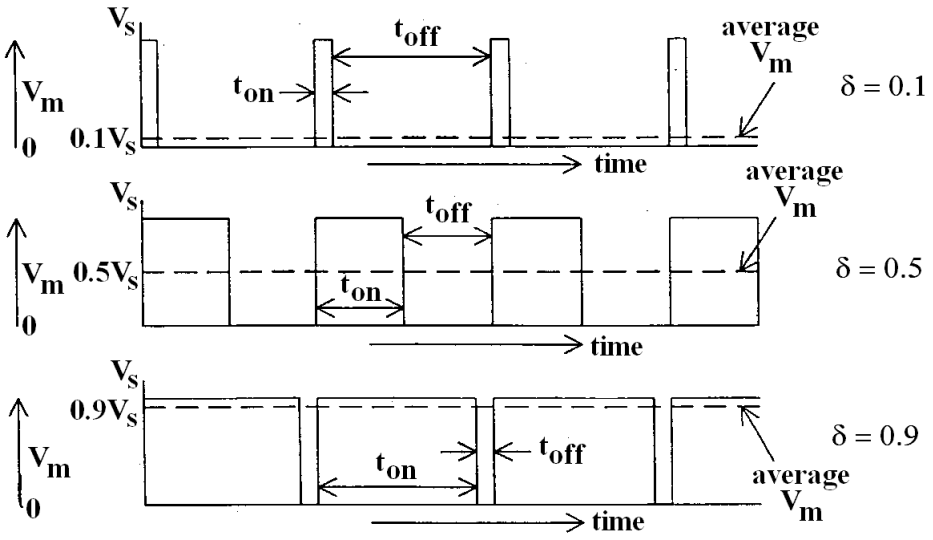

Figure 2.4 Chopped voltage waveforms with various duty cycle ratios, produced from University of Birmingham traction system course notes [16]

2.2.2.2 AC Motor Drives

There is a clear trend towards using AC motors on modern railways all over the world. The main advantage of AC motors is the elimination of commutators, which increases the power density and requires very low maintenance [20]. However, variable voltage and frequency supply are required, making the power electronic converter devices more complex. With the development of the latest generation of power electronic inverters, the GTO (Gate Turn-Off thyristor) with a switching frequency of between 200 and 300 Hz has been replaced by the IGBT (Insulated Gate Bipolar Transistor) with higher frequency, voltage and current capability. An example of the circuit configuration of six controllable switches and diodes is shown in Figure 2.5. With suitable filtering and conditioning, a 'VVVF' (Variable Voltage Variable Frequency) 3-phase supply is fabricated. The principle of the generation of sinusoidal PWM waveform is demonstrated in Figure 2.6. The output pulses are a sequence of rectangular waveforms, which are produced by

comparing a sine wave at the desired motor frequency with a triangular wave at the carrier frequency. The height of PWM pulses equals the DC supply, while the width is proportional to the local sinewave magnitude. Since the inverter is inherently regenerative, the regenerated braking energy can be fed back into the DC supplies.

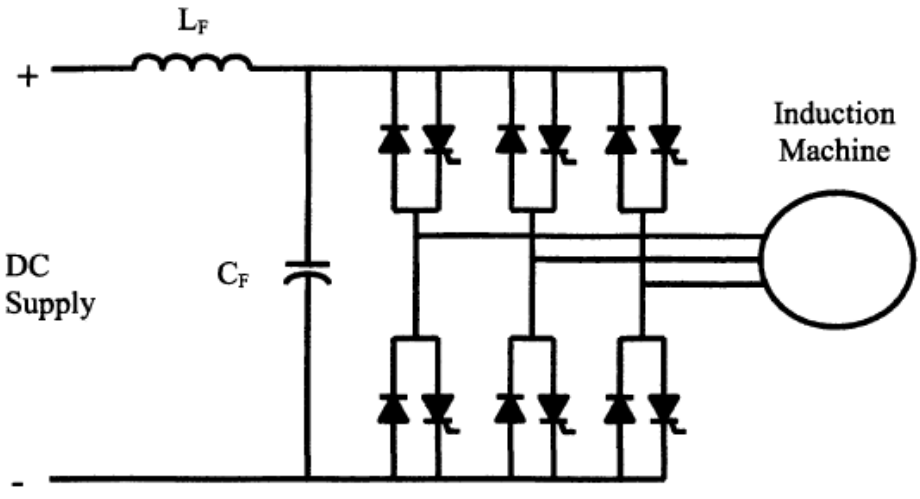

Figure 2.5 Inverter circuit for AC motor drives, produced from University of Birmingham traction system course notes [14]

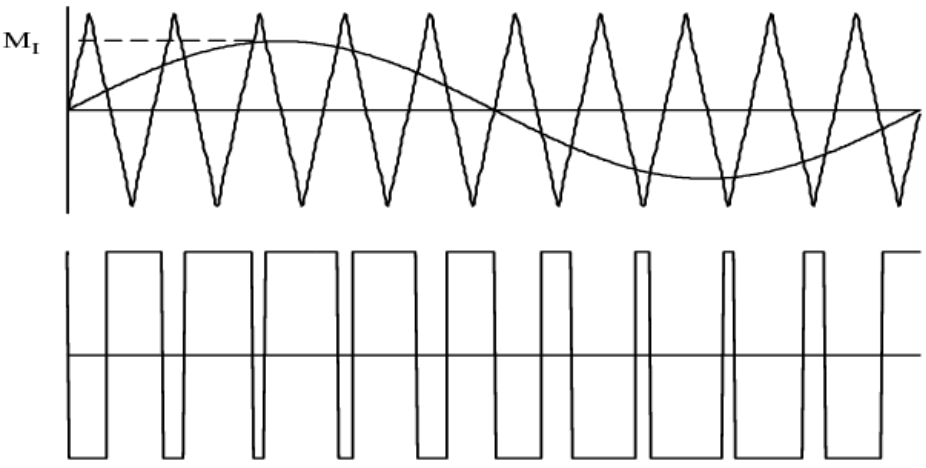

Figure 2.6 Principle of the generation of sinusoidal PWM waveform, produced from University of Birmingham traction system course notes [14]

2.3 Railway Energy Saving Techniques

A typical energy flow chart in railway systems is shown in Figure 2.7. The electrical energy supplies come from substations. Some of the substation energy is dissipated during the electricity transmission. The remaining substation energy is consumed by the train. Some of the train energy is used by auxiliary system and the rest of train energy is used by traction. The train traction energy is dissipated during the conversion from electrical to mechanical. The train kinetic energy results in the movement. Some of the kinetic energy overcomes the motion resistance and some is regenerated during braking. The regenerated braking energy can be used by auxiliary system directly or transferred back to the contact lines to supply other motoring trains in the network. As a result, the substation energy consumption could be reduced.

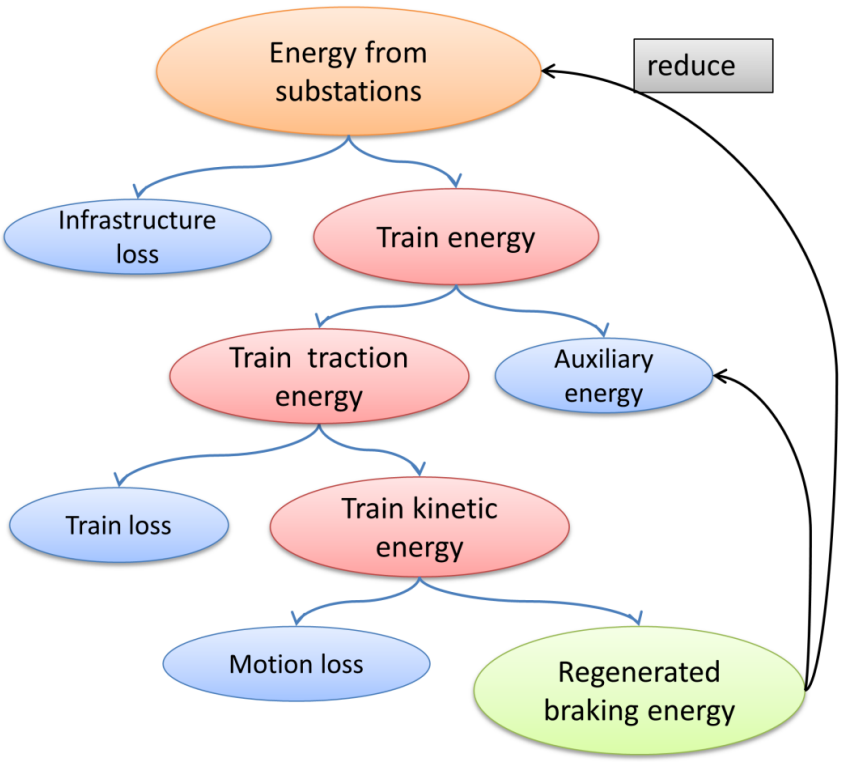

Figure 2.7 Energy flow chart in railway systems

The study of energy saving for railways originally started in the 1960s [21]. The train was assumed to be operated on a straight and flat route. A simple mathematic simulation of train movement was developed. Energy-efficient driving strategies including maximal acceleration and coasting were proposed. During subsequent decades, energy consumption and environmental factors have received more attention and the study of railway energy has become of greater significance. A good overview of energy efficient measurements in urban rail systems has been presented in [10], while energy reduction techniques for general railways have been reviewed in [22, 23] where the energy consumption could be reduced by 20 to 35%.

Energy-saving methods have been explored and examined in [10], including energy-efficient driving, regenerative braking, reduction of traction losses, and smart power management. It is assumed that regenerative braking and energy-efficient driving have greater potential and suitability to reduce energy consumption than other methods. According to the energy sector in railway systems, the techniques of rail energy saving are divided into three different aspects: traction energy optimisation, regenerative energy optimisation and system energy optimisation. In this section, the methodologies used for reducing energy consumption in railways are reviewed.

2.3.1 Traction Energy Optimisation

The energy used for traction accounts for around 60% to 70% of total railway energy consumption [24]. Therefore, the topic of reducing traction energy consumption is of theoretical and practical significance. The traction energy consumption is determined by various factors, mainly including driving styles, track vertical alignments and vehicle characteristics, which will be reviewed in the following sections.

2.3.1.1 Energy-efficient Driving

The train speed profile is determined by train driving controls, which is a key factor influencing the traction energy consumption. An example of three speed profiles with different driving styles is given in Figure 2.8. Speed profile 1 accelerates to a highest speed with a longer coasting pattern, while speed profile 2 accelerates to a medium speed with a shorter coasting pattern. Speed profile 3 accelerates to a lowest speed and remains this speed until braking. There is a large amount of literature studying the impact on energy consumption of different driving controls. Compared with flat-out driving, driving with coasting controls can reduce the energy consumption by about 30% with a 5% increase in journey time [12, 25].

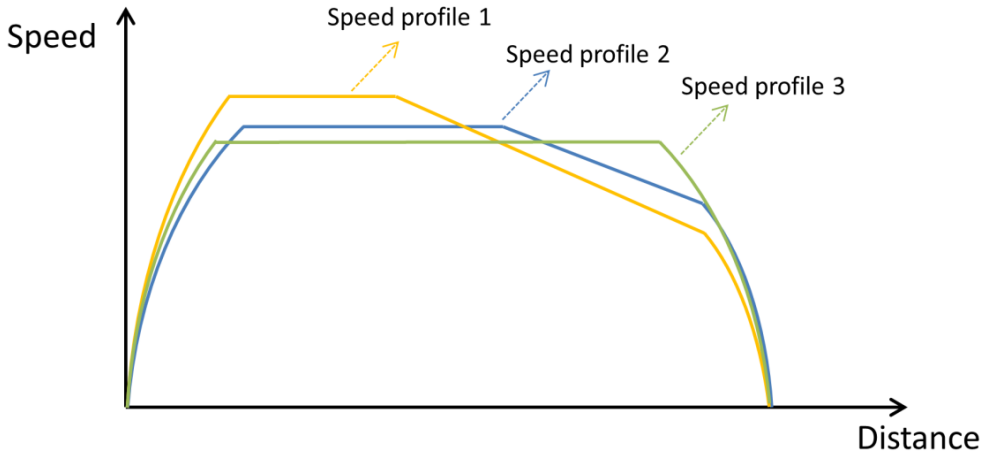

Figure 2.8 Examples of various speed profiles

Energy-efficient driving refers to driving controls with less energy consumption, which has been studied for decades. In 1997, Chang *et al.* proposed a Genetic Algorithm (GA) to optimise train speed profiles using appropriate coasting control with the consideration of energy consumption, delay punctuality and riding comfort [26]. From the preliminary simulation results, the GA provides credible and reasonably fast solutions for this variable

dimensional and multi-objective optimisation problem. The balance of energy consumption and journey time penalty was considered in the driving optimisation [27]. The idea of fuzzy logic was applied in the fitness function with the trade-off between energy and time, which was solved by a GA. A changeable chromosome length GA was proposed in [28] to solve the optimisation problem, which denotes effective performance. Both classical and heuristic approaches were utilised in [29, 30] to identify the necessary coasting points for a metro system. A heuristic method offers a faster and better solution for multiple coasting points compared with classical searching methods, and multi-coasting points control performs better energy saving in a long interstation section than a single coasting point. Different searching algorithms, such as Ant Colony Optimisation (ACO), a Genetic Algorithm (GA), and Dynamical Programming (DP) were compared in optimising single-train and multi-train trajectories in [31, 32]. It was found that Dynamical Programming performed better than GA and ant colony optimisation in searching for energy-efficient driving styles. A multi-train simulator was developed to decrease energy and penalty costs caused by delay [33, 34].

To obtain a fast-response online optimum control system, Howlett *et al.* proposed a mathematical algorithm and constructed an optimal speed profile, proved by Pontryagin Maximum Principle [35-39]. The driving strategies were solved by an analytical algorithm for routes with variable gradients in [40]. A numerical algorithm was proposed to calculate the optimal speed profiles by distributing the journey time into different sections, which achieved fast optimisation [41-43]. A combinatorial optimisation technique was proposed and shown to be capable of significantly reducing computation time and energy consumption [44-46]. The computation time is reduced from hours to less than 30 s, which is suitable for online operation.

Driver Advisory Systems (DAS) have become an effective tool to deliver realisable energy-saving operation information to drivers in recent years [22]. Based on pre-loaded algorithms and data, the on-board DAS is able to provide on-time driving strategies according to current running status. A simple but effective in-cab DAS was introduced in [47]. The trials with a UK train company demonstrated that up to 20% of the energy can be saved for a typical inner-city route with stops every 20 miles.

With the development of automated transit systems and communications-based train control (CBTC), Automatic Train Operation (ATO) is playing an increasingly important role in providing safer and more cost-efficient services. Chang proposed an algorithm of differential evolution (DE) to optimise the fuzzy controllers in ATO to improve the train performance [48]. A multi-objective function comprising energy consumption, time punctuality and riding comfort was optimised by an improved DE algorithm. With the capability of complicated controls by ATO driving, the train speed trajectory was optimised to minimise the energy consumption with constant journey time using an Enhanced Brute Force (EBF) [49]. The optimal ATO speed commands were designed and implemented on the metro lines in Madrid, which reduced the energy consumption by about 13% [50-53]. The principle of practical ATO controls was discussed in [54]. The frequent switches between accelerating and braking are avoided in the optimisation of speed trajectory, which improves the energy savings in the real world. The practical driving controls were studied by monitoring the energy consumption on actual networks [55, 56]. The differences in energy consumption relating to driver manners were observed, and the feedback would be used to enhance driving performance.

2.3.1.2 Track Vertical Alignment

The traction energy consumption can be influenced by various types of track alignments with the same train control action [57]. The station altitude can be designed, for example on the top of hills, which will make the train store potential energy, as shown in Figure 2.9. This potential energy can help the train to accelerate when departing from stations or decelerate when approaching stations. As a result, traction energy can be saved, and the journey time can be reduced [58]. Kim and Chien proposed a method to reduce energy consumption by optimising track alignment, speed limit and schedule adherence [59]. A train performance simulation (TPS) consisting of train traction and track alignment modules was developed in [60].

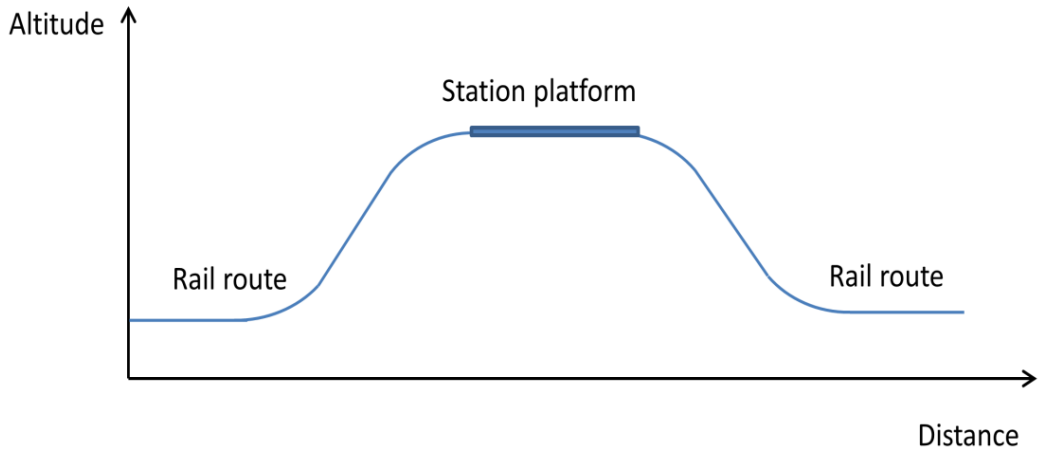

Figure 2.9 An example of the design of a station on the top of a hill

The traction energy and braking energy consumption of different trains on the same combined slope were analysed in [61]. The optimal gradient corresponding to each track combination was found. For short interstation distance, for example, 1000 m, the energy-saving gradient for acceleration or deceleration was found between 18‰ and 30‰. The

optimal gradient decreases with increasing route distance. For example, the energy-saving gradient of a route with 1500 m interstation distance becomes 12‰ to 20‰. A novel optimisation approach to improving energy efficiency by optimising the vertical alignment at stations was proposed in [62]. From the simulation results of Beijing Yizhuang Subway Line, the energy consumption and journey time decrease approximately linearly with the increase of station altitude. The total energy consumption is reduced by 5.6% when optimal vertical alignment is applied.

2.3.1.3 Vehicle Design

Drive chain losses by train power electronic devices comprise 10% to 15% of the total traction energy consumption [22]. The technologies for improving traction motor efficiency have been reviewed in [63, 64]. High-performance materials, for example, low-loss electrical steel sheets and low-resistivity conductors, have been widely explored. The implementation of Permanent Magnet Synchronous Motors (PMSM) is becoming a popular technology, which can achieve a very high efficiency [65]. The traction losses can be reduced because of the permanent magnets. PMSMs are smaller, lighter and allow regenerative braking down to lower speeds, which increases the benefits.

A new design of hybrid vehicles for energy saving was studied in [66-68]. The features of electric, diesel and hydrogen traction were evaluated. Power-management strategies were optimised for hybrid vehicle propulsion systems, where 7% of the energy could be saved [69]. The energy loss by train motion resistance is also significant, at around 10% to 30% of the traction energy consumption [22]. The motion resistance could be reduced by decreasing the mass of vehicles, improving the vehicle shapes, and so on [70, 71].

2.3.2 Regeneration Energy Optimisation

In modern railway systems with regenerative braking implemented, motoring trains collect electricity from substations and trains in regenerative braking. When the train is braking, motors transform mechanical energy available at the drive shaft into electrical energy. Then, the electrical energy is transferred back to the network system to power other trains in traction. For normal regenerative braking, all of the regenerating energy can be transferred into the transmission network to power other trains. However, as regenerative braking can increase the voltage of a train, a high regen voltage will occur when there are not enough motoring trains absorbing the regenerative energy in the power network. In case of a high voltage hazard, some braking energy is prevented from transferring into contact lines. This part of the braking energy is wasted in the on-board braking rheostat as heat until the network voltage is below the safe value [72]. Based on a DC 1500 V metro line in Korea, the reused regenerative braking energy was calculated based on the measurement of catenary voltage and current, where around 21-39% of traction energy was reused due to regenerated braking [73]. Therefore, it is essential to analyse and improve the amount of usable regenerative energy in railways.

The current strategies for improving regenerative braking energy in urban rails have been reviewed in [74], including timetable and trajectory optimisation as well as the implementation of energy storage systems (ESS) and reversible substations. Improving the efficiency of using regenerative energy by braking trajectory and timetable optimisation has been studied in [75, 76]. The Bellman-Ford algorithm was implemented in the optimisation of braking speed trajectory. The regenerative braking energy then increased by 17.23%. The usage of regenerative braking energy can be improved by synchronising

the braking phase with the accelerating phase of trains running in the same power network. A mathematical programming optimisation model was developed to optimise the synchronisation in [77, 78], where a power flow model of the electrical network was used for validation. The optimised timetable improves the energy savings by 7%, without having any effect on the current quality of passenger flow. A train cooperative scheduling rule to synchronise the accelerating and braking actions of successive trains was proposed in [79-82]. Based on a case study of Beijing Metro, the overlapping time of accelerating and braking was improved by around 22% by designing an optimal timetable using a GA.

Energy storage devices can be used to store regenerative braking for reuse. Using energy storage systems not only increases the efficiency of the usage of regenerative braking energy, but also reduces the peak load demand for busy traffic [83]. Ratniyomchai reviewed the developments and applications of energy storage devices [84]. A comparison of batteries, flywheels, electric double layer capacitors and hybrid energy storage devices was presented. The capacity and locations of way-side energy storage devices were optimised to minimise the energy losses in [85, 86]. The charging and discharging control scheme of on-board energy storage systems has been modelled in a multi-train power network simulator [87, 88]. The reference state of charge was optimised by a rule-based approach to improving the robustness of the control system. Practical measurement on a light rail system with energy storage devices was delivered for validation of the modelling method [89-91]. By using the simulation approaches, the system losses could be further reduced. In reversible DC fed systems with inverting substations, the regenerative braking energy can be converted and fed back to AC networks, which increases the network receptivity. The design and simulation of inverting substations is illustrated in [92-94]. However, the impact of using regenerative braking energy is not validated [95].

2.3.3 System Energy Optimisation

System energy consumption in a railway system refers to the energy drawn by substations from the electricity grid, which is net energy consumption of the railway system considering the energy used by electricity transmission and traction as well as the payback of regenerative energy. Compared with the optimisation of traction or regenerative energy consumption, system energy optimisation is more complicated, as it is determined by a number of variables including the power network arrangement, driving styles, timetables and so on.

Most studies of railway system energy optimisation are focused on optimising timetables. A stochastic cooperative scheduling approach to optimising the dwell and the headway times together with coordinating the accelerating and braking phases was proposed in [96]. Based on a case study of Beijing Yizhuang Subway Line, the net energy consumption was reduced by 15.13% compared with operation in the current timetable. Li and Lo proposed an integrated energy-efficient operation modelling approach to jointly optimise the timetable and speed trajectory using a GA. The net energy consumption was reduced by around 20% using the integrated method [97, 98]. Zhao *et al.* presented an approach to minimising the whole-day substation energy consumption for a metro line [99]. The train movement sequence, inter-station journey time, and service intervals were considered in the searching algorithms. A two-train model was formulated to study the cooperative operation in [100]. Energy-efficient control strategies were optimised with the departure headway given, where around 19.2% of the energy consumption was saved. The difference between traction energy and the reused regenerative energy was assumed as the objective to optimise using cooperative train controls in [101, 102].

However, the modelling of a realistic railway traction power network was not considerd, and the transmission loss and regenerative braking loss due to the overvoltage braking were ignored. Miyatake and Ko considered the impact of DC feeding systems, and proposed a simplified approximated numerical algorithm to optimise the train operation. A two-train case was used to demonstrate that this method can be applied to the optimal voltage control of a substation [103, 104]. The energy-saving strategies based on railway power supply systems were investigated in [105-107]. The factors of substation energy consumption in a DC-fed railway system have been presented. Based on a multi-train power network simulation, different scenarios have been analysed to optimise ATO speed profiles with consideration of the energy recovered from regenerative trains [108, 109].

2.4 Hypothesis Development

A comparison of the recent literature on railway energy-saving studies is summarised in Table 2.1. There are a great number of studies on railway energy savings which focus on train driving or timetable optimisation to reduce the traction energy consumption or increase the usage of regenerative braking energy. However, very few of them consider the optimisation of a combination of driving styles, timetables, and the power network to reduce the system energy consumption. Most of them do not consider the relationship between system energy consumption and traction power networks.

Table 2.1 Recent literature on energy-saving studies in railways

Optimisation objective	Decision variables	Publications	Methodology and algorithms
Traction energy	Driving speed	Chang *et al.* [26]	GA
		Bocharnikov *et al.* [27]	GA with fuzzy logic
		Fu *et al.* [28]	GA
		Wong *et al.* [29, 30]	Classical and heuristic
		Lu *et al.* [31]	ACO, GA, DP
		Howlett *et al.* [35-39]	Analytical algorithm
		Su *et al.* [41-43]	Analytical algorithm
		Carvajal *et al.* [50-53]	ATO speed
		Ellis *et al.* [55, 56]	Practical driving
	Track alignment	Kim *et al.* [59, 60]	Simulated annealing
		Hu *et al.* [61]	Energy-saving slope
	Vehicle design	Kondo *et al.* [63, 64]	High-efficiency motors
		Hoffrichter *et al.* [66-68]	Hybrid vehicles
Regenerative braking energy	Braking speed	Lu *et al.* [75]	Bellman-Ford algorithm
	Timetable	Nasri *et al.*[76]	GA
		Ramos *et al.* [77, 78]	Mathematical program
		Yang *et al.* [79-82]	GA
	ESS	Ratniyomchai *et al.* [85, 86]	Capacity and location
		Takagi *et al.* [87, 88]	Control scheme
		Chymera *et al.* [89-91]	Practical application
	Inverting substation	Suzuki *et al.* [92-94]	Simulation design
System energy	Speed & timetable	Li and Lo [97, 98]	GA
		Zhao *et al.* [99]	GA
		Su *et al.* [101, 102]	Analytical algorithm
	Speed & timetable in power networks	Miyatake *et al.* [103, 104]	Numerical algorithm
		Domínguez *et al.* [108, 109]	Particle swarm

The gap in previous literature studies is demonstrated in Figure 2.10. Optimisation, train traction simulation and power supply simulation have been well studied. The combination of optimisation and train traction simulation has also been investigated. However, previous studies of power supply networks usually focus on electrification infrastructure design and

capacity, without the consideration of energy efficiency. The overlap of these three topics has not been investigated.

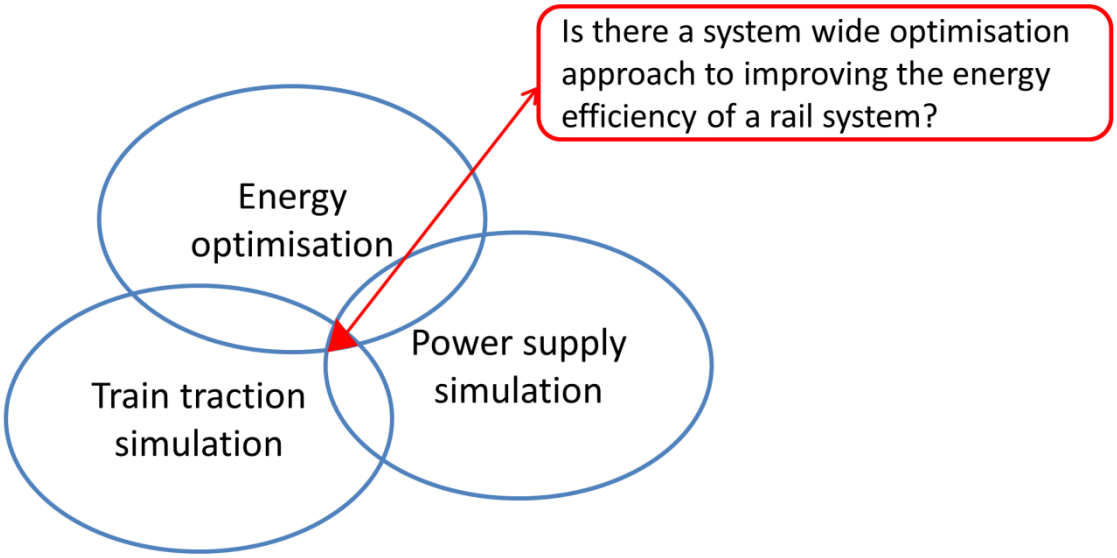

Figure 2.10 The gap in previous literature studies

This thesis proposes the hypothesis: There is a system-wide optimisation approach that can be used to improve the energy efficiency of a railway system. In order to validate the hypothesis, a simulation tool is required to evaluate the energy consumption of a railway system. Train traction modelling and power supply modelling should be considered jointly. Energy optimisation is investigated based on the simulation of integrated systems. Previous energy strategies, for example, driving strategies and timetable design, can be studied and improved for system energy optimisation with the consideration of power network modelling. The feasibility of energy-efficient operation applications should be demonstrated based on case studies.

2.5 Summary

In the first part of this chapter, the arrangement of DC feeding is presented and the features of traction drives in modern railways are introduced. The electrical unity grid provides the 3-phase AC power for the whole railway system. The AC power is rectified by the substation and used to supply the trains for traction. Both AC and DC motors are used currently, controlled by on-board power electronic converters.

This chapter also reviews the previous studies of railway energy optimisation. Based on the energy sector in railway systems, the literature is classified into three sections, namely traction energy optimisation, regenerative energy optimisation and system energy optimisation. By comparing and analysing the prior literature, it is found that system energy optimisation has not been fully studied. This thesis proposes to investigate a system wide optimisation approach to improving the energy efficiency of a railway system. The next chapter illustrates the development of an energy simulator which is used for solving the system energy optimisation problem.

Chapter 3

Railway Integrated System Simulation

3.1 Introduction

Research into computer-based simulation of train movements and power-supply conditions has been ongoing for several decades. In 1978, a computer-based simulator was developed to study the performance characteristics of rapid-transit services [110]. This literature demonstrated the practicability of simulation techniques in solving train movement and power network issues. The linearisation techniques were adopted. The application of diakoptics to solve DC railway power networks was first presented in [111]. Coupled with the sparse matrix techniques, this work improved the efficiency of solving complex railway power networks. In order to examine the non-linear power flows in electrical power networks, algebraic equations with various iterative methods were utilised and applied, for example, the Newton-Raphson iterative method, Point-Jacobi method, Zollenkopf's bifactorisation and Incomplete Cholesky Conjugate Gradient (ICCG) method [89, 112-118].

In terms of train movement and controls, the development of railway signalling and control systems improves transport capacity but increases the complexity of railway modelling. Multiple train simulation under different train signalling systems has been studied in [33,

34, 119]. During recent years, trains with regenerative braking have been widely adopted. These trains can convert kinetic energy into electrical energy to reduce net energy consumption at trains. The efficiency of using regenerative energy has been investigated, and the results indicated that both the braking trajectory and timetable could contribute to the effective usage of braking energy [75, 78]. Based on the power network modelling, energy management techniques for energy storage devices in a power feeding network have also received attention [11, 69, 88, 120].

Previous studies of railway simulation usually separate the modelling of the power network and train traction. Most of the simulation tools are used to design supply infrastructure. In order to investigate the system energy consumption of railways, this chapter presents a simulation method combining the vehicle movement and electrical network model. An improved load flow analysis is proposed to solve the DC-fed railway power network. Based on the data collected from BS-EN50641 British Standard in Railway Applications-Fixed installations [121], a validation test is presented to demonstrate the performance of the load flow solver.

3.2 Train Movement Modelling

3.2.1 Equations of movement

Figure 3.1 indicates the forces on a traction vehicle located on an uphill section of track. The tractive effort (F) applied to a vehicle is used for moving the train against the friction forces (R) and gravitational forces ($Mg\sin(\alpha)$) in moving the mass of the train uphill [17].

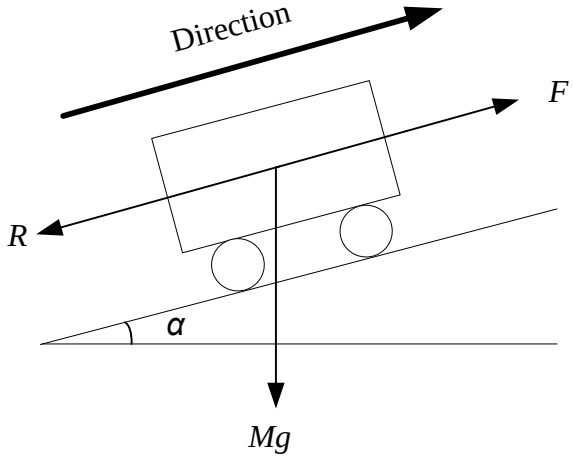

Figure 3.1 Forces on a traction vehicle

The train movement can be determined by standard Newtonian equations of motion. In the longitudinal direction, the motion of the vehicle is governed by the tractive effort, the gradient and the vehicle resistance [122], known as Lomonossoff's equation in (3.1).

$$M_e \frac{\mathrm{d}^2 s}{\mathrm{d}t^2} = F - Mg\sin(\alpha) - R \tag{3.1}$$

Where:

- M_e is the effective mass of the vehicle [kg];
- s is the vehicle position along the track [m];
- t is the time [s];
- F is the tractive effort [N];
- R is the vehicle resistance [N];
- M is the vehicle mass [kg];
- g is the acceleration due to gravity [m/s^2];
- α is the angle of the route slope [rad].

3.2.1.1 Effective Mass

The vehicle mass is the sum of the tare mass and payload in equation (3.2). When a train is accelerated linearly, the rotating parts are also accelerated in a rotational sense. The rotational effect of wheels and motors should be added into the linear train motion by increasing the effective train mass. This rotational inertia effect is called 'rotary allowance' and it is expressed as a fraction of the tare weight of the train (λ_w). The effective mass can be calculated by equation (3.3). The value of the rotary allowance varies from 5% to 15%, which is less for a heavy body with a small number of motored axles and more for a light body with all axles motored [20].

$$M = M_t + M_l \tag{3.2}$$

$$M_e = M_t \times (1 + \lambda_w) + M_l \tag{3.3}$$

Where:

- M_t is the tare mass of the vehicle [kg];
- M_l is the payload [kg];
- λ_w is the rotary allowance.

3.2.1.2 Vehicle Resistance

Train moves in an opposite direction to friction and aerodynamic drag. The main component of vehicle resistance is the rolling resistance, which is related to the weight, shape and speed. The formula for working out rolling resistance is known as the Davis

Equation in (3.4). The Davis coefficients A, B and C are difficult to predict from theoretical calculations, which are usually determined by run-down experiments [123].

$$F_D = A + B\frac{\mathrm{d}s}{\mathrm{d}t} + C\left(\frac{\mathrm{d}s}{\mathrm{d}t}\right)^2 \tag{3.4}$$

Where:

- F_D is Davis resistance [N];
- A is Davis equation constant [N];
- B is Davis equation linear term constant [N/(m/s)];
- C is Davis equation quadratic term constant [$\mathrm{N/(m/s)^2}$].

A further component of train resistance is due to the track curvature. It is called curve resistance as in equation (3.5). The curve resistance has a limited effect when the train is running at a speed less than 200 km/h. In most cases, the curve drag can be assumed to be negligible [124].

$$F_C = \frac{D}{r} \tag{3.5}$$

Where:

- F_C is the curvature resistance [N];
- D is an experimentally determined constant [Nm];
- r is the curve radius [m].

The total train resistance of the vehicle is given in equation (3.6), which mixes equation (3.4) and equation (3.5).

$$R = A + B\frac{\mathrm{d}s}{\mathrm{d}t} + C\left(\frac{\mathrm{d}s}{\mathrm{d}t}\right)^2 + \frac{D}{r} \tag{3.6}$$

3.2.2 Tractive Effort Curve

The tractive effort is produced by the traction motors and overcomes the resistance and gradient. It varies with the types of technology and motors. However, there are several common features used to generalise a tractive effort curve representing most traction systems. The tractive effort curve describes the relationship between tractive effort and the speed of the train. Figure 3.2 describes the tractive effort curve of a suburban train at the nominal voltage in BS EN 50641 Railway Application – Fixed installations [121]. There are three distinct phases in the tractive effort curve. Zone 1 is characterised by constant torque operation. The tractive effort is maintained until the vehicle reaches base speed v_1. The vehicle also reaches the maximum power at v_1. Due to the power limitation in on-board system, the tractive effort decreases at a rate of $1/v$ in zone 2. This is constant power operation. At higher speed, there is a further reduction of tractive effort at a rate of $1/v^2$. This is caused by the motor limitation. The power decreases from the maximum power in zone 3, which can be called reduced power operation. Equations (3.7) and (3.8) are given to indicate the features of the tractive effort curve. The tractive effort can be calculated by the vehicle speed. The maximum mechanical power is given in equation (3.9).

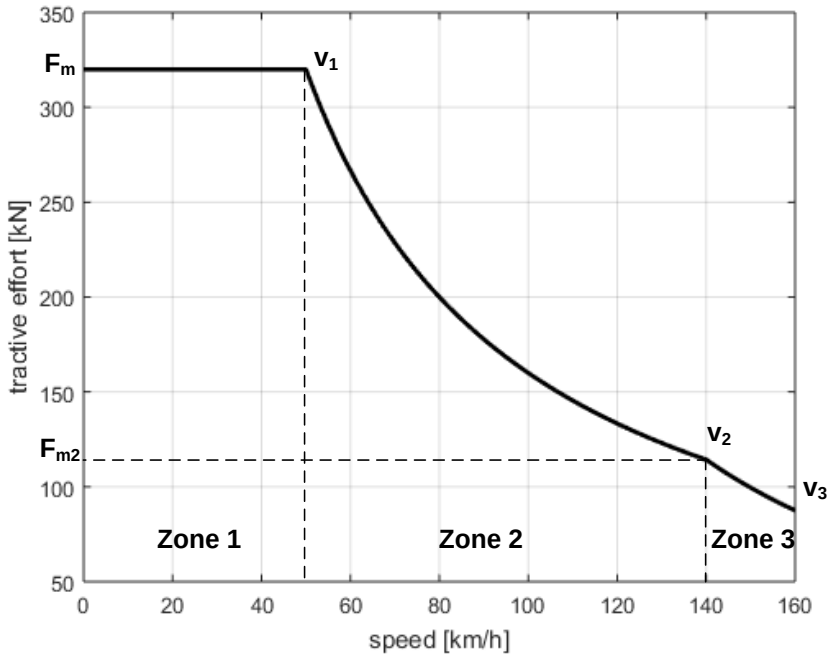

Figure 3.2 Typical tractive effort curve

$$F(v) = \begin{cases} F_m & v < v_1 \\ \dfrac{F_m \times v_1}{v} & v_1 < v < v_2 \\ \dfrac{F_{m2} \times {v_2}^2}{v^2} & v_2 < v < v_3 \end{cases} \tag{3.7}$$

$$F_{m2} = \frac{F_m \times v_1}{v_2} \tag{3.8}$$

$$P_{me\_max} = F_m \times v_1 \tag{3.9}$$

Where:

- F_m is the maximum tractive effort [N];
- F_{m2} is the tractive effort at speed v_2 [N];
- P_{me_max} is the train maximum mechanical power [W].

3.2.3 Train Driving Styles

Train driving control can be generally categorised into four modes: motoring, cruising, coasting and braking [72]. The train speed trajectory can be generated by different driving strategies. Figure 3.3 shows an example of a speed curve with these four modes in sequence.

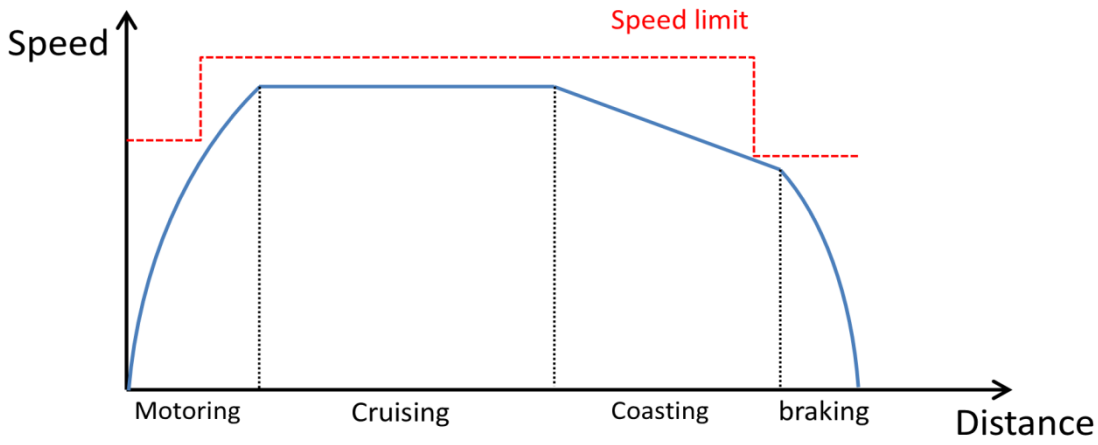

Figure 3.3 An example of a train speed trajectory

The motoring mode is generally active at the beginning of the journey, where it is used to increase the vehicle speed. The tractive effort in the motoring mode is normally higher than the sum of the effort by gradient and the resistance. The acceleration is positive which is given in equation (3.10).

$$\begin{cases} F > Mg\sin(\alpha) + R \\ a = \dfrac{F - Mg\sin(\alpha) - R}{M_e} \end{cases} \tag{3.10}$$

Cruising mode is invoked when the train reaches a higher speed. Partial power is adopted at this time to maintain this speed. The tractive effort in cruising mode is equal to the sum

of the effort by gradient and resistance, as shown in equation (3.11). The acceleration in this mode is equal to zero.

$$\begin{cases} F = Mg\sin(\alpha) + R \\ a = 0 \end{cases} \tag{3.11}$$

When the coasting mode is applied, no traction power is required by the train. Coasting mode consumes zero traction power, which is an energy-efficient driving style. In coasting, the tractive effort is equal to zero. The acceleration is determined by the balance of the forces produced by the gradient and resistance as shown in equation (3.12). The train speed normally decreases in coasting, but it may increase when the train is on a steep downhill.

$$\begin{cases} F = 0 \\ a = \dfrac{-Mg\sin(\alpha) - R}{M_e} \end{cases} \tag{3.12}$$

Braking mode is applied when the train is approaching a stop or a speed limit. In braking mode, both the tractive effort and acceleration are negative as in equation (3.13).

$$\begin{cases} F < 0 \\ a = \dfrac{F - Mg\sin(\alpha) - R}{M_e} \end{cases} \tag{3.13}$$

3.2.4 Motion Simulator Design

A single-train movement is modelled based on the vehicle characteristic and route data. The vehicle characteristic includes vehicle mass, tractive effort parameters and Davis

constants. The route data includes gradient, speed limits and station positions along the route. Figure 3.4 describes the structure of the motion simulator. The driving strategies are treated as dynamic inputs to the single-train motion simulator. The simulator outputs the train speed profile based on the driving styles and fixed inputs. The train power requirement and traction energy consumption can also be computed for further studies.

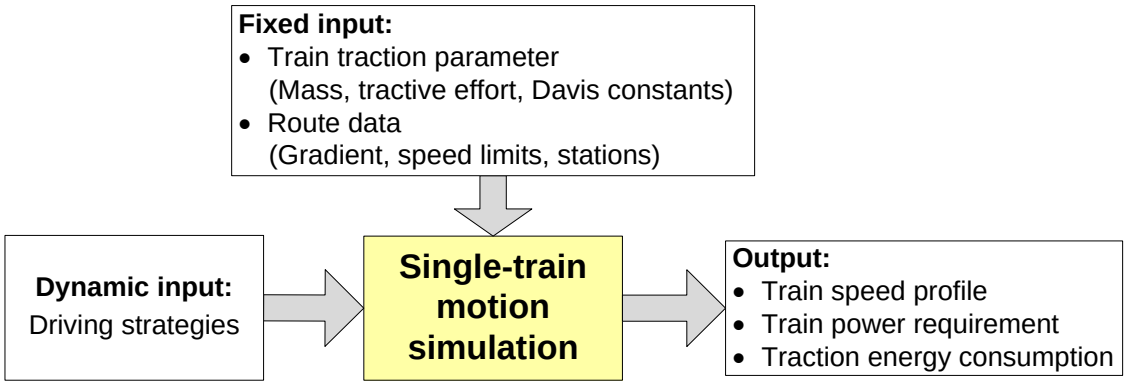

Figure 3.4 Diagram of motion simulator structure

A time-based simulator can be developed using the structure above. A whole journey is discretised in time, and then it becomes a combination of vehicle state at each time step. Figure 3.5 describes an example of the movement of a vehicle. The relationship between distance and time as well as the relation between speed and time can be found in this figure. The time interval is expressed by ΔT. The simulation results with different time intervals have been tested in [125]. The time step with 1 second is proper for energy evaluation, which is used in this thesis. The driving controls are a sequence of tractive effort values at each time step. The tractive effort is assumed as a constant during each time interval. The state of the vehicle including acceleration, speed, position and power can be calculated according to the driving controls at each time step.

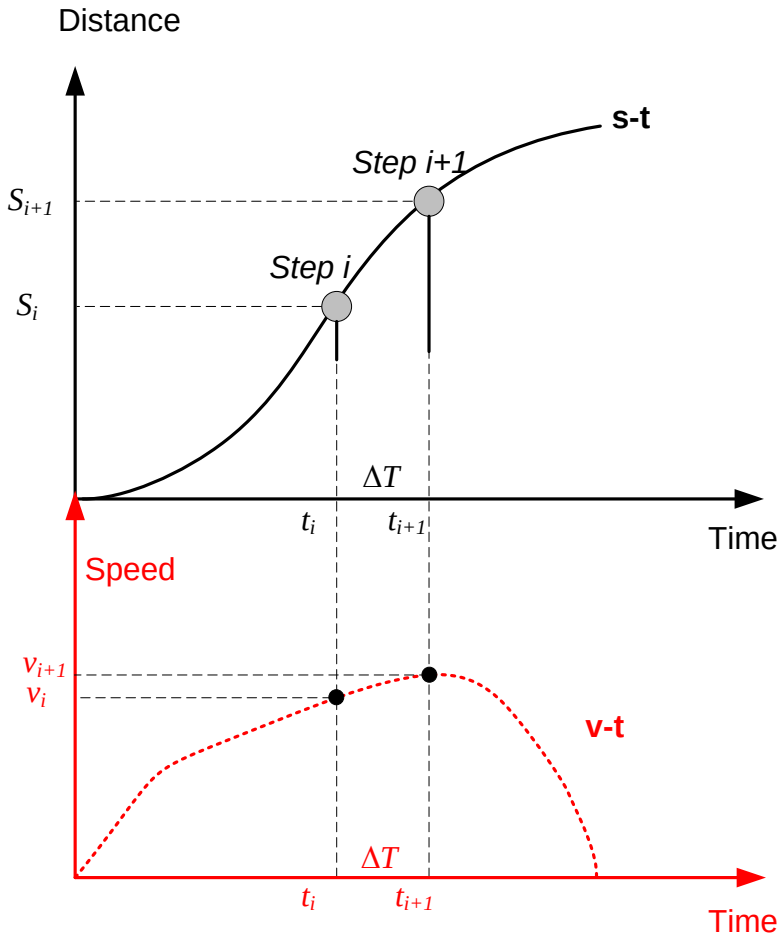

Figure 3.5 Vehicle state switch

If the vehicle state at *step i* is known, and the tractive effort at *step i* is equal to F_i, the acceleration can be calculated by equation (3.14).

$$a_i = \frac{F_i - Mg\sin(\alpha_i) - R_i}{M_e} \tag{3.14}$$

The speed and location at the next step can be calculated by the current state and the driving control, which are given in equations (3.15) and (3.16).

$$v_{i+1} = v_i + a_i \times \Delta T \tag{3.15}$$

$$s_{i+1} = s_i + \left(v_i \times \Delta T + \frac{1}{2} \times a_i \times \Delta T^2\right) \tag{3.16}$$

The mechanical power required by the train in the current state is given in equation (3.17).

$$P_{me\_i} = F_i \times v_i \tag{3.17}$$

In order to analyse the power flow in the power network simulation, the electrical power requirements can be transformed from the mechanical power results as in equation (3.18). The efficiency (η) refers to the whole traction chain from the current collector to the wheel, which is around 85%. The positive mechanical power will lead to a higher positive electrical power requirement. The negative mechanical power is the braking power, which will lead to a lower electric regenerative braking power.

$$P_{el} = \begin{cases} \dfrac{P_{me}}{\eta} & if\ P_{me} \geq 0 \\ P_{me} \times \eta & if\ P_{me} < 0 \end{cases} \tag{3.18}$$

Where:

- P_{me} is the train mechanical power [W];
- P_{el} is the train electrical power [W];
- η is the efficiency of traction chain conversion.

3.3 Power Network Modelling

In a DC railway power network, the traction rectifier substations are the primary electricity source for vehicles. Figure 3.6 presents a typical DC traction power network with multiple

trains on up and down tracks. The rectifier substation is connected to the DC busbar, which feeds the power network in both the up and down tracks. When the transmission line voltage is higher than the substation voltage itself, the rectifier substation will prevent current from flowing back to the AC utility grid. This section introduces the method to simulate the components in the power network by equivalent electric circuits.

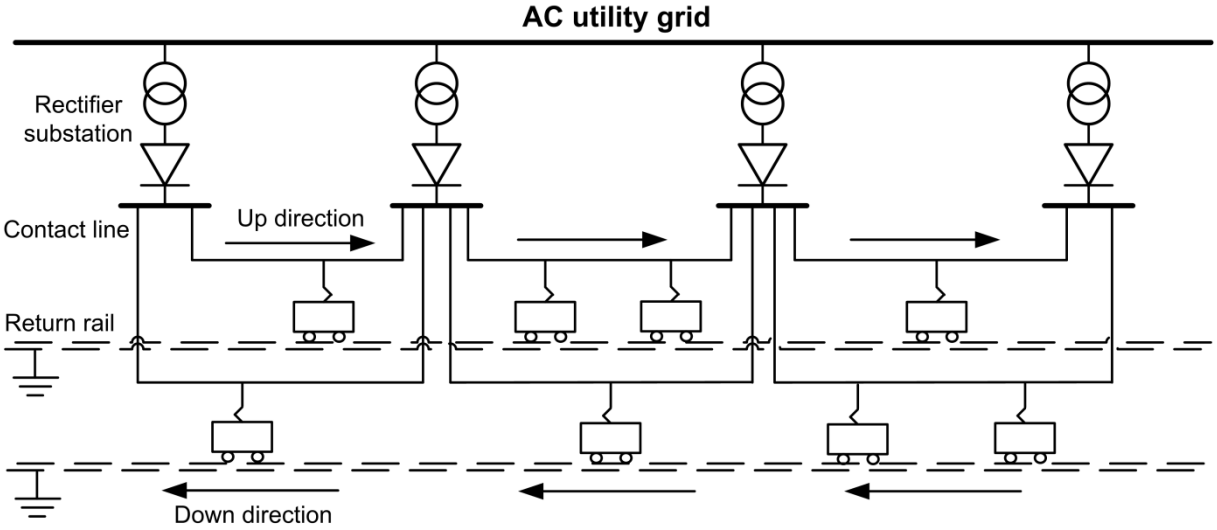

Figure 3.6 Typical DC traction power network

3.3.1 Rectifier substations

Overall, the electrical supply substation is equipped with three phase 6-pulse or 12-pulse rectifiers, as shown in Figure 3.7. With the development of power electronic techniques, equivalent 24-pulse rectifiers are being applied in modern rapid transit systems, where two 12-pulse rectifiers are combined in parallel. The voltage regulation characteristic of the rectifier units is nonlinear, where the ratio of output voltage to current depends on the loads [126]. In order to simplify simulation analysis, this study limits the working region of the rectifier units. Only the voltage regulation characteristic at normal loads is considered in this thesis. Thus, the voltage regulation characteristic can be simplified as linear. For

example, in Figure 3.7, the no-load voltage (850 V) decreases linearly with the current. The rated voltage and current are 750 V and 2500 A, respectively. The equivalent resistance for this rectifier substation can be calculated by equation (3.19).

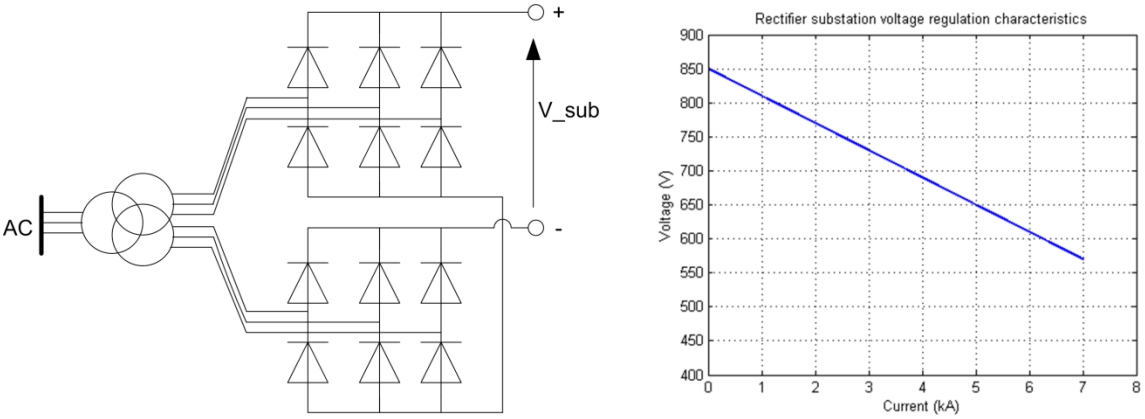

Figure 3.7 12-pulse rectifier unit and voltage regulation characteristics

$$R_{sub} = \frac{\Delta V}{\Delta I} = \frac{V_{noload} - V_{rated}}{I_{rated} - 0} = \frac{850 - 750}{2500 - 0} = 0.04\Omega \tag{3.19}$$

A rectifier substation can be modelled by an ideal voltage source in series with an equivalent source resistance and a diode, as in Figure 3.8. The voltage source is equal to the no-load voltage of the substation.

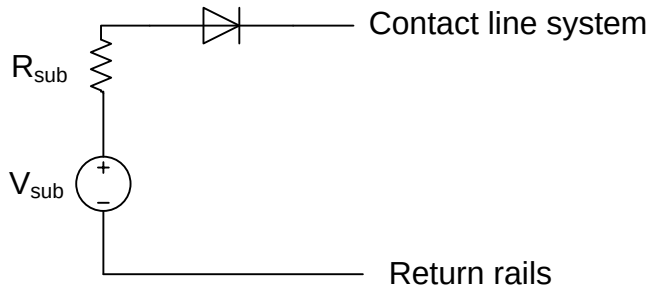

Figure 3.8 Equivalent circuit of rectifier substation

In practice, there are two working modes for a rectifier substation. If the contact line voltage is lower than the no-load voltage, the diode in Figure 3.8 is forward biased and the substation delivers power to the network. In this case, the substation equivalent circuit can be represented as Figure 3.9.

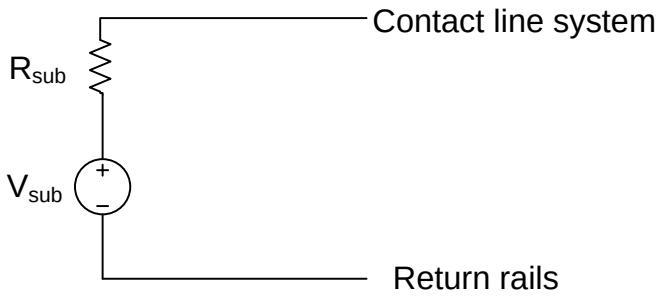

Figure 3.9 Equivalent circuit of rectifier substation switched on

If the contact line voltage is higher than the no-load voltage, the diode in Figure 3.8 is reverse-biased and the substation does not deliver power to the network. The equivalent circuit of the substation is presented in Figure 3.10, where the voltage source is in series with an inner resistor and a very large resistance. The very large resistance is 10^6 Ω in this simulation [116].

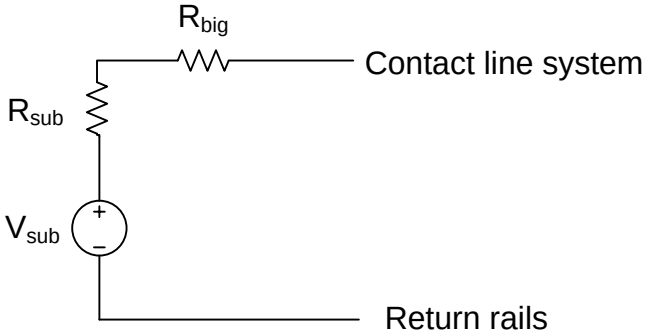

Figure 3.10 Equivalent circuit of rectifier substation switched off

In order to simplify the power flow analysis, the voltage source of the substation model is transformed into a current source using Thevenin's and Norton's theorem, as shown in Figure 3.11. The substation current can be calculated by equation (3.20), where ‘u’ is equal to 0 when the rectifier substation is conducting, and otherwise is equal to 1.

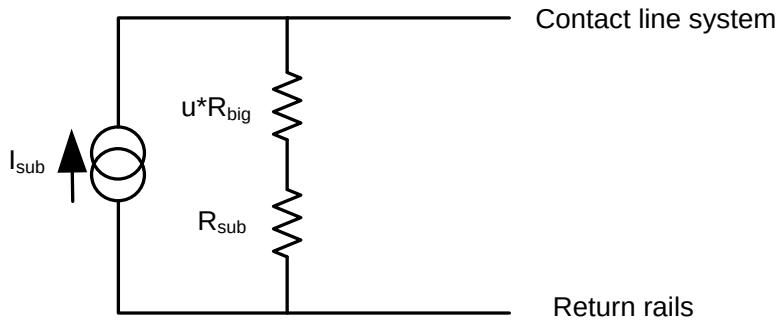

Figure 3.11 Current source circuit of substation model

$$I_{sub} = \frac{V_{sub}}{R_{sub} + u \times R_{big}} \tag{3.20}$$

3.3.2 Dynamic Train Loads

Some previous research used constant current source models or constant efficiency of regenerative braking energy usage to present trains in a traction power network [85, 86, 97, 98]. However, this is not accurate in the study of energy consumption for railways. In railway power systems, modern trains collect electricity behaving as voltage-dependant power loads. The power consumed by trains does not depend on the voltage or current at the pantograph [127]. In this thesis, trains are considered as dynamical power sources or power loads for a better simulation performance.

Train electrical motor power (P_{el}) is explained by equation (3.18) in Section 3.2.4, which is calculated according to the driving controls. Train electrical power is positive when the train is motoring and becomes negative when the train is braking. The auxiliary load of the train is the power used by the air conditioning and lighting power, which is assumed as a constant. The vehicle power demand (P_{train_demand}) is computed by summing the auxiliary load power and electrical power of the motor, given in equation (3.21). This value is treated as an input to the power network simulator.

$$P_{train\_demand} = P_{el} + P_{aux} \tag{3.21}$$

Where:

- P_{train_demand} is the train electrical power demand [W];
- P_{aux} is the train auxiliary load power [W].

The power network simulator will solve the power flow. The train voltage and current can be calculated. P_{train} is the electric power which the traction train receives or the braking train exports, given in equation (3.22). If the train is running in a normal mode, the final train electric power is equal to the train power demand. If not, the train may receive less power compared with the demand, while the braking train may not export all of the electric braking power back to the network. The train modelling methods are illustrated as follows.

$$P_{train} = I_{train} \times V_{train} \tag{3.22}$$

Where:

- P_{train} is the train received electrical power [W].

3.3.2.1 Traction Train

When the train is motoring, it collects power from the power network, transforming the input electrical power into mechanical power. In order to protect the train and supply networks, the train is equipped with automatic devices which are able to adapt the power demand. From the British Standard in Railway applications-Power supply and rolling stock [128], the maximum allowable train current against the train voltage is given in Figure 3.12.

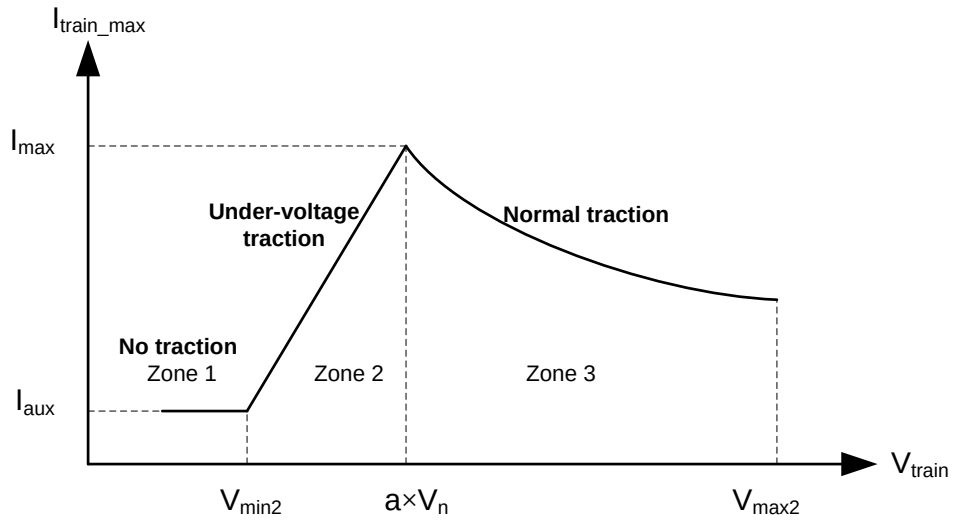

Figure 3.12 Current limitation of traction train

According to the pantograph voltage, the working state of trains is categorised into three zones. In zone 1 where the train voltage is lower than V_{min2}, there is no traction supply from the power network. The train only collects the electricity to feed the auxiliary system. In zone 2, the train is operated in under-voltage traction mode. The train power is limited, even though the train requires higher power. In zone 3, the train is operated in normal traction. V_n is the nominal voltage of the system, and a is the knee point factor which is

lower than 1 (normally between 0.8 and 0.9). When the train voltage is higher than $a \times V_n$, the train can be supplied with maximum traction power. Taken from the British Standard in Railway Applications-Supply voltages of traction systems [129], the voltage characteristics including under-voltage and over-voltage levels for DC railway systems are specified in Table 3.1.

Table 3.1 Voltage permissible limits for DC railways [129]

DC railway systems	Lowest non-permanent voltage V_{min2} [V]	Lowest permanent voltage V_{min1} [V]	Nominal voltage V_n [V]	Highest permanent voltage V_{max1} [V]	Highest non-permanent voltage V_{max2} [V]
DC600	400	400	600	720	800
DC750	500	500	750	900	1000
DC1500	1000	1000	1500	1800	1950
DC3000	2000	2000	3000	3600	3900

For traction trains, the maximum train power demand is the sum of maximum traction power and auxiliary power, as in equation (3.23).

$$P_{train\_demand\_max} = \frac{P_{trac\_me\_max}}{\eta} + P_{aux} \tag{3.23}$$

Where:

- $P_{train\_demand\_max}$ is the maximum train electrical power demand [W];
- $P_{trac\_me\_max}$ is the maximum mechanical traction power [W];
- η is the efficiency of traction chain conversion.

According to the current limitation applied to the current at the current collector shown in Figure 3.12, the maximum current and the auxiliary current of the train are calculated by equation (3.24) and (3.25).

$$I_{max} = \frac{P_{train\_demand\_max}}{a \times V_n} \tag{3.24}$$

$$I_{aux} = \frac{P_{aux}}{V_{min2}} \tag{3.25}$$

If the train voltage is known, the maximum train traction current can be expressed by V_{train} using the equation below:

$$I_{train\_max} = \begin{cases} I_{aux} & if\ V_{train} \leq V_{min2} \\ \dfrac{V_{train} - V_{min2}}{r_{trac\_eq}} + I_{aux} & if\ V_{min2} < V_{train} \leq a \times V_n \\ \dfrac{P_{train\_demand\_max}}{V_{train}} & if\ V_{train} > a \times V_n \end{cases} \tag{3.26}$$

Where the equivalent train under-voltage traction equivalent resistance can be calculated using equation (3.27).

$$r_{trac\_eq} = \frac{a \times V_n - V_{min2}}{I_{max} - I_{aux}} \tag{3.27}$$

At different train voltage levels, the maximum electrical power which the train can collect from the power network is calculated by train current and voltage, as in equation (3.28). The maximum train received power in different zones can be calculated by equation (3.29). The maximum received power curve is shown in Figure 3.13. When the train is operated in no traction zone 1, it is assumed that the auxiliary power can be supplied. When the train is operated in under-voltage traction mode, the train cannot be supplied with enough power when it requires higher power than the limits. In zone 3, the train can be provided with enough power even when it requires the maximum traction power.

$$P_{train\_max} = I_{train\_max} \times V_{train} \tag{3.28}$$

$$P_{train\_max} = \begin{cases} P_{aux} & if\ V_{train} \le V_{min2} \\ \dfrac{(V_{train} - V_{min2}) \times V_{train}}{r_{trac\_eq}} + P_{aux} & if\ V_{min2} < V_{train} \le a \times V_n \\ P_{train\_demand\_max} & if\ V_{train} > a \times V_n \end{cases} \tag{3.29}$$

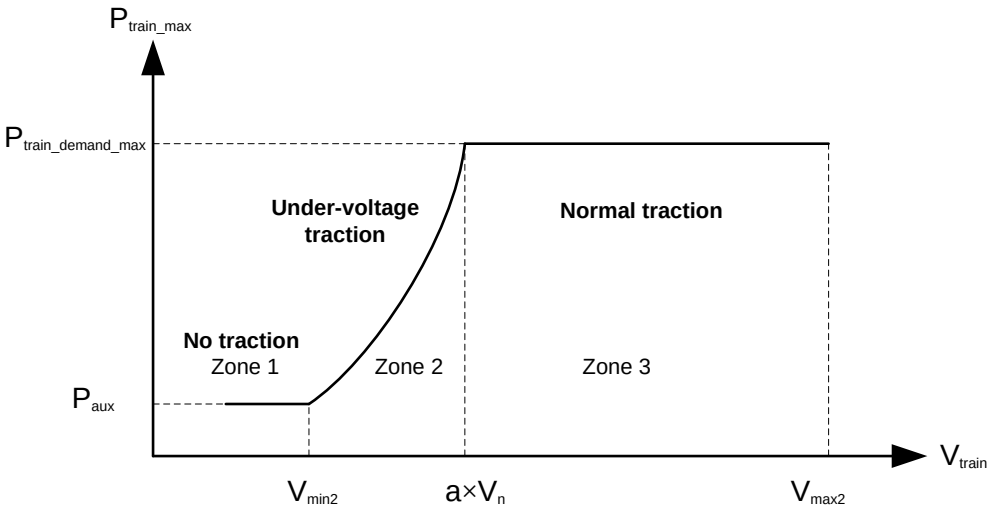

Figure 3.13 Received power limitation of traction train

3.3.2.2 Traction Train Equivalent Circuit

In normal traction mode, the equivalent circuit of the train is shown in Figure 3.14. The train is modelled as a dynamic power load. The received train power is equal to the train power demand. The relation between the train power demand and train power received, as well as the train current and voltage can be expressed in equation (3.30).

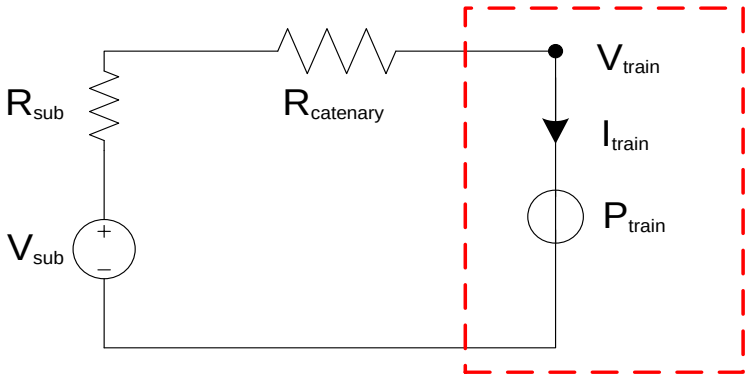

Figure 3.14 Equivalent circuit of traction train in normal operation

$$P_{train\_demand} = P_{train} = I_{train} \times V_{train} \tag{3.30}$$

In under-voltage traction mode, the train can be modelled as Figure 3.15. The train received power is lower than the train power demand, as illustrated in equation (3.31). The train current can be expressed using the train voltage in equation (3.32). It is the sum of the constant train auxiliary current and dynamic traction current which depends on the train voltage.

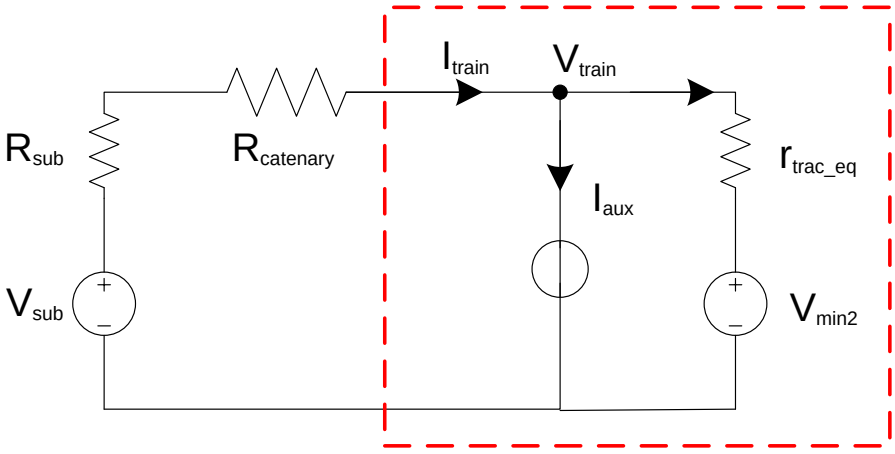

Figure 3.15 Equivalent circuit of traction train in under-voltage

$$P_{train\_demand} > P_{train} = I_{train} \times V_{train} \tag{3.31}$$

$$I_{train} = I_{aux} + \frac{V_{train} - V_{min2}}{r_{trac\_eq}} \tag{3.32}$$

In the non-traction mode, the train current can be assumed as a constant current source. In this abnormal situation, the train receives no traction power. The train can only be operated in this condition for a short period [121].

3.3.2.3 Braking Train

When the train is in regenerative braking, the motor will transform the mechanical power of the drive shaft into electrical power. The regenerated power can be used by the on-board auxiliary system and the surplus regenerated power can be transferred back to the network system feeding other motoring trains. In normal regenerative braking mode, all of the regenerative braking power can be transferred back to the network. However, the regenerative braking can increase train voltage, and a high regen voltage will occur when there are not enough motoring trains absorbing the regenerative energy in the power network. In the case of a high voltage hazard, some of the braking energy cannot be transferred to contact lines. Instead, the energy is wasted in the on-board braking rheostat as heat, when the regen voltage is in excess of a safe value. In the overvoltage regenerating mode, the train current will be limited automatically by the electronic devices. The maximum allowable train current against the train voltage is given in Figure 3.16 [128]. The braking train can be operated in normal regeneration mode when the train voltage is lower than V_{max1}, which is specified in Table 3.1. Normally, the braking train voltage is higher than V_n. When the train voltage exceeds V_{max1}, the train will be operated in over-

voltage mode. The maximum train current is limited and becomes zero when the train voltage reaches V_{max2}.

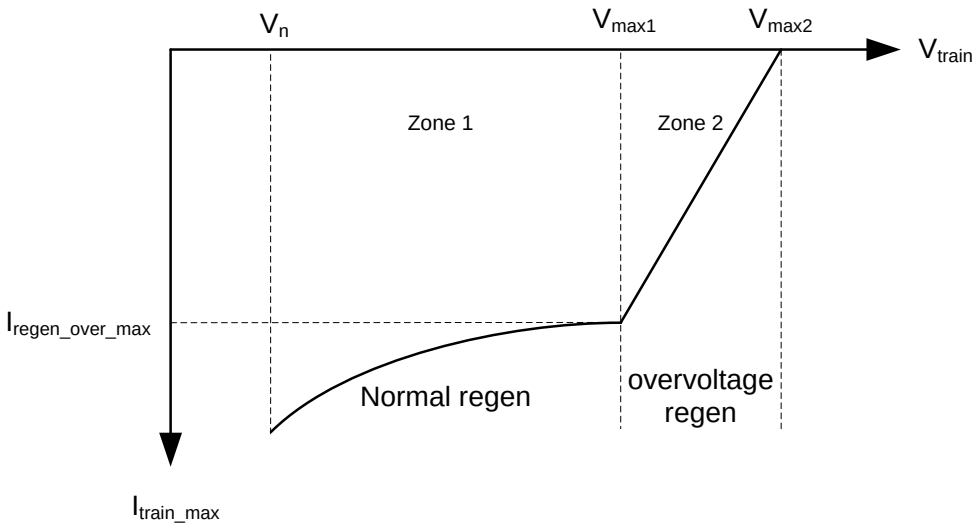

Figure 3.16 Current limitation of braking train

Regarding the braking train, the maximum train power that can be transferred into the power network is the maximum electric braking power plus auxiliary power, as in equation (3.33).

$$P_{train\_demand\_max} = P_{brake\_me\_max} \times \eta + P_{aux} \tag{3.33}$$

Where:

- $P_{brake\_me\_max}$ is the maximum mechanical braking power [W].

According to Figure 3.16, in over-voltage regeneration mode, the train current at V_{max1} is given in equation (3.34).

$$I_{regen\_over\_max} = \frac{P_{train\_demand\_max}}{V_{max1}} \tag{3.34}$$

If the train voltage is known, the maximum braking train current can be expressed by V_{train} using the equation below:

$$I_{train\_max} = \begin{cases} \dfrac{P_{train\_demand\_max}}{V_{train}} & if\ V_{train} \le V_{max1} \\ \dfrac{V_{train} - V_{max2}}{r_{brake\_eq}} & if\ V_{max1} < V_{train} \le V_{max2} \end{cases} \tag{3.35}$$

The equivalent train over-voltage braking equivalent resistance can be calculated by equation (3.36).

$$r_{brake\_eq} = \frac{V_{max1} - V_{max2}}{I_{regen\_over\_max}} \tag{3.36}$$

At different train voltage levels, the maximum electrical power which the train can transfer into the power network is given in equation (3.37). The maximum train exported power in different working zones can be calculated by equation (3.38). The maximum exported power curve is described in Figure 3.17. When the train is operated in normal regeneration zone 1, all of the electrical braking power can be exported. When the train is operated in overvoltage regeneration mode, the train can only export part of the total electrical braking power. When train voltage is equal to V_{max2}, no electrical braking power can be transferred into the power network.

$$P_{train\_max} = I_{train\_max} \times V_{train} \tag{3.37}$$

$$P_{train\_max} = \begin{cases} P_{train\_demand\_max} & if\ V_{train} \leq V_{max1} \\ \dfrac{(V_{train} - V_{max2}) \times V_{train}}{r_{brake\_eq}} & if\ V_{max1} < V_{train} \leq V_{max2} \end{cases} \quad (3.38)$$

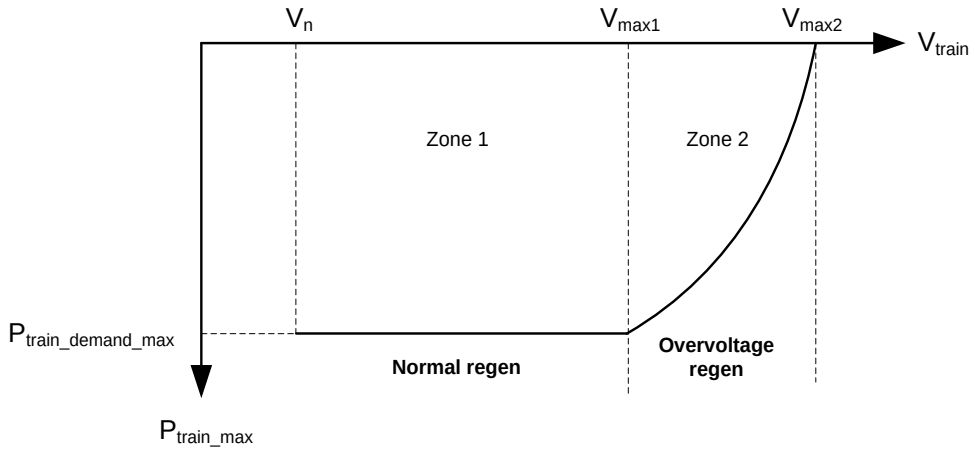

Figure 3.17 Exported power limitation of braking train

3.3.2.4 Braking Train Equivalent Circuit

In normal regeneration mode, the equivalent circuit of the train is shown in Figure 3.18. The train is modelled as a dynamic power load. The train exported power is equal to the train power demand. The relation between the train power demand, train power received and the train current and voltage can be expressed in equation (3.39).

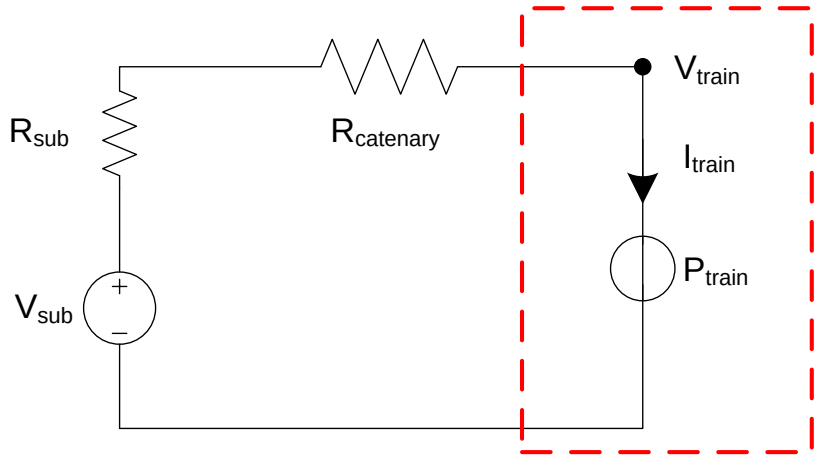

Figure 3.18 Equivalent circuit of braking train in normal operation

$$P_{train\_demand} = P_{train} = I_{train} \times V_{train} \tag{3.39}$$

In overvoltage regeneration mode, the train is modelled as in Figure 3.19. The train exported power is lower than the train power demand as in equation (3.40). The train current can be expressed using the train voltage as shown in equation (3.41).

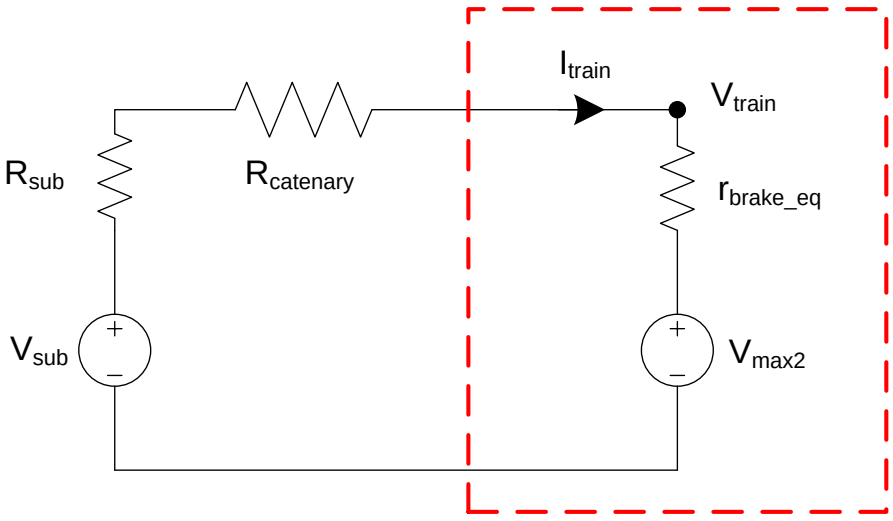

Figure 3.19 Equivalent circuit of braking train in over-voltage

$$\left|P_{train\_demand}\right| > \left|P_{train}\right| = \left|I_{train} \times V_{train}\right| \tag{3.40}$$

$$I_{train} = \frac{V_{train} - V_{max2}}{r_{brake\_eq}} \tag{3.41}$$

3.3.3 Admittance Matrix Construction

An example of the railway system equivalent circuit is described in Figure 3.20, which consists of the equivalent models of substations and trains as explained in previous sections. The paralleling post connects the contact lines on both tracks for reducing transmission losses as well as improving line voltages. It is modelled by a zero-resistance conductor connecting two contact lines. The substation connects with the busbar to feed both tracks. In practice, the rails bond together every 250 or 500 meters. Two tracks can be modelled by one combined return rail for admittance simplification with a reasonably low error [130]. The conductor resistors are used to represent the overhead line and return running rail resistance, which are split by trains, substations and parallel posts. The resistance of the contact line and lumped rail depends on the length and resistivity of the conductor as in equation (3.42), where ρ_c and ρ_r refer to the resistivity of contact line and return rail per track. The resistivity of overhead conductor systems is in the range of 30 to 90 mΩ/km, whereas it is between 8 and 20 mΩ/km for the third rail [14, 124]. The resistivity of the return rail is around 20 mΩ/km/track [121].

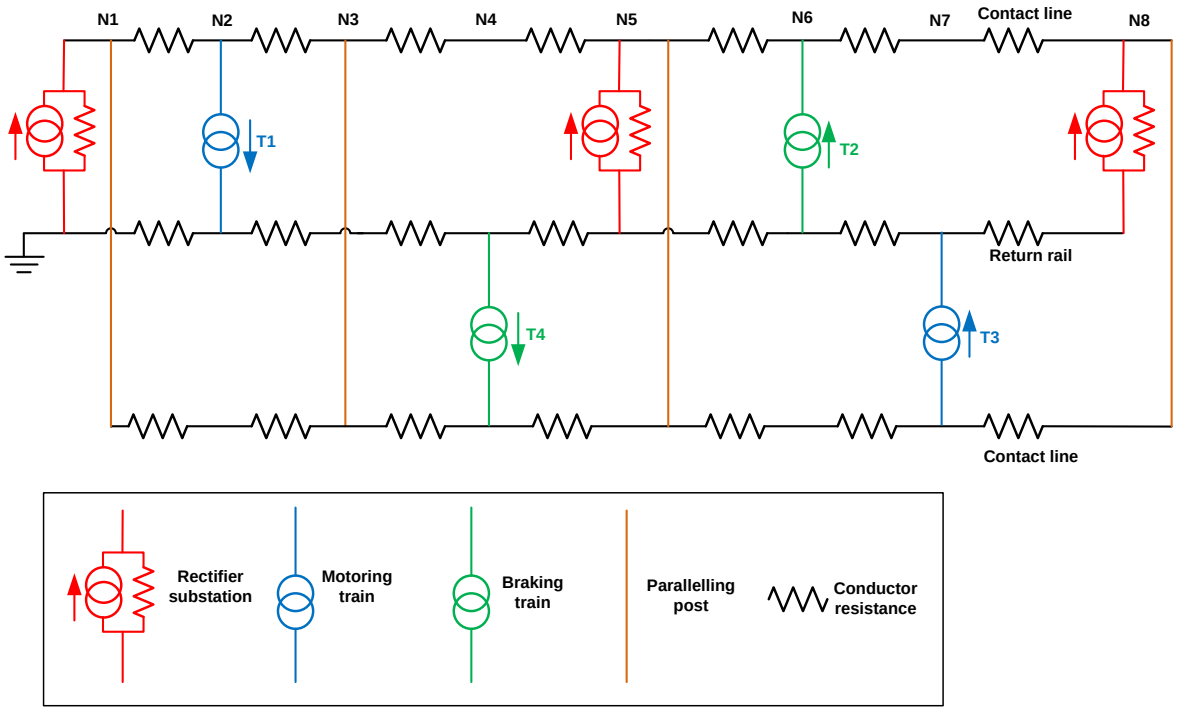

Figure 3.20 An example of railway system equivalent circuit

$$\begin{cases} R_c = L \times \rho_c \\ R_r = L \times \dfrac{\rho_r}{2} \end{cases} \tag{3.42}$$

The admittance matrix of a railway power network circuit is complex. With the chain circuit topology of railway equivalent circuit, the admittance matrix can be constructed conveniently [131]. Figure 3.21 describes a chain circuit topology of railway equivalent circuit with 3 paralleling layers. The circuit is classified by N-1 serial conductors and N shunt sections. The serial conductors represent the split resistances of contact lines and lumped rails. The shunt sections include the parallel posts, substations and trains, which can separate the conductor lines.

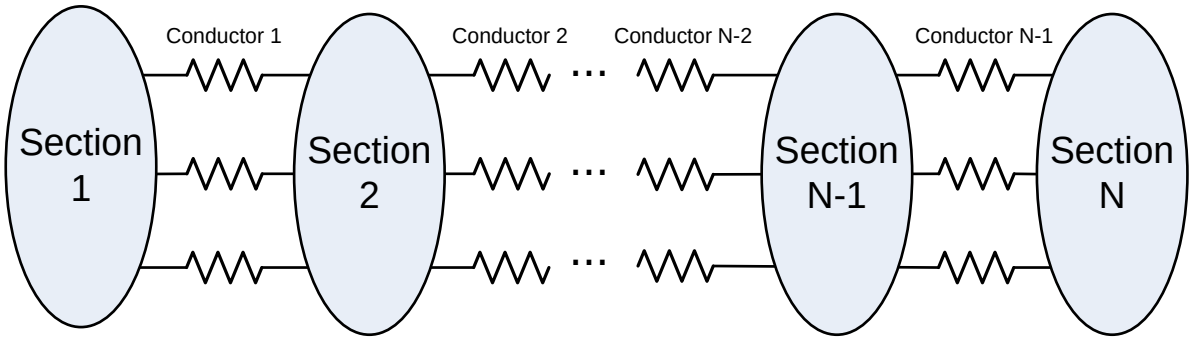

Figure 3.21 Chain circuit topology of railway equivalent circuit

The nodal analysis equation can be applied to solve the power flow of the railway network in equation (3.43). The admittance matrix of the whole network (Y) is a 3N×3N matrix, while both the current and voltage vector is a 1×3N matrix. Matrix Y is composed of the admittance matrix of each serial conductor element (Y_c) and shunt element (Y_s), which are 3×3 matrices. The admittance matrix of the whole network is expressed in equation (3.44), which is a sparse matrix.

$$I = Y \times V \tag{3.43}$$

$$Y = \begin{bmatrix} Y_{s1}+Y_{c1} & -Y_{c1} & 0 & & \\ -Y_{c1} & Y_{c1}+Y_{s2}+Y_{c2} & -Y_{c2} & \cdots & 0 \\ 0 & -Y_{c2} & Y_{c2}+Y_{s3}+Y_{c3} & & \\ & \vdots & & \ddots & \vdots \\ & 0 & & \cdots & Y_{cN-2}+Y_{sN-1}+Y_{cN-1} \quad -Y_{cN-1} \\ & & & & -Y_{cN-1} \quad Y_{cN-1}+Y_{sN} \end{bmatrix} \tag{3.44}$$

The current and voltage vectors in equation (3.43) are both 1×3N matrices, which are composed of nodal voltage vector (V_s) and current vectors (I_s) of each shunt section, as in equation (3.45) and (3.46). Both V_s and I_s are 1×3 matrices. According to the features of

the railway power network, the serial and shunt elements can be concluded by the following forms.

$$V = \begin{bmatrix} V_{s1} \\ V_{s2} \\ V_{s3} \\ \vdots \\ V_{sN-1} \\ V_{sN} \end{bmatrix} \tag{3.45}$$

$$I = \begin{bmatrix} I_{s1} \\ I_{s2} \\ I_{s3} \\ \vdots \\ I_{sN-1} \\ I_{sN} \end{bmatrix} \tag{3.46}$$

3.3.3.1 Serial Conductor Elements

The serial conductors consist of the contact lines and the lumped rails. The resistance can be calculated by equation (3.42). One section of serial conductors is shown in Figure 3.22. The admittance matrix of this part can be expressed in equation (3.47).

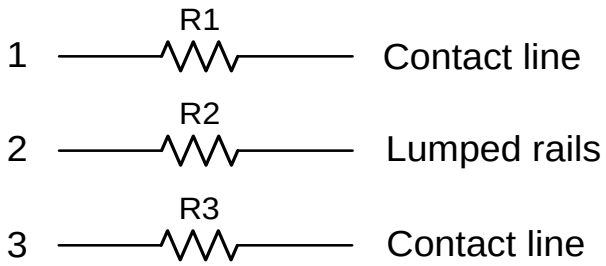

Figure 3.22 Serial conductor element

$$Y_c = \begin{bmatrix} \frac{1}{R_1} & 0 & 0 \\ 0 & \frac{1}{R_2} & 0 \\ 0 & 0 & \frac{1}{R_3} \end{bmatrix} \tag{3.47}$$

3.3.3.2 Shunt Resistance

The shunt resistance is a basic model for the shunt section, which connects paralleling conductor lines. An example is shown in Figure 3.23. The admittance for this element is expressed in equation (3.48). The self-admittances (Y_{s11} and Y_{s22}) and the mutual admittances (Y_{s12} and Y_{s21}) are equal to $\frac{1}{R}$.

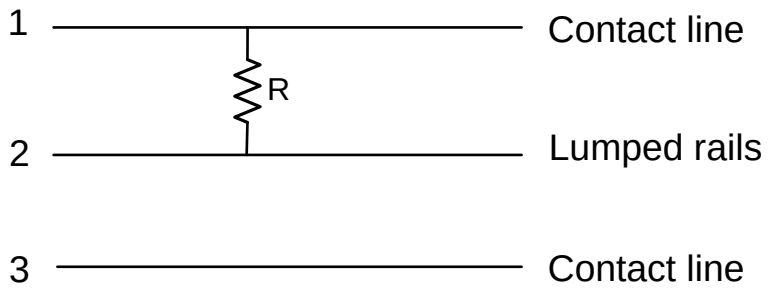

Figure 3.23 Shunt resistance

$$Y_s = \begin{bmatrix} \frac{1}{R} & -\frac{1}{R} & 0 \\ -\frac{1}{R} & \frac{1}{R} & 0 \\ 0 & 0 & 0 \end{bmatrix} \tag{3.48}$$

The parallel post which connects two contact lines is shown in Figure 3.24. According to the admittance matrix structure of a shunt resistance, the parallel post can be assumed as a

very small resistor connecting both contact lines. Therefore, the admittance matrix of the parallel post can be expressed in equation (3.49), where the small resistance (R_{small}) is set to $10^{-6}\,\Omega$ in this thesis [116].

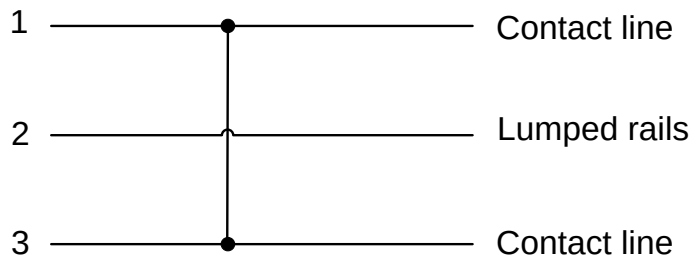

Figure 3.24 Parallel post

$$Y_s = \begin{bmatrix} \frac{1}{R_{small}} & 0 & -\frac{1}{R_{small}} \\ 0 & 0 & 0 \\ -\frac{1}{R_{small}} & 0 & \frac{1}{R_{small}} \end{bmatrix} \tag{3.49}$$

Similarly, for a grounding connection in Figure 3.25, the admittance matrix can be written as in equation (3.50). The self-admittance Y_{s22} is equal to $\frac{1}{R_{small}}$, while all the mutual admittances are equal to zero.

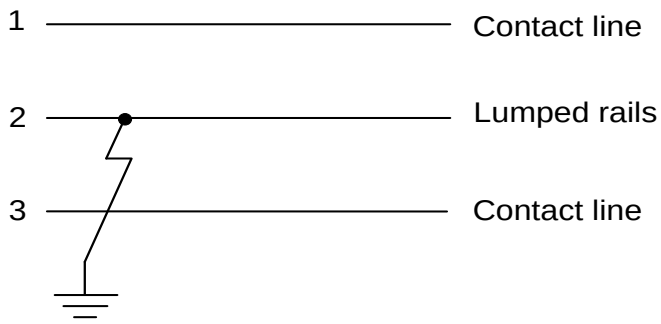

Figure 3.25 Grounding connection

$$Y_s = \begin{bmatrix} 0 & 0 & 0 \\ 0 & \frac{1}{R_{small}} & 0 \\ 0 & 0 & 0 \end{bmatrix} \tag{3.50}$$

3.3.3.3 Substations

The substation is composed of a current source, a resistance and parallel post. The ideal current source does not affect the admittance matrix. The admittance matrix of a substation can be calculated by equation (3.51), which is the sum of the admittance matrix of a shunt resistance and parallel post. The current vector of the substation can be calculated according to the substation current, as in equation (3.52). I_{s_sub11}, I_{s_sub12} and I_{s_sub13} are the currents flowing through line 1, line 2 and line 3, respectively.

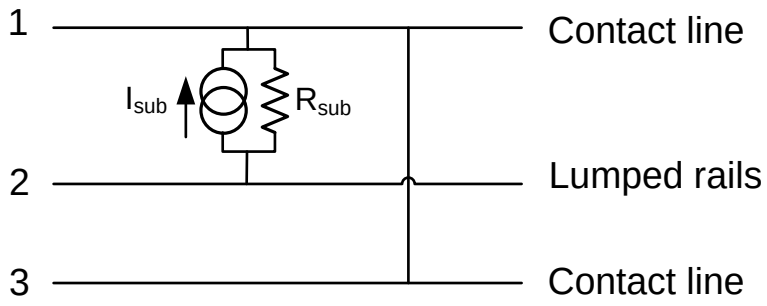

Figure 3.26 Substation element

$$Y_{sub} = \begin{bmatrix} \frac{1}{R_{sub}} & -\frac{1}{R_{sub}} & 0 \\ -\frac{1}{R_{sub}} & \frac{1}{R_{sub}} & 0 \\ 0 & 0 & 0 \end{bmatrix} + \begin{bmatrix} \frac{1}{R_{small}} & 0 & -\frac{1}{R_{small}} \\ 0 & 0 & 0 \\ -\frac{1}{R_{small}} & 0 & -\frac{1}{R_{small}} \end{bmatrix} \tag{3.51}$$

$$I_{s\_sub} = \begin{bmatrix} I_{sub} \\ -I_{sub} \\ 0 \end{bmatrix} \tag{3.52}$$

3.3.3.4 Trains

There are several equivalent circuits for different working modes of trains. The models of traction and braking trains at the up-direction track in normal operation are presented in Figure 3.27 and Figure 3.28.

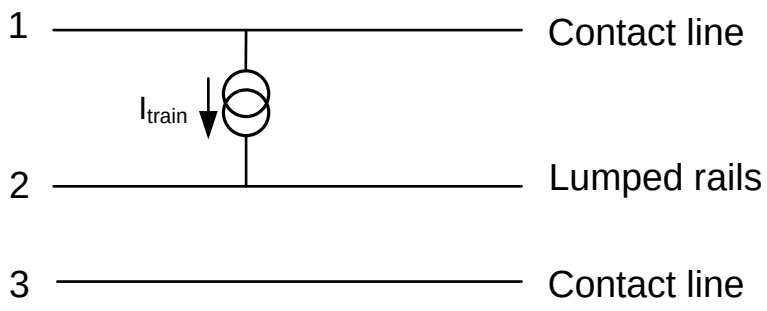

Figure 3.27 Traction train in up direction

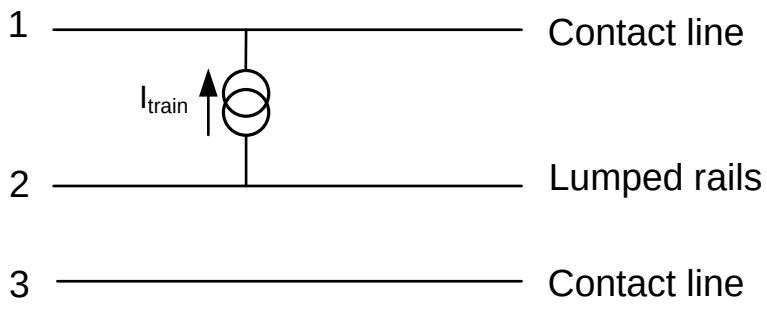

Figure 3.28 Braking train in up direction

Since the model of the trains in normal operation does not consist of a resistance, the admittance matrix is a null matrix in equation (3.53). The current vector depends on the

direction of train current. For the traction train in up-direction in Figure 3.27, the train collects the current from the up-tract contact line and the current returns back to lumped rails. Therefore, the current vector can be expressed in equation (3.54). As for the braking train in Figure 3.28, the braking train regenerates power and feeds the contact lines. Therefore, the current vector can be expressed in equation (3.55).

$$Y_{train} = \begin{bmatrix} 0 & 0 & 0 \\ 0 & 0 & 0 \\ 0 & 0 & 0 \end{bmatrix} \tag{3.53}$$

$$I_{t\_trac\_up} = \begin{bmatrix} -I_{train} \\ I_{train} \\ 0 \end{bmatrix} \tag{3.54}$$

$$I_{t\_brake\_up} = \begin{bmatrix} I_{train} \\ -I_{train} \\ 0 \end{bmatrix} \tag{3.55}$$

The model of a traction train in under-voltage operation is shown in Figure 3.29, which can be transformed from the equivalent circuit of traction train in under-voltage in Figure 3.15. Two current sources and a resistance are connected in parallel between the contact line and lumped rails. The admittance matrix and current vector can be expressed in equation (3.56) and (3.57).

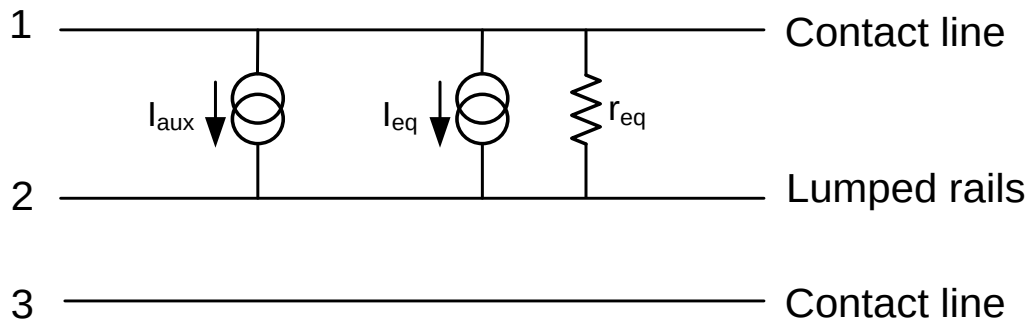

Figure 3.29 Traction train in under-voltage operation

$$R_{train} = \begin{bmatrix} \frac{1}{r_{eq}} & -\frac{1}{r_{eq}} & 0 \\ -\frac{1}{r_{eq}} & \frac{1}{r_{eq}} & 0 \\ 0 & 0 & 0 \end{bmatrix} \tag{3.56}$$

$$I_{train} = \begin{bmatrix} -I_{aux} \\ I_{aux} \\ 0 \end{bmatrix} + \begin{bmatrix} -I_{eq} \\ I_{eq} \\ 0 \end{bmatrix} \tag{3.57}$$

The model of a traction train in under-voltage operation is shown in Figure 3.30, which can be transformed from the equivalent circuit of braking train in over-voltage in Figure 3.19. A current source and a resistance are connected in parallel between the contact line and lumped rails. The admittance matrix and current vector can be expressed in equation (3.58) and (3.59).

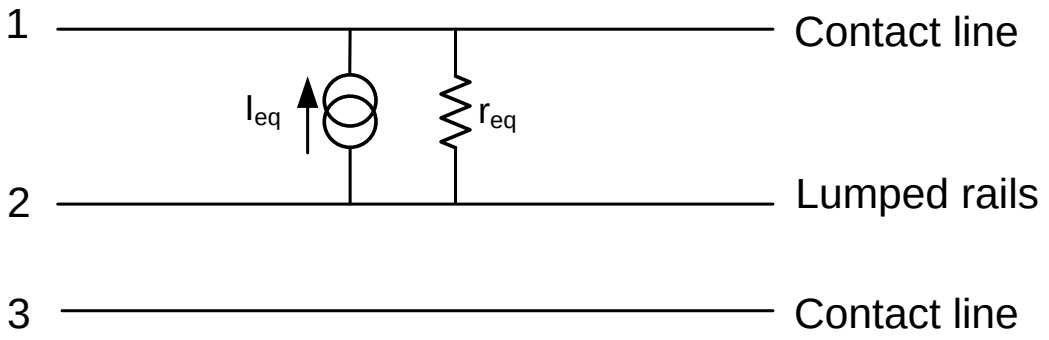

Figure 3.30 Braking train in over-voltage operation

$$R_{train} = \begin{bmatrix} \frac{1}{r_{eq}} & -\frac{1}{r_{eq}} & 0 \\ -\frac{1}{r_{eq}} & \frac{1}{r_{eq}} & 0 \\ 0 & 0 & 0 \end{bmatrix} \tag{3.58}$$

$$I_{train} = \begin{bmatrix} I_{eq} \\ -I_{eq} \\ 0 \end{bmatrix} \tag{3.59}$$

3.4 Load Flow Solver

The railway system equivalent circuit is made up of the voltage sources and resistance, which are linear components, a power source (train) which is a nonlinear component, as well as the diode which is a piecewise component. To solve the load flow problem for the railway power network, an iterative method with piecewise analysis is required. There are various iterative approaches used for solving the load flow for railway systems, as introduced in Section 3.1. Most of these iterative methods start from a certain initial guess, and the stopping criteria are based on the train power mismatches. However, it is difficult

to prove the accuracy mathematically. The load flow solver in this thesis integrates the current-vector iterative method with the train/substation working mode detection algorithm to obtain an accurate solution for a DC-fed railway network.

3.4.1 Current-vector Iterative Method

When all the substations are switched on and the trains are operated in a normal working mode, the whole railway power network is a linear circuit, which consists of voltage sources (substations), current sources (trains) and resistors (transmission network). If one train is assumed as a load, the rest of the circuit becomes a linear two-terminal circuit. According to Thevenin's theorem, the linear two-terminal circuit can be replaced by an equivalent circuit comprised of an equivalent voltage source in series with an equivalent resistor [132], as shown in Figure 3.31. The equivalent voltage is the open-circuit voltage at terminals. The equivalent resistance is the input resistance at terminals when the independent sources are turned off.

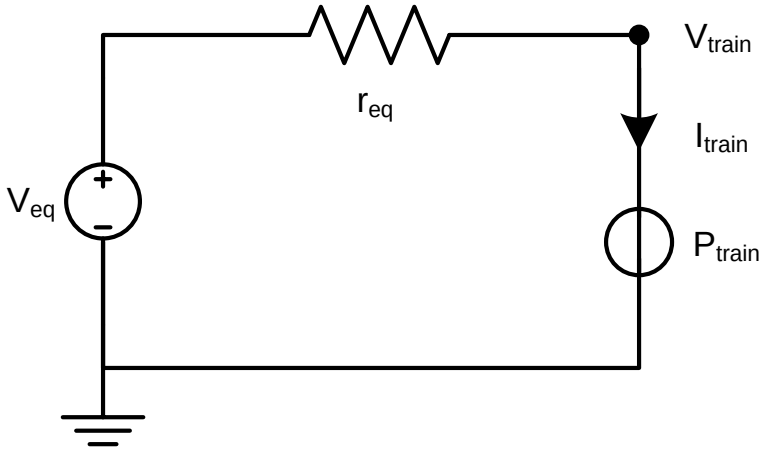

Figure 3.31 Thevenin's equivalent circuit of a railway network

The train power demand is a known value. The train voltage can be obtained by solving equation (3.60). For a system with only one train, the voltage sources (substations) are connected in parallel with the same voltage. It is obvious that the equivalent voltage is equal to the no-load voltage of the substation. For a multi-train system, the equivalent voltage for one train depends on the state of the other trains. If most of the other trains are regenerating braking power, the equivalent voltage for this train could be higher than the substation voltage. When most of the other trains are requiring traction power, the equivalent voltage for this train could be lower than the substation voltage.

$$P_{train\_demand} = \frac{(V_{eq} - V_{train})}{r_{eq}} \times V_{train} \tag{3.60}$$

If the equivalent voltage and resistance are confirmed, a quadratic formula shown as in equation (3.60) can be obtained. There are two theoretical solutions for a quadratic formula. The load power flow analysis aims to find the solution with higher train voltage, which is the actual train voltage in the railway network. The current-vector iterative method is presented below:

- Step 1: Initialise all the train voltage by the no-load voltage of the substation as in equation (3.61).

$$V_{train\_n}{}^{(0)} = V_{sub} \tag{3.61}$$

- Step 2: Calculate the train current at the next iteration by equation (3.62).

$$I_{train\_n}^{(1)} = \frac{P_{train\_demand\_n}}{V_{train\_n}{}^{(0)}} \tag{3.62}$$

- Step 3: Update nodal voltages by nodal analysis by equation (3.63), where the power network admittance construction is illustrated in Section 3.3.3. The train voltage at this iteration can be updated at this step. The nodal analysis equation (3.63) is equivalent to equation (3.64) which is obtained from the Thevenin's equivalent circuit in Figure 3.31.

$$\left[V^{(1)}\right] = [Y]^{-1} \times \left[I^{(1)}\right] \tag{3.63}$$

$$V_{train\_n}^{(1)} = V_{eq\_n} - r_{eq\_n} \times {I_{train\_n}}^{(1)} \tag{3.64}$$

- Step 4: Calculate train power at this iteration by equation (3.65).

$${P_{train\_n}}^{(1)} = {V_{train\_n}}^{(1)} \times {I_{train\_n}}^{(1)} \tag{3.65}$$

- Step 5: Check whether the difference of calculated train power and train power demand is within the criteria. If so, the current-vector iterative method ends. If not, repeat step 2 using the updated train voltage.

Figure 3.32 and Figure 3.33 describe the geometrical interpretation of the current-vector iterative approach for a traction train. The parabola represents the P-V relation of equation (3.60). The straight green line represents the P-V relation of equation (3.62). The straight green line moves with the iteration. The intersection of the parabola and the straight line denotes the train power result of the iteration. The initial train voltage is the substation voltage. For common cases, the initial voltage is higher than the final result. Thus, the straight line moves anticlockwise until converging to the solution, as shown in Figure 3.32. For some abnormal cases, the initial voltage could be lower than the final solution. The straight line moves clockwise until it converges to the solution. It is evident that the

solution can be found by a current-vector iterative approach regardless of the level of initial voltage.

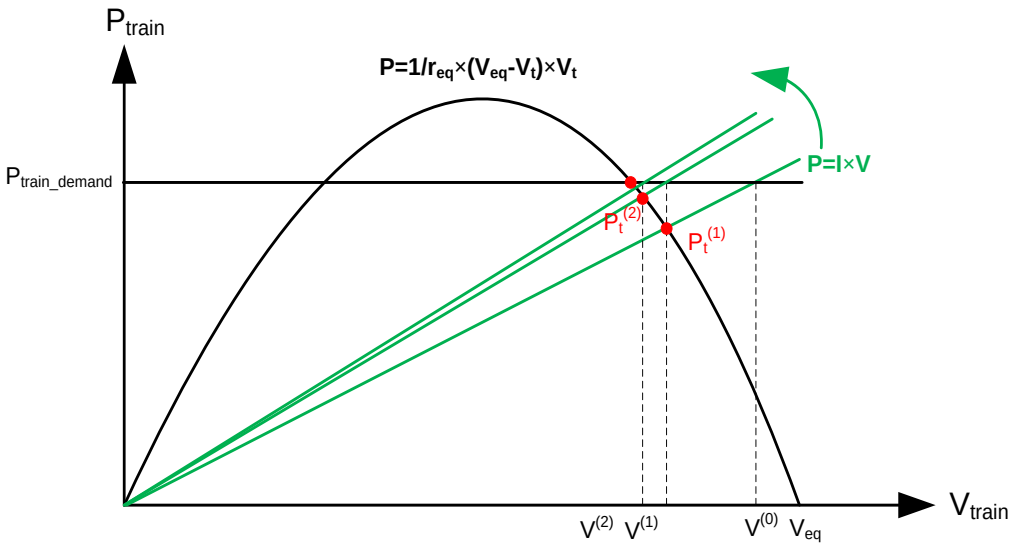

Figure 3.32 Geometrical interpretation for a traction train

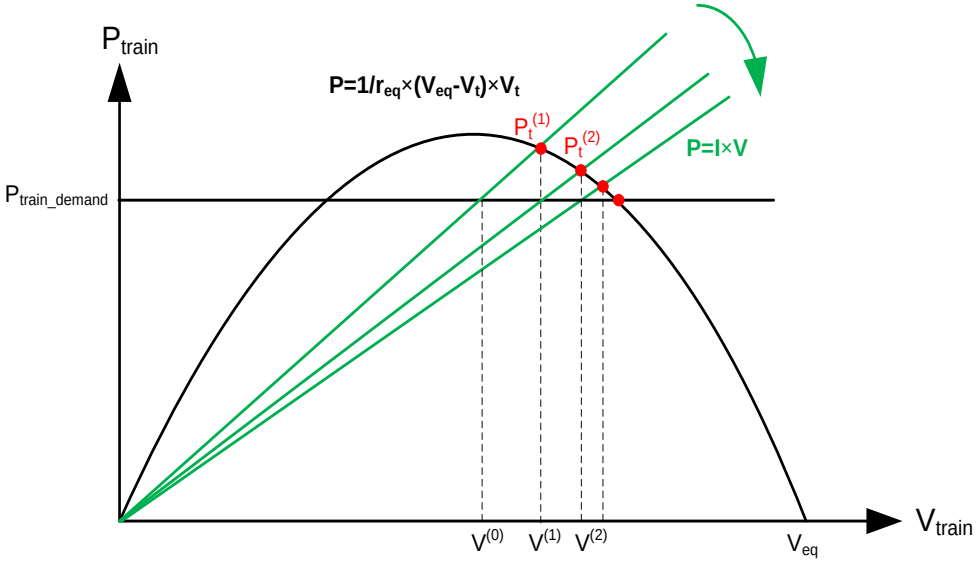

Figure 3.33 Geometrical interpretation for a traction train

Figure 3.34 demonstrates the geometrical interpretation of the current-vector iterative approach for a regenerative braking train. The train power demand is negative for the braking train. The movement of the straight green line is always close to the solution on both sides in sequence. Whatever the initial train voltage is, the load flow solution can be found.

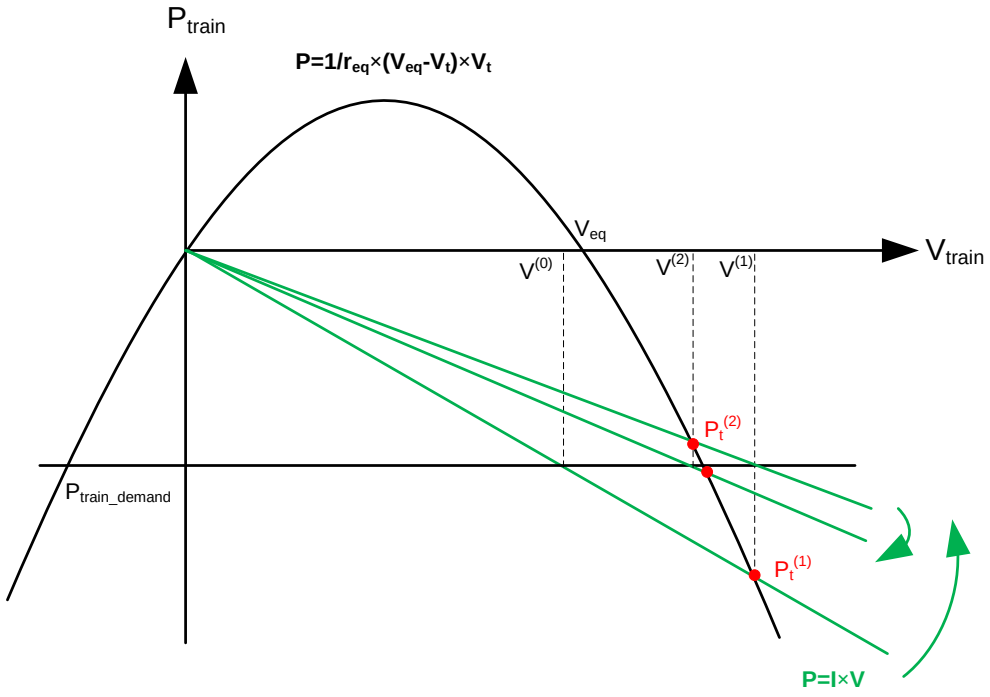

Figure 3.34 Geometrical interpretation for a regenerative braking train

3.4.2 Working Mode Selection Algorithm

The nodal voltages can be found when the current-vector iterative method converges. Sometimes, the voltage of the train or substation mismatches the model used in the admittance matrix. Therefore, a working mode selection algorithm is required to check if

the working mode matches the nodal voltage. If the current-vector iterative method converges, the following checks should be conducted:

- Step 1: Over-voltage regeneration train check: if the voltage of the normal regenerating train is higher than the highest permanent voltage V_{max1}, and the current exceeds the current limitation, change the normal regeneration train model into the over-voltage model and then rebuild the admittance matrix. If not, go to step 2;
- Step 2: Over-power regeneration train check: if the power of the over-voltage regeneration train exceeds the power limitation, change the over-voltage model into the normal regeneration model and then rebuild the admittance matrix. If not, go to step 3;
- Step 3: Under-voltage traction train check: if the voltage of the normal traction train is lower than the under-voltage limitation $a \times V_n$, and the current exceeds the current limitation, change the normal traction train model into the under-voltage model and then rebuild the admittance matrix. If not, go to step 4;
- Step 4: Over-power traction train check: if the power of the under-voltage traction train exceeds the power limitation, change the under-voltage model into the normal traction model and then rebuild the admittance matrix. If not, go to step 5;
- Step 5: Substation voltage check: if the voltage of the substation mismatches its working mode, change the substation model to match the voltage level and then rebuild the admittance matrix. If not, the load flow analysis is correct and the power network simulation ends.

The current-vector iterative method converges in most cases. However, if the working modes of substations and train change, the current-vector iterative method may not converge to find the solutions. The geometrical interpretation of the situation when the current-vector iterative method cannot converge is shown in Figure 3.35. This is because the train power demand is too high, which exceeds the capacity of the power network. The working mode selection algorithm is capable of detecting this situation. If the current-vector iterative method does not converge, in order to increase the capacity of the power network, all substations should be switched on. The substations are switched off due to the high regenerative power. All braking trains should be set to the over-voltage model to prevent substations from switching off.

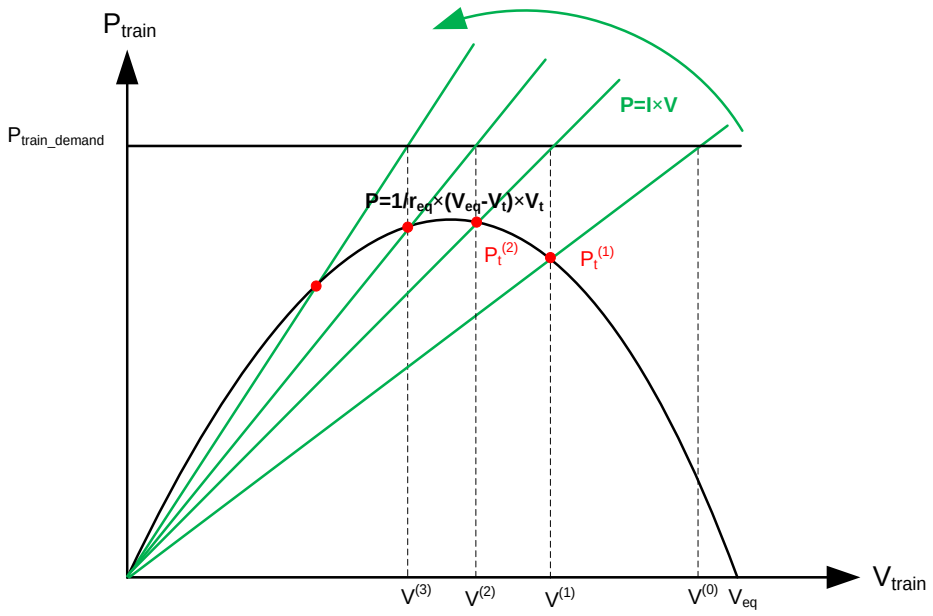

Figure 3.35 Geometrical interpretation of divergence

A flow chart of the structure of the power network simulation is presented in Figure 3.36. The power network simulator collects the network parameters and data from the motion

simulation and then solves the power network by admittance matrix formulation, load flow solving and working mode selection.

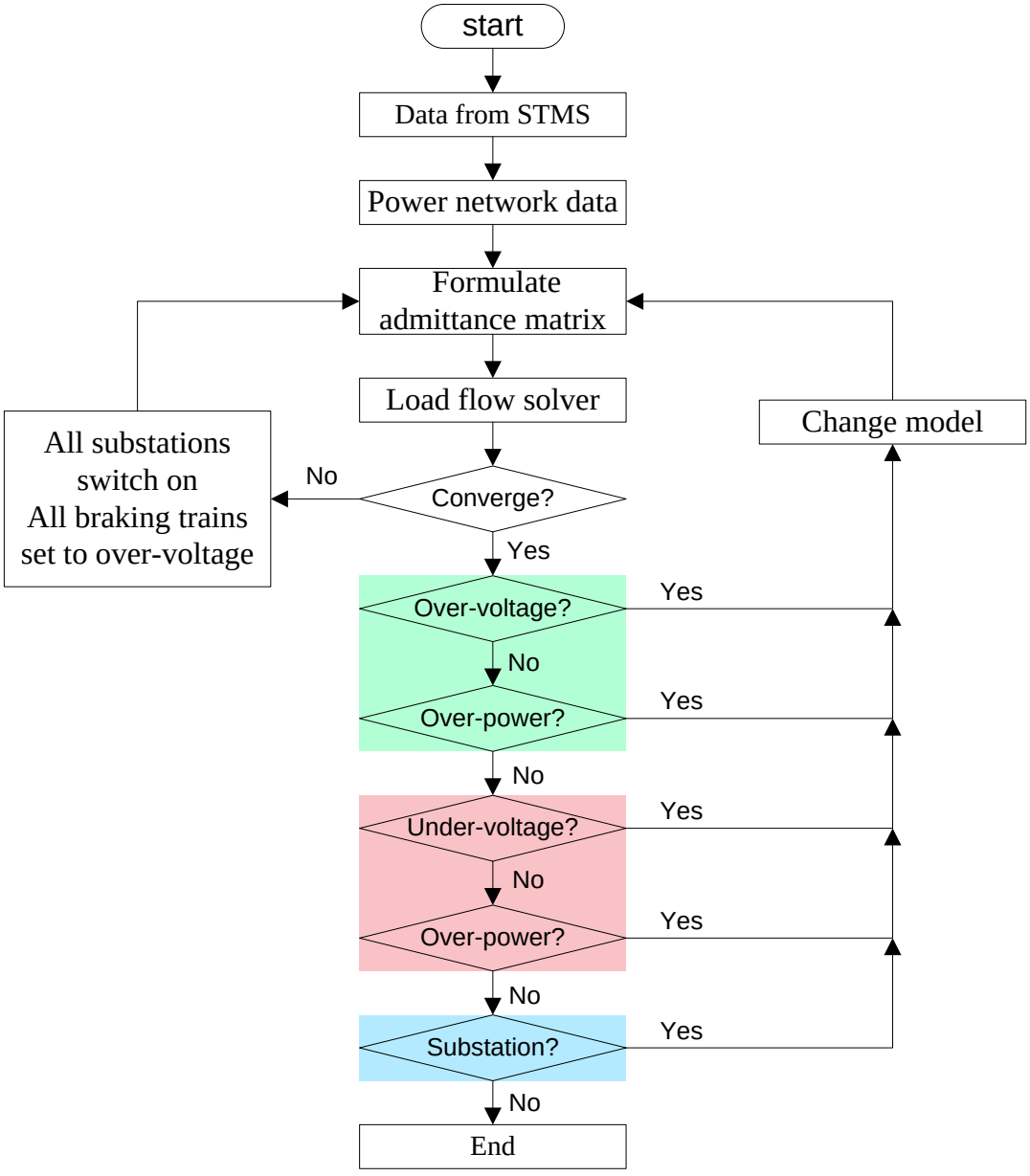

Figure 3.36 Structure of the power network simulation

3.4.3 Load Flow Validation Test

The fixed data of the train and power network for the test is shown in Table 3.2. The power network data is collected from BS-EN50641 British Standard in Railway Applications-Fixed installations [121]. The dynamic data including train location and power demand can lead to different results. TINA, which is a circuit simulator, is employed to validate the load flow calculation [133]. Some typical scenarios with different dynamic inputs are tested and illustrated in this section.

Table 3.2 Fixed data for the validation test

Item	Quantity	Units
Route length	8000	m
Substation No. 1 position	0	m
Substation No. 2 position	5000	m
Substation No. 3 position	8000	m
Paralleling post position	2500	m
Traction system nominal voltage	1500	V
Substation no-load voltage	1800	V
Substation source resistance	0.01	Ω
Highest permanent voltage V_{max1}	1850	V
Highest non-permanent voltage V_{max2}	1950	V
Under-voltage limitation	1350	V
Contact line system resistance	29	mΩ/km/track
Return rail system resistance	20	mΩ/km/track
Train maximum electric power	8000	kWh

3.4.3.1 Test 1: Normal Traction and Regeneration

The train location and power demand are assumed as dynamic inputs in this validation test. Regarding the normal traction and regeneration test, the train data is presented in Table 3.3. There are four trains in the power network. Two trains are motoring, and the other two are braking.

Table 3.3 Train data inputs for test 1

	Location [m]	Power [kW]
Train_up1	1000	8000
Train_up2	7000	8000
Train_down1	3000	-3000
Train_down2	6000	-3000

The results from the power network simulator are presented in Table 3.4. It takes 7 times of iteration and no working mode is changed. The voltage, current and power of trains and substations are obtained. All the trains and substations are working in the normal mode. In order to validate the simulation results, the circuit is formulated in TINA, as shown in Figure 3.37. All the trains are modelled as voltage sources in TINA, using the values from the power network simulator. TINA is able to analyse the DC circuit and output the nodal voltage and current. The results from TINA are reported in Table 3.4. The current and power results from TINA are almost the same with the results from the simulator in Matlab. The average power difference is within 0.07%. This proves the accuracy of the power network simulation.

Table 3.4 Results for test 1

	Results from Matlab			Results from TINA		
Number of iterations	7			-		
Number of working mode changes	0			-		
	Voltage [V]	**Current [A]**	**Power [kW]**	**Voltage [V]**	**Current [A]**	**Power [kW]**
Train_up1	1654	4838	8002	1654	4840	8005
Train_up2	1661	4816	7999	1661	4820	8006
Train_down1	1794	-1672	-3000	1794	-1670	-2996
Train_down2	1813	-1655	-3001	1813	-1660	-3010
Substation No. 1	1770	3025	5354	1770	3020	5345
Substation No. 2	1791	859	1538	1790	859	1538
Substation No. 3	1776	2449	4349	1770	2440	4319

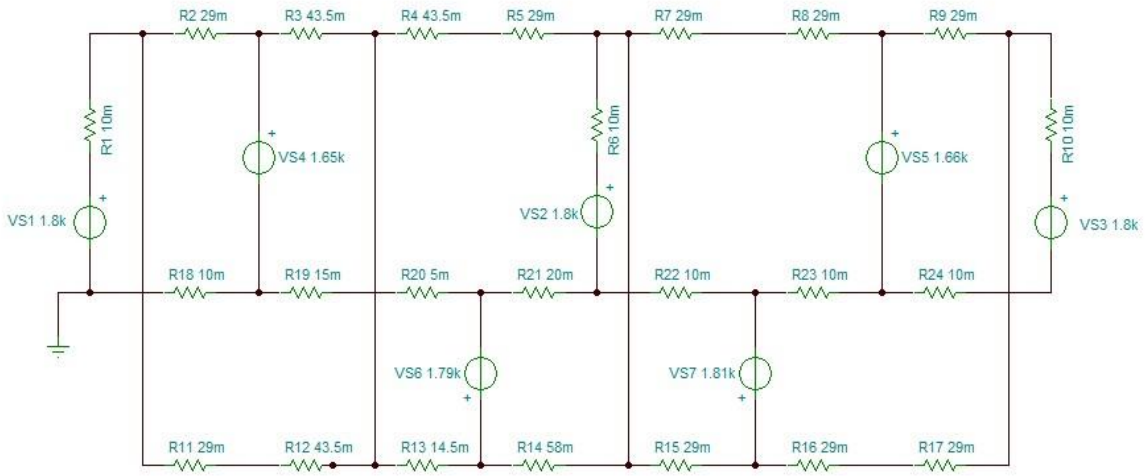

Figure 3.37 TINA model for test 1

3.4.3.2 Test 2: Overvoltage Regeneration

Table 3.5 presents the train data to validate the scenario of overvoltage regeneration. Two trains are motoring, requiring 8000 kW and 3000 kW, respectively. The other two trains are braking, regenerating 8000 kW and 8000 kW, respectively. The sum of regenerating power is higher than the sum of traction power.

Table 3.5 Train data inputs for test 2

	Location [m]	**Power [kW]**
Train_up1	1000	8000
Train_up2	7000	3000
Train_down1	3000	-8000
Train_down2	6000	-8000

After 7 times of iteration and 2 times of working mode change, the results from the power network simulation are obtained, as shown in Table 3.6. Two braking trains are overvoltage, with voltages that are higher than 1850 V. Part of the electric braking power

can be reused by the network, which is 5054 kW and 3425 kW, respectively. Two motoring trains are working in normal operation, and can obtain sufficient power. The first substation is switched on, supplying 5388 kW. The voltages of other substations are higher than the substation no-load voltage. As a result, these two substations are switched off, supplying no power. The simulation results are validated by TINA. The TINA circuit is demonstrated in Figure 3.38. Two traction trains are modelled as the voltage sources with the values from the power network simulator. Two overvoltage braking trains are modelled as voltage sources connecting with over-voltage braking equivalent resistances in series, according to the method illustrated in Section 3.3.2. As substations No. 2 and No. 3 are switched off, they are connected with a very large resistance in TINA. The DC analysis results are illustrated in Table 3.6. The current and power results are almost the same as the results from the simulator in Matlab, which can prove the accuracy with agreement of 0.06% difference.

Table 3.6 Results for test 2

	Results from Matlab			**Results from TINA**		
Number of iterations	7			-		
Number of working mode changes	2			-		
	Voltage [V]	**Current [A]**	**Power [kW]**	**Voltage [V]**	**Current [A]**	**Power [kW]**
Train_up1	1693	4725	7999	1693	4730	8008
Train_up2	1818	1650	3000	1818	1650	3000
Train_down1	1888	-2677	-5054	1888	-2680	-5060
Train_down2	1909	-1794	-3425	1909	-1790	-3417
Substation No. 1	1781	3025	5388	1781	3030	5396
Substation No. 2	1880	0	0	1880	0	0
Substation No. 3	1843	0	0	1843	0	0

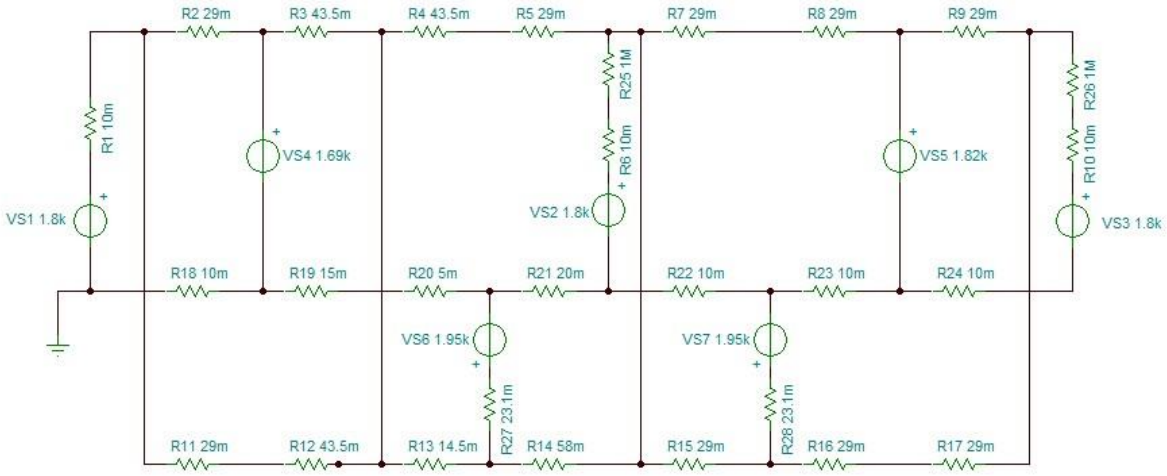

Figure 3.38 TINA model for test 2

3.4.3.3 Test 3: Mixture of Every Working Mode

In the most complex case, all the normal, under-voltage and overvoltage trains are operated at the same time. The train data for this test is demonstrated in Table 3.7. Three trains are motoring with the maximum traction power. These three trains are located close together, at 1000 m, 2000 m, and 3000 m, respectively. Another train is braking with 8000 kW and is far away from the other trains at 6000 m.

Table 3.7 Train data inputs for test 3

	Location [m]	**Power [kW]**
Train_up1	1000	8000
Train_up2	2000	8000
Train_down1	3000	8000
Train_down2	6000	-8000

The results from the power network simulation are illustrated in Table 3.8. It takes 10 iterations and 4 times of working mode changes for this scenario. Two of the traction trains are working in normal mode, which can obtain sufficient power of 8000 kW. The other

traction train located at 2000 m is operated at under-voltage (1320 V). This train only obtains 7154 kW. The braking train is operated at overvoltage, regenerating 6202 kW. The first two substations are switched on, while the last one is off. The TINA circuit for validation is shown in Figure 3.39. The TINA results in Table 3.8 are consistent with the results from the simulator for this scenario, within 0.03% of difference.

Table 3.8 Results for test 3

	Results from Matlab			**Results from TINA**		
Number of iterations	10			-		
Number of working mode changes	4			-		
	Voltage [V]	**Current [A]**	**Power [kW]**	**Voltage [V]**	**Current [A]**	**Power [kW]**
Train_up1	1400	5714	8000	1400	5710	7994
Train_up2	1320	5420	7154	1320	5420	7154
Train_down1	1370	5841	8002	1370	5840	8001
Train_down2	1873	-3311	-6202	1873	-3310	-6200
Substation No. 1	1703	9692	16505	1703	9690	16502
Substation No. 2	1760	3971	6989	1760	3970	6987
Substation No. 3	1841	0	0	1841	0	0

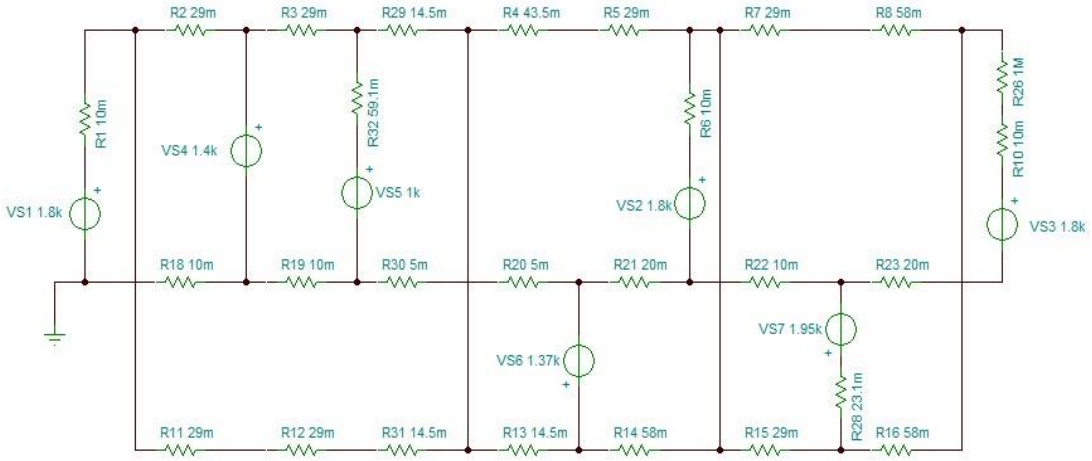

Figure 3.39 TINA model for test 3

3.5 Summary

This chapter describes the development of a railway system simulator, which integrates the modelling of train movement and the traction power network. The model is capable of dealing with under-voltage and overvoltage for accurate energy consumption evaluation.

A brief literature review of the railway modelling is first presented. In Section 3.2, the kinetic model of train movement is demonstrated. In Section 3.3, the electric models of the elements in the traction power network are illustrated. The method to construct the admittance matrix is explained, which is used to solve the power flow of the network. The algorithm to solve power flow for a nonlinear railway power network is presented in Section 3.4. A current-vector iterative method with a working mode selection algorithm is utilised in this simulator. Finally, power network simulation results are compared with the circuit analysis by TINA. Typical scenarios including normal operation, under-voltage traction, overvoltage regeneration and mixed working modes of substations are considered. The results show that the power difference by load flow analysis and TINA is with 0.1%.

The system integrated simulator demonstrated in this chapter is used as a tool to evaluate the energy performance for a railway system. Based on the results from the simulator, the energy flow through the whole system is evaluated and analysed in the next chapter. The feasibility of energy optimisation will be illustrated.

Chapter 4

System Energy Evaluation

4.1 Introduction

Regenerating trains are commonly used on many DC fed railway systems. The kinetic energy of the train can be partially converted back into electricity when braking, and can be reused in other accelerating trains. Train operating companies are therefore able to benefit from energy cost discounts when regeneration is active. The energy consumed by railway systems is mainly used by trains for traction [24]. Compared with an AC system with 25 kV, the lower voltage supply of a DC system will lead to higher transmission losses for the same rated power. As a consequence, energy loss analysis has to be considered in the energy study of DC electrified railways [134]. The usage of regenerated braking energy depends on the receptivity of the power network. However, the efficiency of regenerative braking energy has not been fully understood.

In this chapter, a method to evaluate the energy flow for the whole railway system is introduced. With the multi-train energy evaluation, the energy flow is analysed including the energy supplied by the substations, the energy wasted in the power transmission network, the energy used by the train in traction and regenerated by braking trains. The Beijing Yizhuang Subway Line is used as a case study to understand the feature of energy

flows. The energy consumption for the system with and without regeneration in operation is compared. The potential of energy optimisation is identified based on the energy loss analysis.

This chapter is an expanded version of the studies that resulted in a journal paper 'Energy evaluation of the power network of a DC railway system with regenerating trains', which is published in *IET Electrical Systems in Transportation* [72]. The author of this thesis is the first author of the journal paper and made the major contribution to the paper. This chapter is reproduced by permission of the Institution of Engineering & Technology.

4.2 Multi-Train Energy Simulation

4.2.1 Simulator Structure

Based on the railway system modelling methods illustrated in chapter 3, a Multi-Train Energy Simulator (MTES) has been developed to evaluate the energy flow in a railway system. The structure of the MTES is shown in Figure 4.1.

This simulator combines single-train motion simulation and multi-train power network simulation. The dynamical input parameters (driving strategies) with fixed input (traction and route data) are imported into the motion simulator. Then, the output single train trajectory and power requirement with a whole-day timetable and power network parameters are imported into the power network simulator, which will export the electrical energy consumption, including substation and transmission losses, as well as the actual used and wasted regenerative energy. According to the energy evaluation results from the

multi-train power network simulation, the dynamic inputs (driving strategies and timetable) can be modified to optimise the total energy consumption.

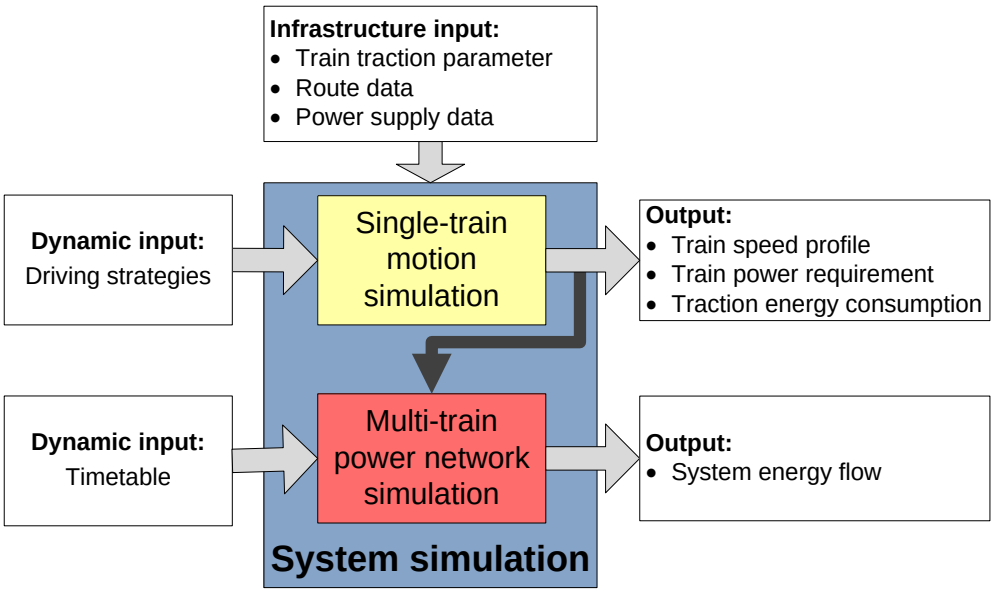

Figure 4.1 Diagram of MTES structure

4.2.2 Energy Flow

In order to study the energy efficiency of the whole railway system (up to the substations), the typical energy flow diagram through the DC-fed railway is shown in Figure 4.2. There are three layers, namely substation level, catenary system level and train level. The substations collect electricity from the national electricity grid to feed the whole railway system.

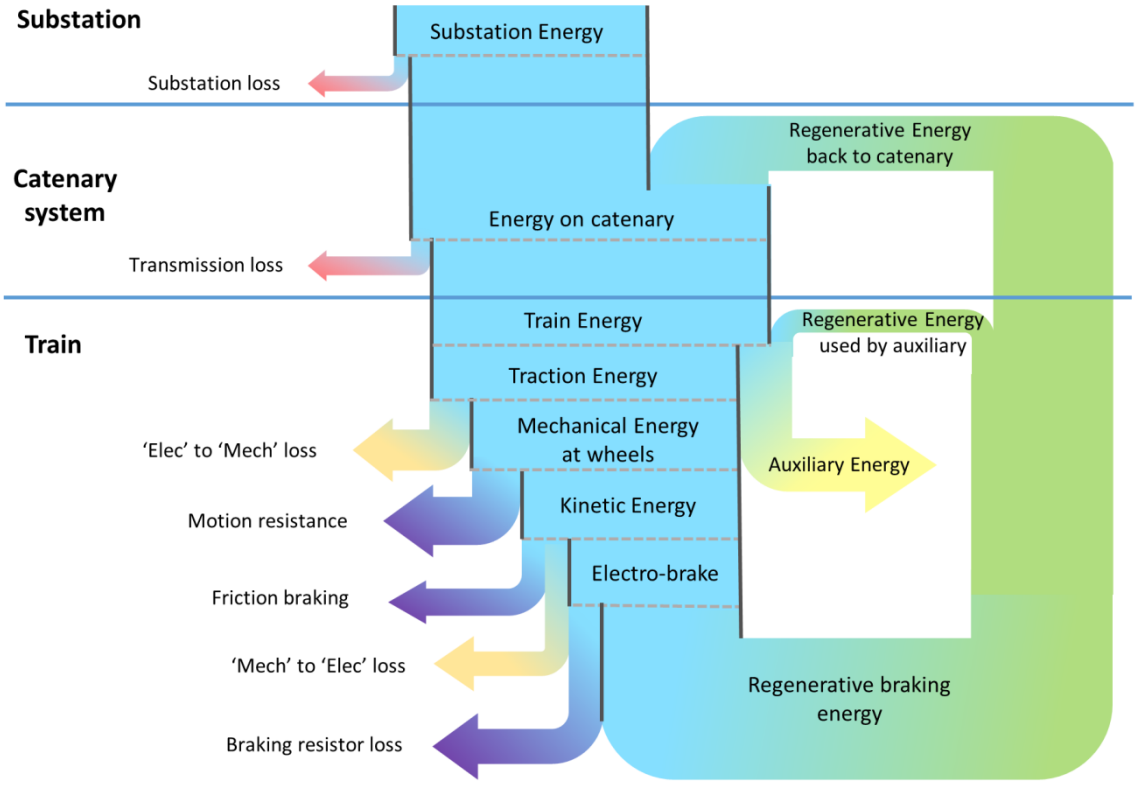

Figure 4.2 Energy flow of DC-fed railway

The substation energy is the bill paid by the railway operators. From the load flow analysis, the voltage and current of each substation can be obtained. The substation energy consumption is computed by integrating all substation instantaneous power over the train operation time, as shown in equation (4.1).

$$E_{sub} = \int_0^T \sum_{n=1}^{N_s} (V_{sub\_n}(t) \times I_{sub\_n}(t))\, dt \tag{4.1}$$

Where:

- E_{sub} is the substation energy consumption;
- N_s is the number of substations;

- T is the total time of train operation;
- V_{sub_n} is the instantaneous voltage of a substation;
- I_{sub_n} is the instantaneous current of a substation.

Due to the internal resistance of substations, some energy will be dissipated inside the substations as heat. The electrical losses within each substation are determined by the losses in the transformer and diodes [72]. However, as the substation loss does not have a significant effect on the system energy evaluation and optimisation, for simplicity, the substation loss is approximated using the equivalent substation inner resistance, explained in Section 3.3.1. Thus, the substation energy loss is given in equation (4.2).

$$E_{sub\_loss} = \int_0^T \sum_{n=1}^{N_s} (R_{sub} \times (I_{sub\_n}(t))^2)\, dt \tag{4.2}$$

Where:

- E_{sub_loss} is the substation energy loss;
- R_{sub} is the equivalent resistance of the rectifier substation for estimating the loss.

After the losses from substations, the rest of the substation energy can be transferred to the catenary. The energy on the catenary combines some of the substation energy and the regenerative braking energy which is transferred back to the catenary system. As the current goes through the resistive transmission lines, some energy is dissipated as heat. The energy loss in transmission is given in equation (4.3). The resistance of the transmission conductor is a time-varying variable, which is obtained according to the train locations and network, which is illustrated in Section 3.3.3.

$$E_{trans\_loss} = \int_0^T \sum_{n=1}^{N_c} (R_n(t) \times (I_n(t))^2)\, dt \tag{4.3}$$

Where:

- E_{trans_loss} is the transmission loss;
- N_c is the number of power transmission conductors;
- $R_n(t)$ is the resistance of a piece of transmission conductor at time *t*;
- $I_n(t)$ is the current of a piece of transmission conductor at time *t*.

Trains receive the electricity from pantographs which connect with the transmission lines. The train power depends on the voltage and current at the pantograph, which is solved by a load flow solver. Thus, the train energy can be computed by integrating all train instantaneous power over the time, as shown in equation (4.4).

$$E_{train} = \int_0^T \sum_{n=1}^{N_t} (V_{train\_n}(t) \times I_{train\_n}(t))\, dt \tag{4.4}$$

Where:

- E_{train} is the train energy consumption at the pantograph;
- N_t is the number of trains in the network;
- $V_{train\_n}(t)$ is the voltage of a traction train at time *t*;
- $I_{train\_n}(t)$ is the current of a traction train at time *t*.

The train energy and some of the regenerative braking energy are used for train traction and the auxiliary system, as shown in equation (4.5).

$$E_{train} + E_{regen\ to\ train} = E_{traction} + E_{aux} \tag{4.5}$$

Where:

- $E_{regen\ to\ train}$ is the regenerative energy used by the on-board auxiliary system;
- $E_{traction}$ is train electrical traction energy consumption;
- E_{aux} is on-board auxiliary energy consumption.

The auxiliary power is assumed as constant for a train. Therefore, the auxiliary energy consumption can be calculated by integrating the power of the on-board auxiliary system over the time, shown in equation (4.6).

$$E_{aux} = \int_0^T \sum_{n=1}^{N_t} P_{aux}(t)\, dt \tag{4.6}$$

When the train is braking, a small part of the regenerative braking energy is used by the on-board auxiliary system directly. This energy can be calculated by the overlapping of auxiliary power and electric braking power, as shown in equation (4.7)

$$E_{regen\ to\ train} = \int_0^T \sum_{n=1}^{N_t} min\{P_{aux}(t),\ P_{elec\_brake\_n}(t)\}\, dt \tag{4.7}$$

The train traction energy is the electricity consumed by the train for traction, which depends on driving styles. It is the sum of the mechanical energy at the wheels and the conversion loss. The mechanical energy at the wheels depends on the train tractive effort and train speed, given in equation (4.8).

$$E_{mech} = \int_0^T \sum_{n=1}^{N_t} (F_{traction\_n}(t) \times v_n(t))\, dt \tag{4.8}$$

Where:

- E_{mech} is the mechanical energy at the wheels;
- $F_{traction\_n}(t)$ is the tractive effort of a traction train at time *t*;
- $v_n(t)$ is the speed of a train at time *t*.

As discussed in train motion simulation, some energy is dissipated by transforming from electrical to mechanical energy. The relation between train mechanical energy and electrical energy consumption is expressed in equation (4.9). In this thesis, the efficiency (η) refers to the whole traction chain from pantograph to wheels and is assumed as a constant. The energy loss of the conversion from electrical to mechanical energy can be calculated by equation (4.10).

$$E_{mech} = E_{traction} \times \eta \tag{4.9}$$

$$E_{traction\_loss} = E_{traction} \times (1 - \eta) \tag{4.10}$$

Where:

- η is the efficiency of electrical to mechanical conversion;
- $E_{traction\_loss}$ is the energy loss of the conversion from electrical to mechanical.

The mechanical energy at the wheels is used to move the train and overcome the motion resistance. The energy loss on motion resistance is given in equation (4.11).

$$E_{motion\_loss} = \int_0^T \sum_{n=1}^{N_t} (R_n(t) \times v_n(t))\, dt \tag{4.11}$$

Where:

- E_{motion_loss} is the energy loss on motion resistance;
- $R_n(t)$ is the motion resistance of a traction train at time *t*.

All the trains are assumed to be operated in a circle. The final potential energy by gradient is zero. Thus the rest of the mechanical energy is train kinetic energy consumption, given in equation (4.12). This kinetic energy is not the maximum kinetic energy obtained by the train at running, but the part of the kinetic energy which is dissipated by the braking system.

$$E_{kinetic} = E_{mech} - E_{motion\_loss} \tag{4.12}$$

Where:

- $E_{kinetic}$ is the kinetic energy of trains dissipated by braking.

A blending of the electric and mechanical brake is commonly used in modern trains. Electric braking uses the traction motor as a generator to regenerate braking energy. Friction braking is used when the motor cannot provide sufficient braking effort. Therefore, part of the kinetic energy of the train is dissipated by friction braking. The rest of it is converted into electricity by electric braking with some loss of energy in the mechanical to electrical conversion, as shown in Figure 4.2. The efficiency (η) of the mechanical to electrical conversion is assumed to be the same as the electrical to

mechanical conversion in equation (4.9). The amount of electricity regenerated by electric braking can be expressed in equation (4.13).

$$E_{elec\_brake} = (E_{kinetic} - E_{fric\_brake}) \times \eta \tag{4.13}$$

$$E_{brake\_loss} = (E_{kinetic} - E_{fric\_brake}) \times (1 - \eta) \tag{4.14}$$

Where:

- E_{elec_brake} is the electricity converted by electric braking;
- E_{fric_brake} is the energy dissipated by friction braking as heat;
- E_{brake_loss} is the energy loss of the conversion from mechanical to electrical.

Most trains with regenerative braking are also fitted with braking resistors in case the regenerative energy is not receptive. The regenerative braking energy equals the electric braking energy subtracted by the energy dissipated by the braking resistor, as in equation (4.15).

$$E_{regen} = E_{elec\_brake} - E_{r\_loss} \tag{4.15}$$

Where:

- E_{regen} is the regenerated braking energy;
- E_{r_loss} is the energy dissipated by the braking resistor.

Part of the regenerated energy is used by the on-board auxiliary system directly and the rest of the regenerated energy flows back to the catenary system.

$$E_{regen} = E_{regen\ to\ train} + E_{regen\ to\ network} \tag{4.16}$$

Where:

- $E_{regen\ to\ network}$ is the regenerated energy drawn back to the catenary system.

The regenerative energy fed back to the network can be computed by integrating all of the braking train's instantaneous power on the pantograph over the time, as shown in equation (4.17).

$$E_{regen\ to\ network} = \int_0^T \sum_{n=1}^{N_t} (V_{regen\_train\_n}(t) \times I_{regen\_train\_n}(t))\, dt \tag{4.17}$$

Where:

- $V_{regen\_train\_n}(t)$ is the voltage of a regenerative braking train at time *t*;
- $I_{regen\_train\_n}(t)$ is the current of a regenerative braking train at time *t*.

4.3 Energy Loss Analysis

The majority of the energy consumption in railway systems is used for train traction. In order to understand and improve the energy efficiency of railway systems, the energy loss through the whole network has to be studied. The power of the auxiliary system is constant and depends on the usage of electric auxiliary equipment on board. The auxiliary energy usage is not the main factor for the system energy consumption and it cannot be reduced by traction operation optimisation. To simplify the study of energy evaluation and efficient regenerative braking, the auxiliary power is assumed as zero in this thesis. Thus, equation

(4.16) can be simplified into equation (4.18). The total regenerative energy equals the regenerative energy back to the catenary system. As a result, equation (4.5) can be simplified into equation (4.19). The train energy consumption at the pantograph equals the train electrical traction energy consumption.

$$E_{regen} = E_{regen\ to\ network} \tag{4.18}$$

$$E_{train} = E_{traction} \tag{4.19}$$

As for the energy flow analysis, the energy balance equation for the whole railway network can be expressed in equation (4.20).

$$E_{sub} + E_{regen} = E_{train} + E_{sub\_loss} + E_{trans\_loss} \tag{4.20}$$

4.3.1 Energy Loss in Network

The energy loss in the network refers to the electricity loss during the transmission from the substation to the train, which includes the substation loss and transmission loss as given in equation (4.21).

$$E_{network\_loss} = E_{sub\_loss} + E_{trans\_loss} \tag{4.21}$$

From equation (4.2) and (4.3), it can be found that the network loss is related to contact line resistance and line current. As a consequence, the network loss principally depends on the voltage level and material of the railway system as well as the traction demand [10]. A coefficient to characterise the amount of network loss is defined in order to compare different scenarios. The ‘network loss coefficient’ is given in equation (4.22).

$$C_n = \frac{E_{network\_loss}}{E_{train}} \tag{4.22}$$

Where:

- C_n is the network loss coefficient.

The network loss coefficient denotes the electricity transmission efficiency performance of the electrical infrastructure. In general, a railway system with a higher voltage level can lead to a lower network loss coefficient. The typical values for network loss coefficient can be around 18%, 14%, 8% and 6% for 600 V, 750 V, 1500 V and 3000 V DC networks, respectively [135]. The contact line resistivity is another factor of the value of the network loss coefficient. With the development of superconducting cables using high-temperature superconducting materials, the feeding loss in the power supply network could be reduced [120].

4.3.2 Energy Loss in Traction

Based on equation (4.9) to (4.12), the traction energy equals the sum of traction conversion loss, the motion loss and the train kinetic energy, shown as in equation (4.23).

$$E_{traction} = E_{traction\_loss} + E_{motion\_loss} + E_{kinetic} \tag{4.23}$$

The traction conversion loss comprises 10% to 15% of total traction energy consumption [22]. The majority of the loss is from motor inefficiency. To reduce this loss requires more efficient motor designs, for example, selecting improved materials or using permanent magnet synchronous motors. The study of motor efficiency is not considered in this thesis, and the efficiency of traction conversion is assumed to be a constant. The energy used to

overcome motion resistance comprises 10% to 50% of total traction energy. From equation (4.11), the amount of the motion loss depends on the motion resistance and vehicle speed. The motion resistance depends on the Davis coefficients and route curvature configuration, as discussed in equation (3.6). The method to reduce motion resistance is not the main objective of this thesis. The speed should be considered to reduce motion loss. The vehicle obtains kinetic energy when accelerating. Some of the kinetic energy is used to overcome the motion resistance. The rest of the kinetic energy will be converted into heat or electricity by the braking system. The amount of kinetic energy dissipated by the braking system is related to vehicle speed. This thesis focuses on the design of an energy-efficient driving profile to reduce the traction energy consumption.

Coasting control is one of the most significant efficient driving controls. During coasting, no tractive power is applied and the acceleration is determined by the force balance of gradient and resistance. In general, the kinetic energy of the train is reduced to overcome the motion resistance. Figure 4.3 and Figure 4.4 present the velocity and energy consumption profiles without and with coasting, respectively. The time taken by both drivings is the same, but the traction energy consumption is reduced by 17.6%. In Figure 4.3, the train accelerates to 60 km/h and then cruises until braking. When the train is cruising, partial tractive power is applied to keep the same speed and the tractive energy increases with the increasing motion energy loss. In Figure 4.4, the train accelerates to a higher speed of 70 km/h and then cruises for a short period. After cruising, the train starts to coast. During coasting, no tractive power is applied and the tractive energy keeps the same. The motion energy loss still increases when the train is coasting, but this energy is covered by train kinetic energy. The train brakes until it coasts to 47 km/h.

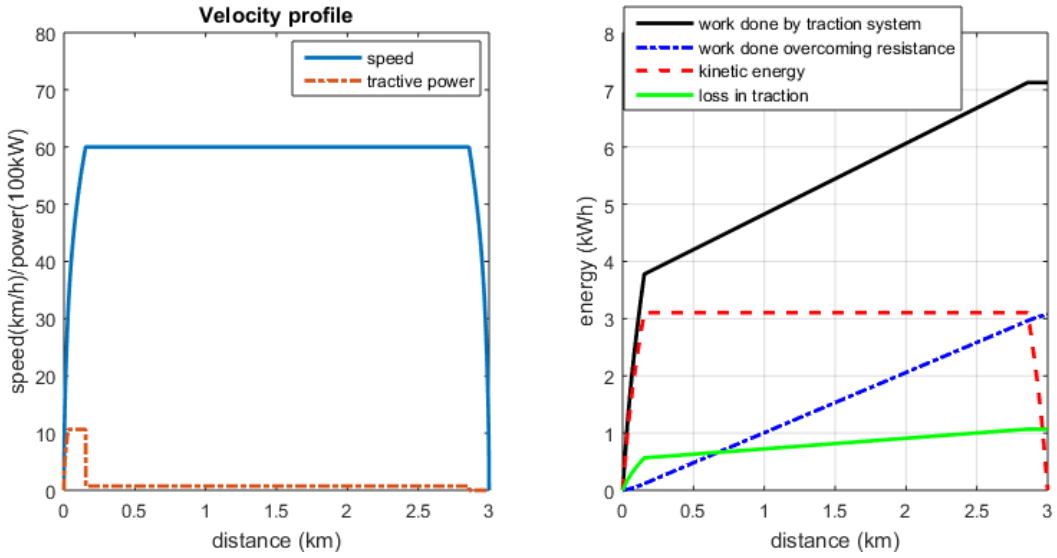

Figure 4.3 Speed profile and traction energy case 1

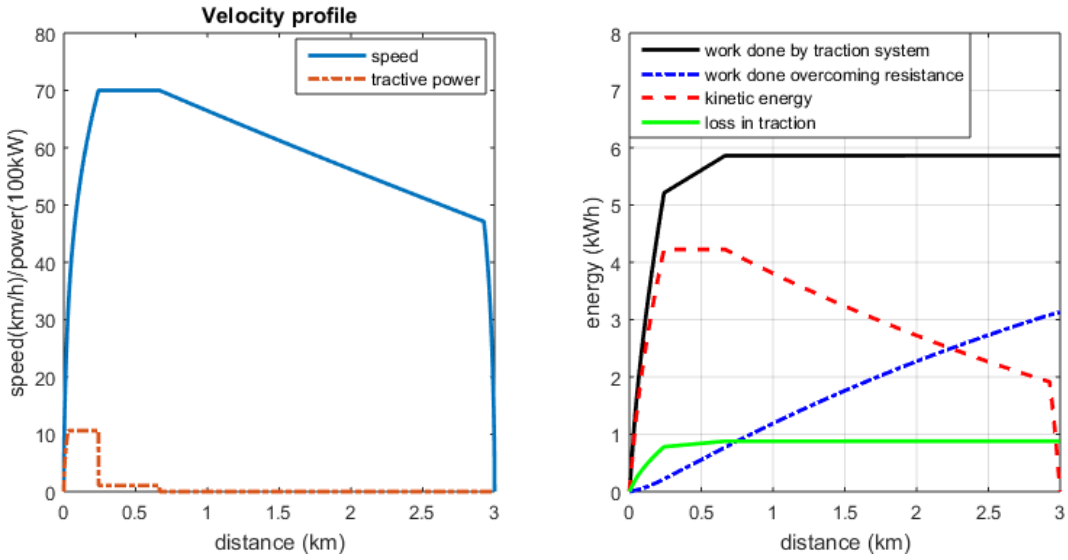

Figure 4.4 Speed profile and traction energy case 2

The detailed energy comparison is shown in Table 4.1. For the same route with the same running time, driving with proper coasting controls can reduce the traction energy consumption by 17.6% (from 7.11 kWh to 5.86 kWh). The traction loss is reduced relatively. The motion loss for the driving with coasting is slightly higher due to the high-

speed running, but the kinetic energy is reduced significantly, which is the main reason for traction energy saving. In terms of global energy optimisation, if all of the kinetic energy can be reused without losses, optimising the motion energy loss is the only way to reduce the system energy consumption. Nevertheless, it is not possible due to the nature of the efficiency of conversion from kinetic energy to electricity. Therefore, traction energy consumption optimisation by reducing kinetic energy is still a good solution to saving system energy for railways, although the motion loss may be increased.

Table 4.1 Comparison

Item	**Driving without coasting**	**Driving with coasting**
Distance (km)	3	3
Journey time (s)	194	194
Traction energy (kWh)	7.11	5.86 (-17.6%)
Traction loss (kWh)	1.07	0.88
Motion loss (kWh)	3.07	3.12
Kinetic energy dissipated by braking(kWh)	2.97	1.86

4.3.3 Energy Loss in Regenerative Braking

Kinetic energy is converted by the braking system, and part of it is converted into electricity and reused by trains. The energy flow during braking is shown in equation (4.24). Since the regenerative energy can be reused, the energy loss during braking includes the friction braking energy, the electric braking conversion loss and the energy loss by electric braking resistance.

$$E_{kinetic} = E_{fric\_brake} + E_{brake\_loss} + E_{r\_loss} + E_{regen} \tag{4.24}$$

Friction braking is used when the motor cannot provide sufficient braking effort. For most metro trains, the electric braking is sufficient for normal braking requirements. Friction braking is only applied when the train is approaching a stop with very low speed. In this thesis, the energy dissipated by friction braking is assumed as zero, which is reasonable for a metro system energy study. Therefore, the energy flow through the braking system can be simplified, as shown in equation (4.25).

$$E_{kinetic} = E_{brake\_loss} + E_{r\_loss} + E_{regen} \tag{4.25}$$

The energy loss of the conversion from mechanical to electrical depends on the efficiency of the power conversion system, which is assumed as a constant in this thesis. Therefore, the energy dissipated by the braking resistor is the main factor to influence the amount of regenerated energy. The energy wasted in braking resistance is due to the overvoltage of the braking train. When the number of motoring trains is insufficient to absorb the regenerative energy, a high voltage will appear. This is because the train voltage can be increased by regenerative braking. In case of a high voltage hazard when the network voltage exceeds a safe value, some braking energy should be wasted in the onboard braking rheostat as heat instead of being transferred to contact lines.

In order to evaluate the efficiency of using the regenerative braking energy, the regeneration efficiency is defined in equation (4.26). High regeneration efficiency means a high receptivity of the network.

$$\eta_{regen} = \frac{E_{regen}}{E_{elec\_brake}} = \frac{E_{regen}}{E_{regen} + E_{r\_loss}} \tag{4.26}$$

A simple study of the regeneration efficiency has been carried out based on a 750 V railway system with a 15 km route, as shown in Figure 4.5. There are three substations along the route. There are two trains running in the network, one traction train and one braking train.

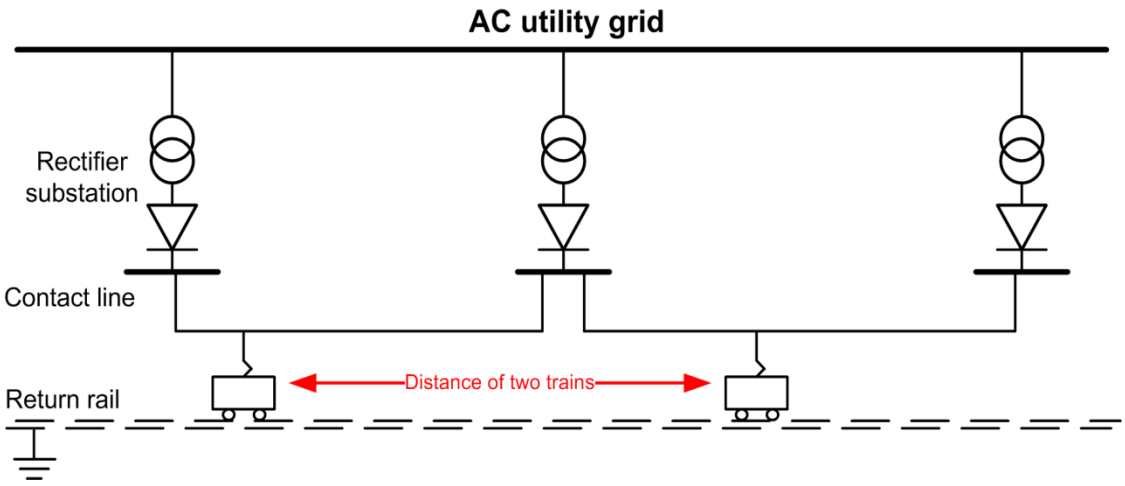

Figure 4.5 Railway network diagram

The power flow of this network by varying the distance between these two trains is computed. The regeneration efficiency based on the braking train instantaneous power is calculated at different distances from the traction train, as shown in Figure 4.6. When the distance between two trains is within 2 km, 100% regeneration efficiency can be achieved. The regeneration efficiency decreases when the distance increases further. Finally, the efficiency reduces to 23% when the distance is 15 km. Therefore, the distance between traction trains and braking trains is the main factor to change the efficiency of regeneration. In general, a short distance leads to high regeneration efficiency. In a railway system with busy traffic it is easier to achieve high regeneration efficiency compared with a railway system with less traffic or long headways.

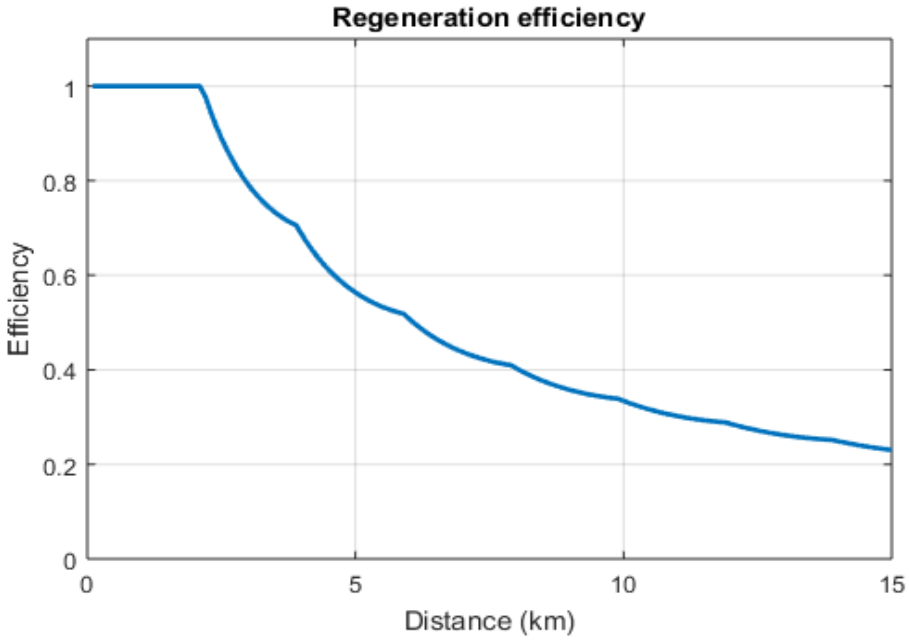

Figure 4.6 The receptiveness of regenerative energy between two trains

From the power results shown in Figure 4.7, the substation power increases with the train distance. The train traction power remains the same with 2000 kW. The substation power is related to the network loss and regeneration power. When the distance is within 2 km, although the regeneration power is 2000 kW with 100% efficiency, the substation power varies a lot with the change in network loss. Therefore, the regeneration efficiency is significant to substation energy consumption, but the network loss cannot be neglected.

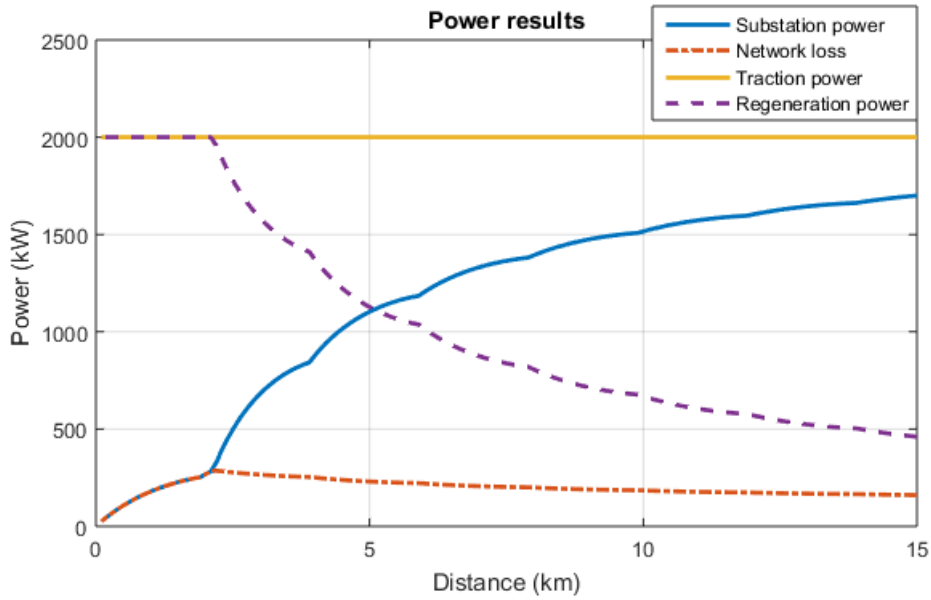

Figure 4.7 Power results

4.4 Case Study

The Beijing Yizhuang Subway Line (BYSL) in China has been in operation since 2010. It is a significant subway line which links the suburbs of Beijing and the city centre. Trains are operated by an Automatic Train Operation (ATO) system for a certain service. For the rest of the time, trains are driven by human drivers. In order to assess the energy performance of the current operation of BYSL, two no-load driving tests were conducted in September 2014. One of them is the current ATO driving test, and the other is human driving with energy-efficient driving strategies. In this case study, the practical data for simulating BYSL is presented. The ATO driving speed profiles are used in this case study and the energy consumption is evaluated by the system energy simulator. The simulation results and field test results are illustrated and compared.

4.4.1 Modelling Formulation

4.4.1.1 Route Data

The Beijing Yizhuang Subway Line covers a length of 22.73 km and contains 14 stations including both underground and over ground segments. The station location data is presented in Table 4.2. A diagram of the route vertical alignment and train station locations is shown in Figure 4.8.

Table 4.2 Station location

No.	Station	Location (m)
1	Yizhuang	0
2	Ciqu	1334
3	Ciqunan	2620
4	Jinghailu	4706
5	Tongjinanlu	6971
6	Rongchang	9309
7	Rongjing	10663
8	Wanyuan	11943
9	Wenhuayuan	13481
10	Yizhuangqiao	14474
11	Jiugong	16456
12	Xiaohongmen	18822
13	Xiaocun	20097
14	Songjiazhuang	22728

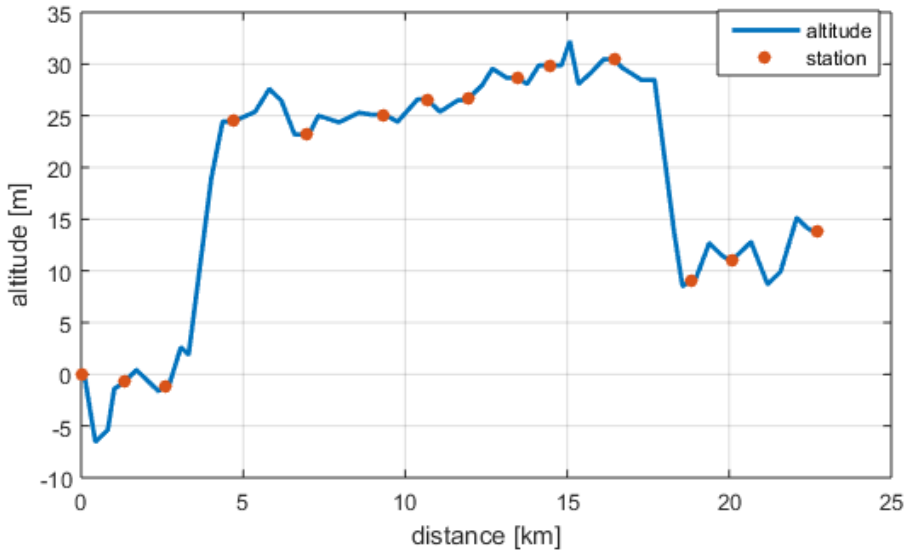

Figure 4.8 Route vertical alignment and train station location

The speed limits are demonstrated in Figure 4.9. The speed limit is marked as zero at each station. The maximum speed is 80 km/h for this route. Lower speed limits are applied when the train departs from or arrives at a station.

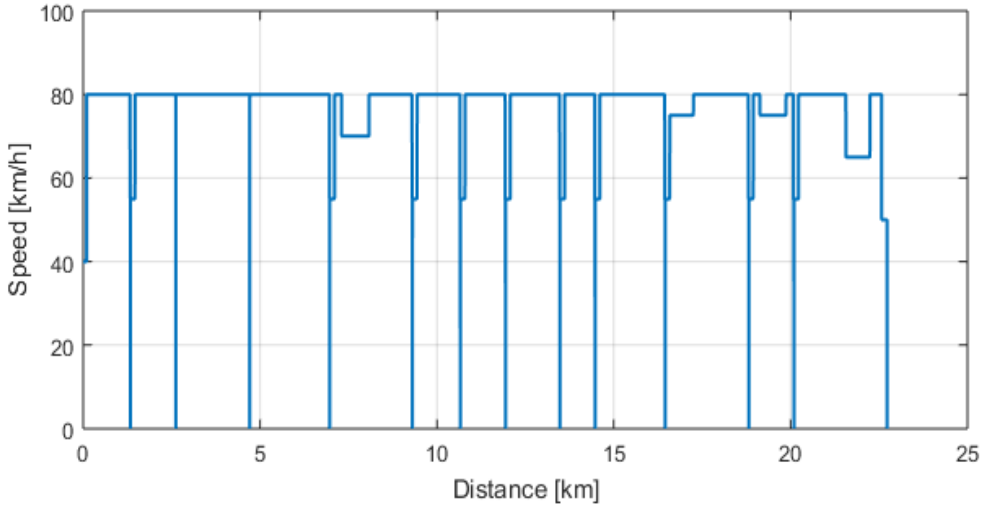

Figure 4.9 Speed limits

4.4.1.2 Vehicle Data

The train operated in the Beijing Yizhuang Subway Line is formatted by 6 carriages. 3 of them are equipped with motors (M1 to M3), while the other carriages are trailers (T1 to T3). The tare weight of each carriage is shown in Table 4.3.

Table 4.3 Vehicle tare mass [tonnes]

Car No.	**T1**	**M1**	**T2**	**M2**	**M3**	**T3**	**Total**
Vehicle tare mass	33	35	28	35	35	33	199

The passenger weight of each carriage for different scenarios is presented in Table 4.4.

Table 4.4 Passenger mass [tonnes]

Car No.	**T1**	**M1**	**T2**	**M2**	**M3**	**T3**	**Total**
AW0 (no load)	0	0	0	0	0	0	0
AW2 (normal load)	13.56	15.24	15.24	15.24	15.24	13.56	88.08
AW3 (over load)	17.40	19.50	19.50	19.50	19.50	17.40	112.8

The tractive effort characteristic is introduced in Section 3.2.2. Based on the general equation (3.7), the tractive parameters for different scenarios of BYSL are shown in Table 4.5. The tractive effort curve in Figure 4.10 describes the relationship between tractive effort and velocity in different scenarios.

Table 4.5 Tractive characteristics

	F_m [kN]	**F_{m2} [kN]**	**V_1 [km/h]**	**V_2 [km/h]**
AW0 (no load)	200	200	51.3	51.3
AW2 (normal load)	289	228.8	38	48
AW3 (over load)	312	228.8	35.2	48

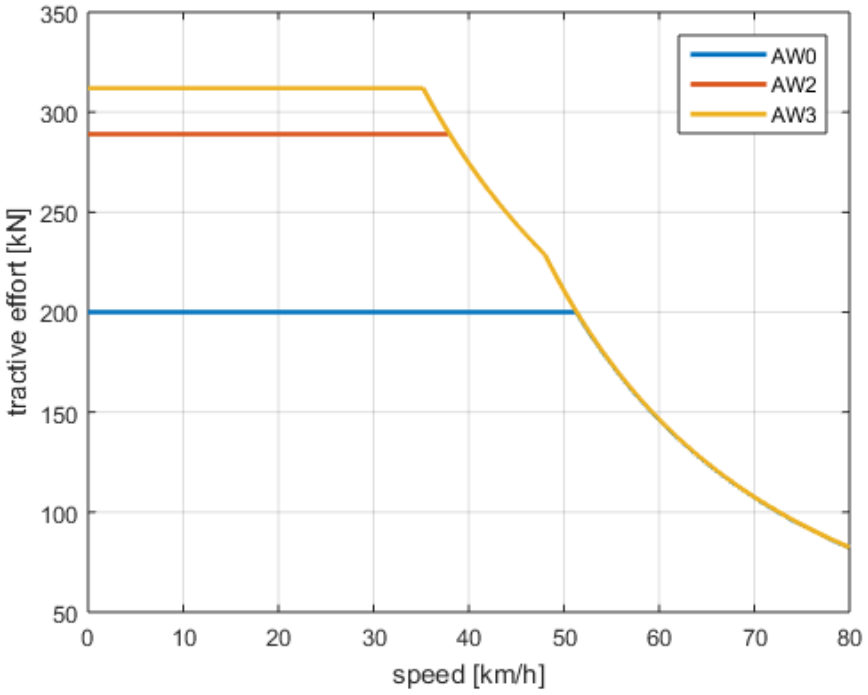

Figure 4.10 Tractive effort curve

The regenerative braking effort characteristic is given in Table 4.6 and the braking effort curve is described in Figure 4.11.

Table 4.6 Regenerative braking effort characteristics

	F_m [kN]	**F_{m2} [kN]**	**V_1 [km/h]**	**V_2 [km/h]**
AW0 (no load)	167	167	77.8	77.8
AW2 (normal load)	239	232	64	66
AW3 (over load)	255	232	60	66

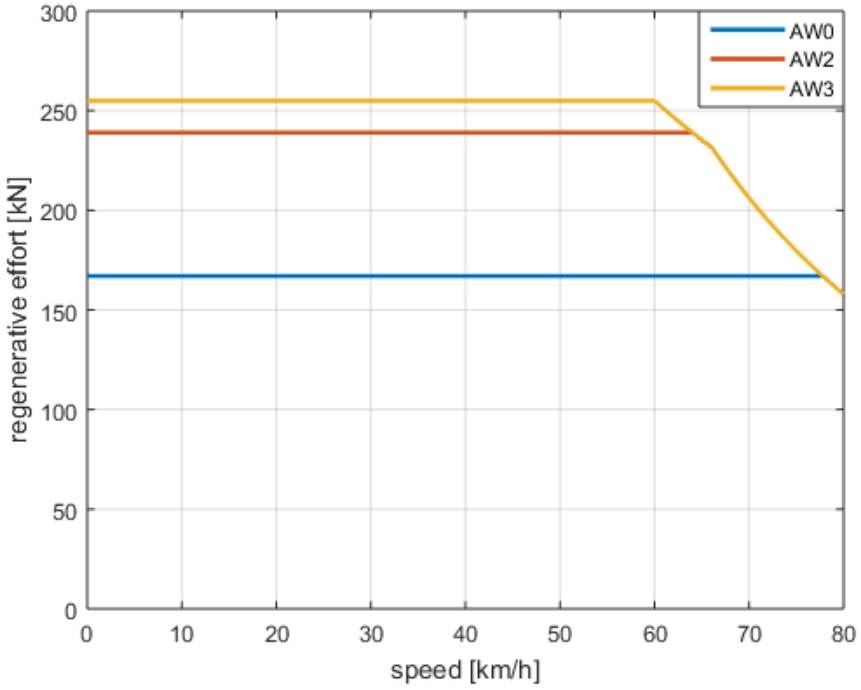

Figure 4.11 Regenerative braking effort curve

The resistance to motion is given in equation (3.6). The curvature resistance is neglected in this thesis. The Davis coefficients for different scenarios are shown in Table 4.7 and the motion resistance curve is shown in Figure 4.12.

Table 4.7 Davis constants

	A [kN]	**B [kN/(km/h)]**	**C [kN/(km/h)^2]**
AW0 (no load)	2.4180	0.0280	0.0006575
AW2 (normal load)	3.4818	0.0403	0.0006575
AW3 (over load)	3.7799	0.0437	0.0006575

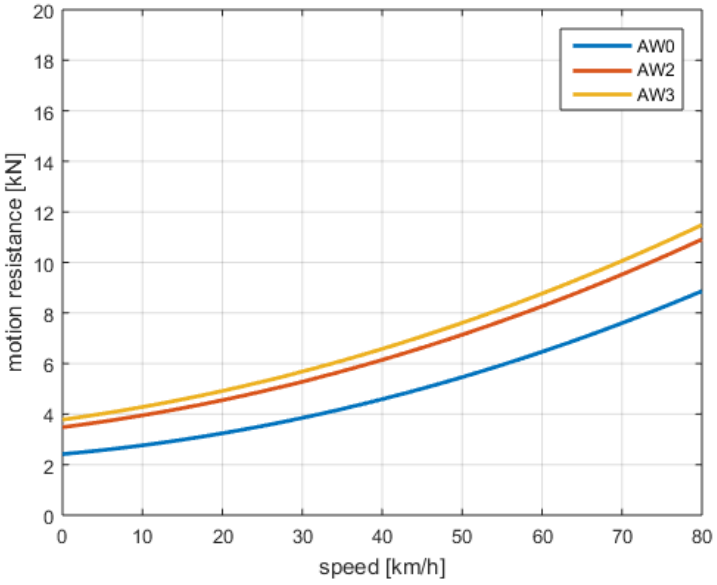

Figure 4.12 Motion resistance curve

4.4.1.3 Power Network Data

The electrical network is comprised of 12 rectifier substations with nominal 750 V supply, shown in Table 4.8. For the power network simulation, the substation is modelled as a voltage source with a no-load voltage of 850 V. The equivalent internal resistance is 0.02 Ω. The resistance rate for the overhead line and return rail are 15 μΩ/m and 10 μΩ/m, respectively.

Table 4.8 Substation location

	Substation	**location (m)**
1	Yizhuang	0
2	Ciqunan	2620
3	Jinghailu	4706
4	Tongjinanlu	6971
5	Rongchang	9309
6	Rongjing	10663
7	Wenhuayuan	13481

8	Yizhuangqiao	14474
9	Jiugong	16456
10	Xiaohongmen	18822
11	Xiaocun	20097
12	Songjiazhuang	22728

4.4.1.4 Timetable

The first and last trains of BYSL depart Yizhuang Station at 5:30 and 22:05, respectively. At peak hours (from 5:30 to 9:00 and from 16:00 to 19:00), the headway is 6 minutes, and at off-peak hours, the headway is 11 minutes. There are in total 121 cycles including 65 cycles with short headway and 56 cycles with long headway. The current operational timetable is shown in Table 4.9. It is allowed to be within 5 seconds for each interstation running.

Table 4.9 Current operational timetable

	Station	**Running time (s)**	**Dwell time (s)**
1	Yizhuang	-	40
2	Ciqu	105	45
3	Ciqunan	101	35
4	Jinghailu	140	30
5	Tongjinanlu	148	30
6	Rongchang	160	30
7	Rongjing	103	30
8	Wanyuan	99	30
9	Wenhuayuan	113	30
10	Yizhuangqiao	85	35
11	Jiugong	134	30
12	Xiaohongmen	155	30
13	Xiaocun	104	30
14	Songjiazhuang	193	30
Up-direction total		1640	455
Turnaround		-	180
1	Songjiazhuang	-	30
2	Xiaocun	190	30
3	Xiaohongmen	106	30

4	Jiugong	156	30
5	Yizhuangqiao	131	35
6	Wenhuayuan	86	30
7	Wanyuan	112	30
8	Rongjing	100	30
9	Rongchang	103	30
10	Tongjinanlu	163	30
11	Jinghailu	147	30
12	Ciqunan	135	35
13	Ciqu	100	45
14	Yizhuang	103	40
Down-direction total		1632	455
Cycle total		3272	1090

4.4.2 Current Driving

Trains on BYSL are driven by the ATO system and human operation jointly. In order to validate the simulation calculation and evaluate the current system energy consumption, the current driving data of ATO are collected by the on-board Train Information Measurement System (TIMS) of BYSL. The date includes the traction effort, power, time, speed, location and voltage. According to the collected train speed data, the train speed trajectory and mechanical power can be simulated by the Single Train Motion Simulator (STMS), shown in Figure 4.13 and Figure 4.14. The existing operation is to drive the train to the maximum target speed (approximately 75 km/h), and then maintain a constant speed (cruising mode) until the braking train approaches the station stop. However, due to the limitations of the ATO speed tracking algorithm and the traction characteristic, the train control is switched between motoring and braking modes frequently in order to maintain the cruising speed.

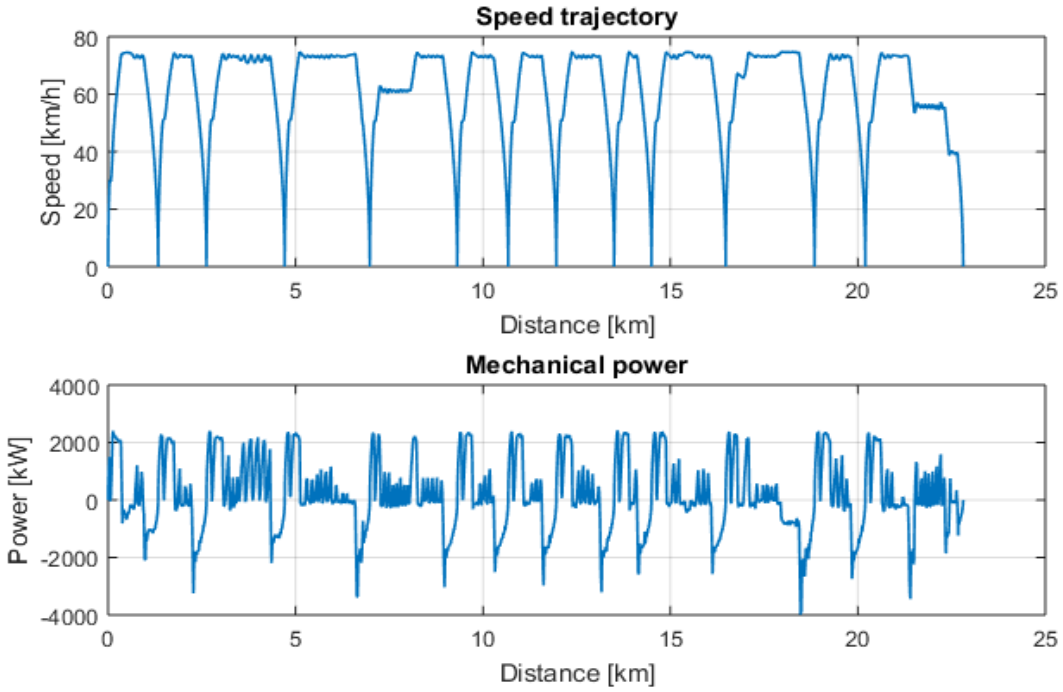

Figure 4.13 ATO driving profiles for up-direction

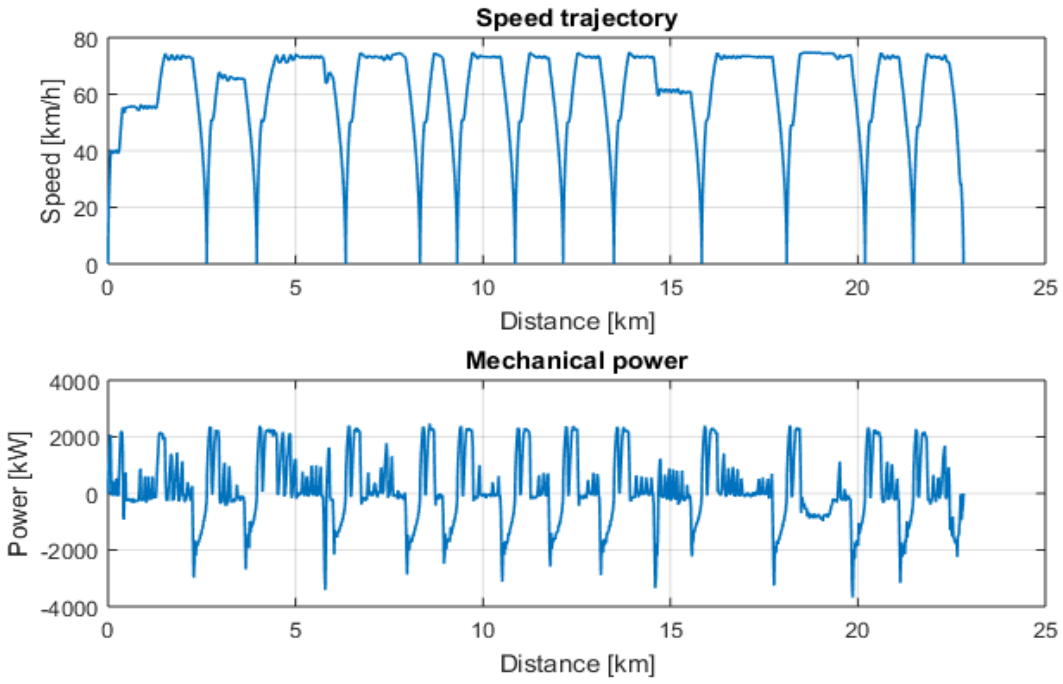

Figure 4.14 ATO driving profiles for down-direction

The traction energy consumption and electrical braking energy for each interstation journey are shown in Table 4.10 and Table 4.11. The measured energy values come from the TIMS, and the simulated energy values are from the STMS according to the real speed trajectory. It is found that the average difference of the energy results between the measured and simulated values is less than 3%, which validates the accuracy of STMS. It notes that the braking energy is much lower than traction energy between the 3rd station (Ciqunan) and 4th station (Jinghualu) due to a steep uphill. Most of the traction energy is used to cover the potential energy, and less braking is used. In addition, for the interstation journey between the 11th station (Jiugong) and 12th station (Xiaohongmen), the braking energy is relatively high, because the corresponding route is a steep downhill.

Table 4.10 Train energy consumption for up-direction

	Station	**Measured electrical tractive energy (kWh)**	**Simulated electrical tractive energy (kWh)**	**Measured electrical braking energy (kWh)**	**Simulated electrical braking energy (kWh)**
1	Yizhuang	-	-	-	-
2	Ciqu	16	16.50	6	9.50
3	Ciqunan	17	18.32	11	10.78
4	Jinghailu	33	33.95	9	8.78
5	Tongjinanlu	23	21.00	12	10.97
6	Rongchang	24	22.63	13	11.21
7	Rongjing	16	18.13	10	9.64
8	Wanyuan	17	17.38	9	9.92
9	Wenhuayuan	19	20.08	12	10.39
10	Yizhuangqiao	16	17.07	10	9.67
11	Jiugong	20	20.48	12	10.70
12	Xiaohongmen	20	18.34	20	18.20
13	Xiaocun	21	20.53	10	10.72
14	Songjiazhuang	26	25.25	11	12.62
	total	268	269.64	145	143.10

Table 4.11 Train energy consumption for down-direction

	Station	Measured electrical tractive energy (kWh)	Simulated electrical tractive energy (kWh)	Measured electrical braking energy (kWh)	Simulated electrical braking energy (kWh)
1	Songjiazhuang	-	-	-	-
2	Xiaocun	26	23.34	12	13.45
3	Xiaohongmen	16	15.53	10	9.66
4	Jiugong	32	34.19	10	10.39
5	Yizhuangqiao	21	20.22	13	10.70
6	Wenhuayuan	15	15.74	10	9.78
7	Wanyuan	17	17.83	9	10.69
8	Rongjing	16	17.34	11	9.84
9	Rongchang	15	17.00	9	10.12
10	Tongjinanlu	19	21.22	11	11.74
11	Jinghailu	21	21.20	10	10.45
12	Ciqunan	12	15.25	18	18.34
13	Ciqu	20	18.88	11	10.79
14	Yizhuang	18	16.85	9	9.11
	total	248	254.60	143	145.07

4.4.3 Energy Evaluation Results

Trains in a metro system run repetitively and periodically when the headway is constant. During the headway period, each train in a multi-train system finishes one part of the cycle running, and the sum of each train running is the whole cycle journey. Therefore, the sum of each train's traction energy during the headway period is actually the single train traction energy consumption of one cycle. The system energy evaluation for this study is always the energy consumption during the headway period rather than that of the whole day's operation time.

Figure 4.15 describes the energy results during a headway period with regeneration turned off versus different headways, which range from 240 s to 900 s. The traction energy and

braking energy are 524 kWh and 288 kWh, respectively, which are fixed values with different headways. The substation energy consumption ranges from 550 kWh to 562 kWh, and there is only 2% difference with various headways. As the regeneration is turned off, all of the electric braking energy is dissipated by the braking resistor. The regeneration energy is zero in this case. The network loss ranges from 26 kWh to 38 kWh, which is the reason for the substation energy changing. Although the network loss changes a lot relative to itself, it does not significantly affect the substation energy consumption.

The efficiency results are shown in Figure 4.16. The regeneration efficiency is zero as no regeneration energy is reused. The network loss coefficient ranges from 5% to 7%, and trends to reduce with the increase of headway. This is because the average current through a network of busy traffic with low headway is higher than that through a network of quiet traffic. Therefore, the substation energy consumption trends to decrease a little with the increase of headway.

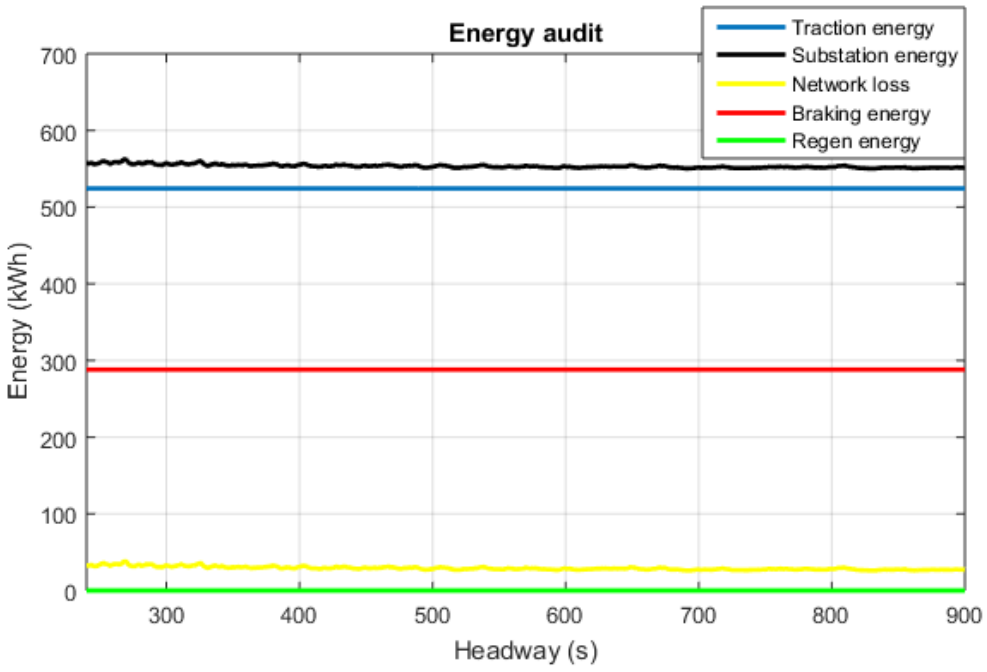

Figure 4.15 Energy consumption with regeneration turned off

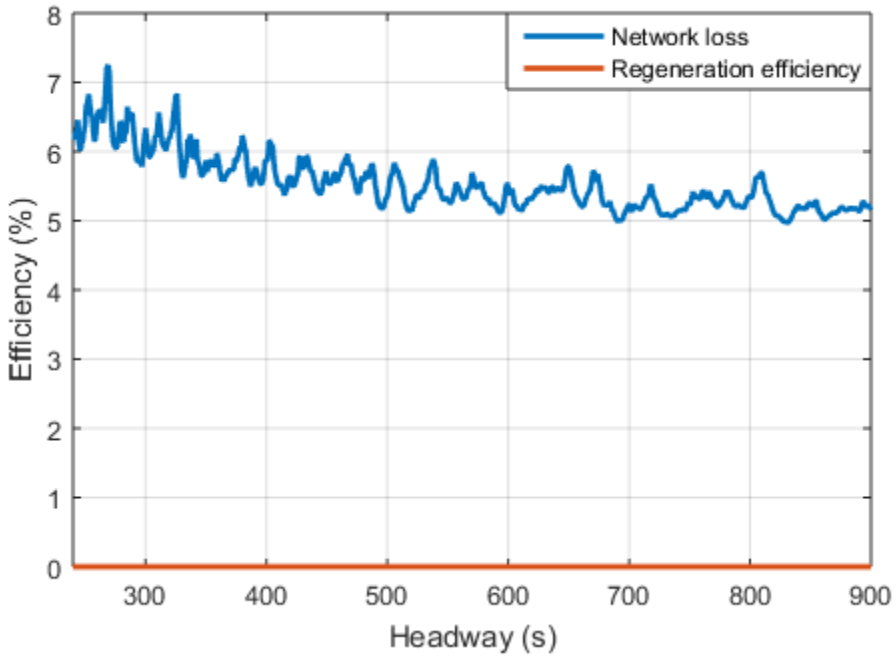

Figure 4.16 Efficiency with regeneration turned off

Figure 4.17 indicates the energy results with regenerating trains. As there are no changes in train trajectory, the result of traction and braking energy are also the same as the results without regeneration. The energy consumption at the substations ranges from 291 kWh to 446 kWh. The minimum and maximum of substation energy consumption occur when the headway is 245 s and 842 s, respectively. In principle, over 35% of the energy saving from the substation can be achieved by 'optimising' the headway. However, in practice, even small deviations in timings of a single train could result in a significant reduction (or even increase) in the effective use of regenerated power. Compared with the average substation energy consumption for the system without regeneration, the energy is reduced by 20% to 48% by having regeneration. By utilising the regeneration braking energy, at least 20% of substation energy can be saved. The regenerated energy ranges from 109 kWh (842 s headway) to 288 kWh (245 s headway), with 62% of the difference. The highly variable use of regenerated energy is not simply related to headway. This is because the station

positions are at unequal distances and the braking and accelerating trains randomly overlap. However, it is clear that high regeneration energy results for short headways happen more frequently than long headways. The network losses when regeneration is turned on are a little higher, ranging from 29 kWh to 42 kWh. But this is not significant compared to the net energy reduction.

The regeneration efficiency and network loss coefficient with different headways is shown in Figure 4.18. The regeneration efficiency ranges from 38% when headway is 842 s to 92% when headway is 245 s. The higher regeneration efficiency can be achieved when the headway is shorter. The network loss coefficient ranges from 6% to 8%, and there is no clear trend with the increasing of headway. This is because the regenerative braking draws the current back to the network, which increases the average current through the network, even when the network is not busy.

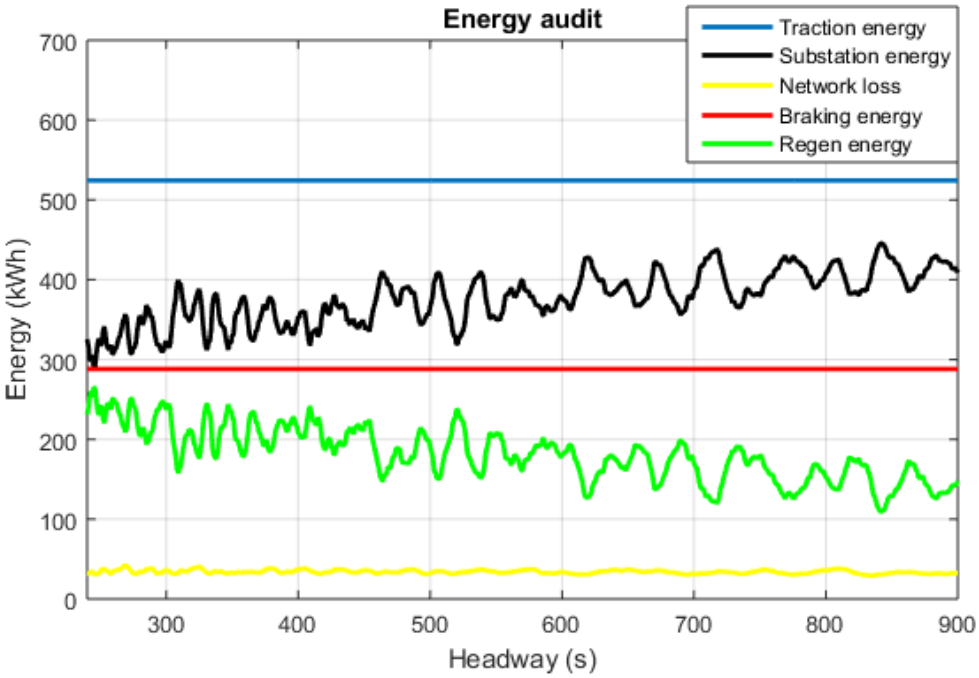

Figure 4.17 Energy consumption with regeneration turned on

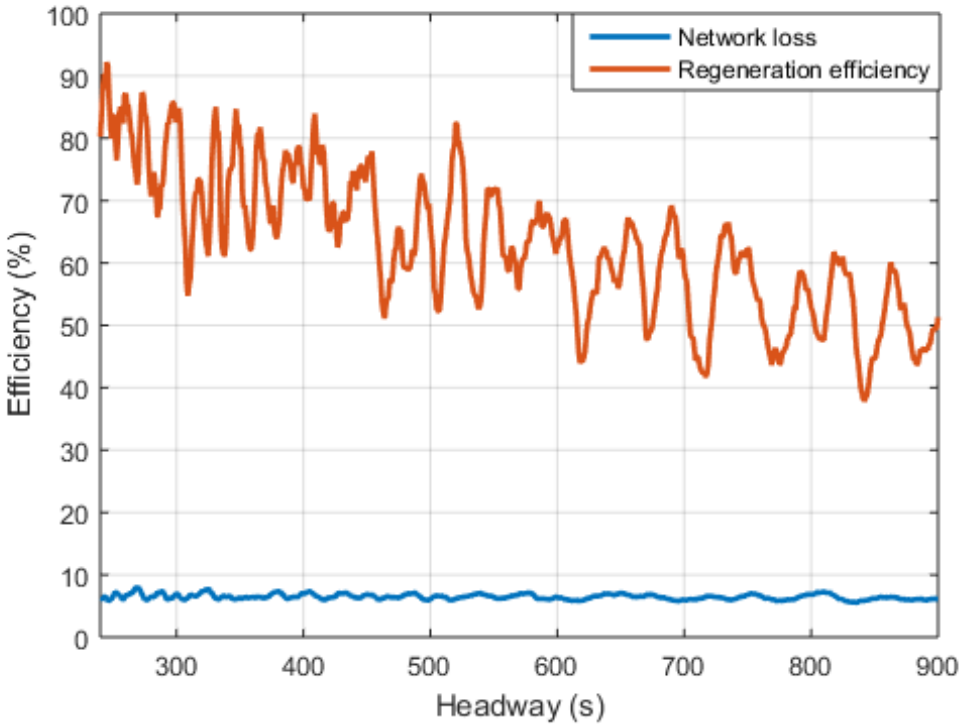

Figure 4.18 Efficiency with regeneration turned on

4.4.4 Case Study Conclusion

A whole system energy evaluation is studied based on the data of the Beijing Yizhuang Subway Line. The energy consumption is calculated according to current driving by the ATO system. The energy audit result shows different system energy consumption with the regeneration braking on and off as well as the energy consumption with various headways. It has been noted that the system energy consumption with regeneration on can be reduced by 20% to 48% compared with the system with regen off, although the transmission loss is slightly increased due to higher current transmission. Although the vehicles used on BYSL are capable of regenerating braking energy, for some reason regeneration is switched off. The system energy consumption with regeneration turned on can benefit from timetable

optimisation, which can, in principle, increase the efficiency of regenerative energy utilisation. By optimising the timetable, 35% of substation energy can be saved.

As energy-efficient driving strategies with coasting controls are not applied in current ATO driving, speed trajectory optimisation should be studied to reduce the traction energy consumption. The substation energy consumption is variable due to the complex interaction between the headway, the inter-station journey time, and line receptivity. Small changes in the otherwise constant headway vary the effective use of available regenerated energy significantly. Therefore, the further research will also focus on developing various algorithms to optimise driving strategies and timetable jointly, based on the detailed energy audit simulation.

4.5 Summary

This chapter presents an energy evaluation method based on the simulation of train motion and the power network. Section 4.1 introduces the background and importance of system energy flow studies for railways. Section 4.2 illustrates the calculation of the energy flow of DC fed railway systems. In Section 4.3, the energy loss dissipated in the whole railway network is discussed. The traction energy can be reduced by 17.6% with coasting controls. The use of regenerative braking energy depends on the distance between trains. A two-train model denotes that the regeneration efficiency is 100% when the distance is within 2 km and decreases to 23% when the distance is 15 km. Based on a case study of Beijing Yizhuang Subway Line in Section 4.4, the energy consumption with different operation controls is evaluated and compared. The results indicate that regenerating trains have a significantly lower substation demand, but slightly more energy is lost within the network.

The results also denote that the available regenerative energy and total substation demand vary with the timetable, and there is a 35% difference in substation energy consumption between the best and worst headways.

Based on the results from this chapter, it is found the traction energy can be effectively reduced by optimising driving controls. Although the eco-driving has been studied for a long time, few researches have investigated the application of eco-driving. Chapter 5 presents the approaches to reducing traction energy and its applications. In Chapter 6, a system optimisation approach will be proposed, which integrates traction energy and regenerative braking energy optimisation.

Chapter 5

Traction Energy Optimisation and Its Application

5.1 Introduction

Traction energy consumption accounts for 60% to 70% of the total energy consumption in railway systems [24]. Traction energy saving using energy-efficient driving strategies is a significant area of study. The previous literature has been reviewed in Chapter 2.

Although the theory of energy-efficient driving has been studied for a long time, few of the results have been tested and used in practice [136]. In this chapter, energy-efficient train driving strategies are illustrated and a field test to validate the performance of energy saving is presented. Two optimisation methods, Brute Force (BF) and Genetic Algorithm (GA), are demonstrated and compared. These methods are used to search for the driving controls with minimum traction energy consumption subject to the journey time constraints. According to the optimal driving styles, a Driving Advisory System (DAS) is designed to advise a human driver how to achieve efficient driving. The field test was carried out on the Beijing Yizhuang Subway Line. The driver was instructed by the DAS to apply energy-

efficient driving controls. The energy consumption with typical current driving and optimal driving were recorded during the field test.

5.2 Energy-efficient Driving Modelling

5.2.1 Train Driving Controls

Train movement modelling was introduced in Chapter 3. With the fixed train and route parameters, the train speed trajectory is produced by driving controls. Energy-efficient driving has been studied for a long time, and coasting control has been proved to be an energy-efficient operation by the Pontryagin maximum principle [38, 137]. Train movement operation in this thesis includes motoring, cruising, coasting and braking. In the study of energy-efficient driving controls, it is proved that maximum tractive and braking power should be applied when the train is motoring and braking for the best energy savings [40, 41]. The partial tractive power operation is only used when the train is cruising. As for a long and complex interstation distance route (with multiple speed limits, or many gradient changes, for example), multiple cruising and coasting controls may achieve better energy-efficiency compared with single cruising and coasting controls. However, with the typical characteristics of metro systems, the distance to the next station is generally short. While multi-coasting commands are possible, in practice single cruising and coasting controls have been shown to achieve good energy efficiency [29]. Therefore, in this thesis, the train speed trajectory is produced by two single dynamic inputs, the cruising and coasting speeds. Figure 5.1 illustrates the structure of the motion simulation with the fixed and dynamic inputs.

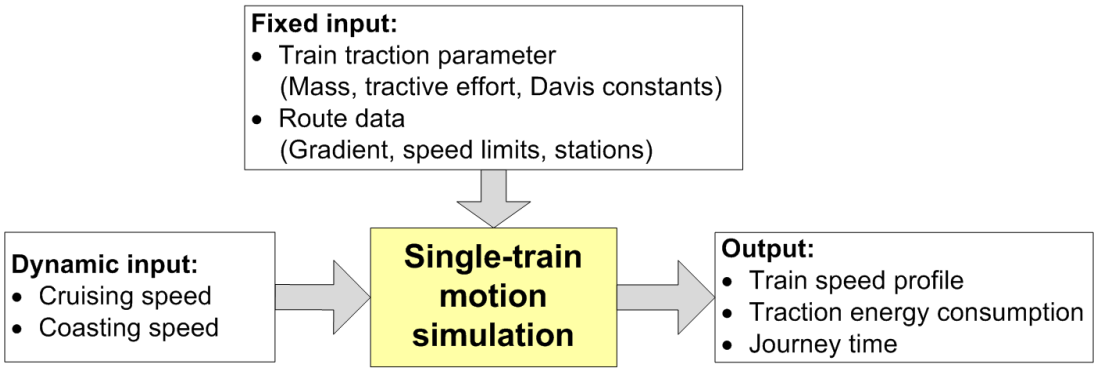

Figure 5.1 Structure of train motion simulation

The cruising speed is defined as the speed at which the train starts its cruising phase, while the coasting speed is defined as the speed when the train finishes its coasting phase and changes to braking. A sample of a train speed profile is shown in Figure 5.2. The cruising speed and coasting speeds are 70 and 50 km/h, respectively. From the tractive power curve in Figure 5.2, it can be found that, when the train is motoring, the tractive power increases to the maximum tractive power. Partial tractive power is applied when the train is cruising. No tractive power is required when the train is coasting or braking.

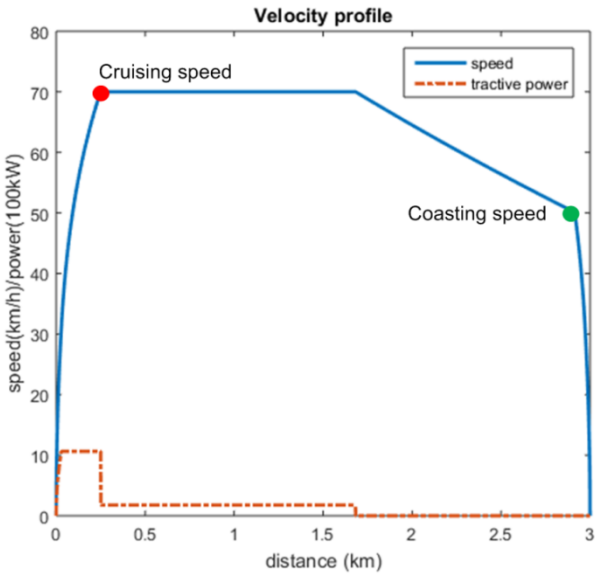

Figure 5.2 A sample of speed trajectory with driving controls

5.2.2 Traction Energy Consumption

The tractive energy consumption depends on the driving controls including cruising speed and coasting speed, as shown in equation (5.1), where f defines the relationship between the two driving controls and the traction energy consumption calculated using the simulator.

$$E_{traction} = f(v_{cr}, v_{co}) \tag{5.1}$$

Where:

- $E_{traction}$ is the train electrical traction energy consumption;
- v_{cr} is the cruising speed;
- v_{co} is the coasting speed.

The train running time is expressed in equation (5.2), where g represents the simulation process to calculate the train running time.

$$T = g(v_{cr}, v_{co}) \tag{5.2}$$

Where:

- T is the running time.

Train energy consumption can be traded off against running time. In theory, energy consumption is relatively reduced when running time increases. Figure 5.3 illustrates this formulation graphically. Each point in Figure 5.3 represents the energy consumption against running time resulted by a random driving control. The best driving operations with

the lowest energy consumption for each second are shown in red, which constitute the bottom line of the driving results.

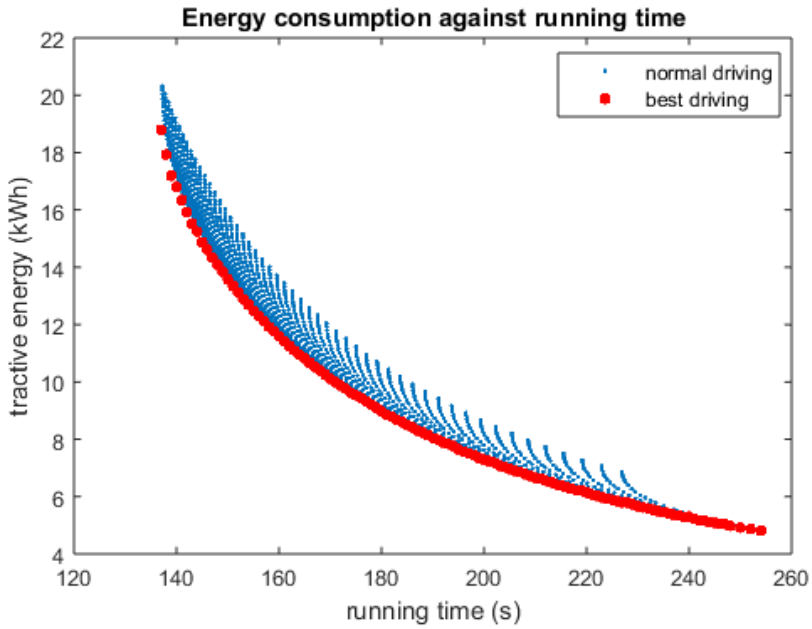

Figure 5.3 Result of energy consumption on running time

Train traction energy optimisation aims to reduce energy consumption within the running time constraints. An example of driving operations with three different driving patterns is shown in Figure 5.4. All three operations take the same running time but have different energy consumption costs. From the speed trajectory curves, the first driving cruises at the highest speed (80 km/h) and coasts until it reaches the lowest speed (48 km/h), while the third driving cruises at the lowest speed (66 km/h) and coasts until it reaches the highest speed (56 km/h). However, the second driving costs the lowest energy, followed by the first driving. The tractive energy profile shows the energy consumption during the running. As shown in Table 5.1, the first driving with a higher cruising speed costs more motion energy loss (5.95 kWh). This is because the high-speed running increases the motion resistance. With the same journey time, a high cruising speed leads to low coasting speed

and late braking. Thus, the kinetic energy may be reduced, which is 1.91 kWh for the first driving. As for the third driving, the motion loss is lower, but the kinetic energy is higher resulting in the highest total tractive energy consumption. Therefore, a balance between cruising speed and coasting speed needs to be considered, and the best combination should be found.

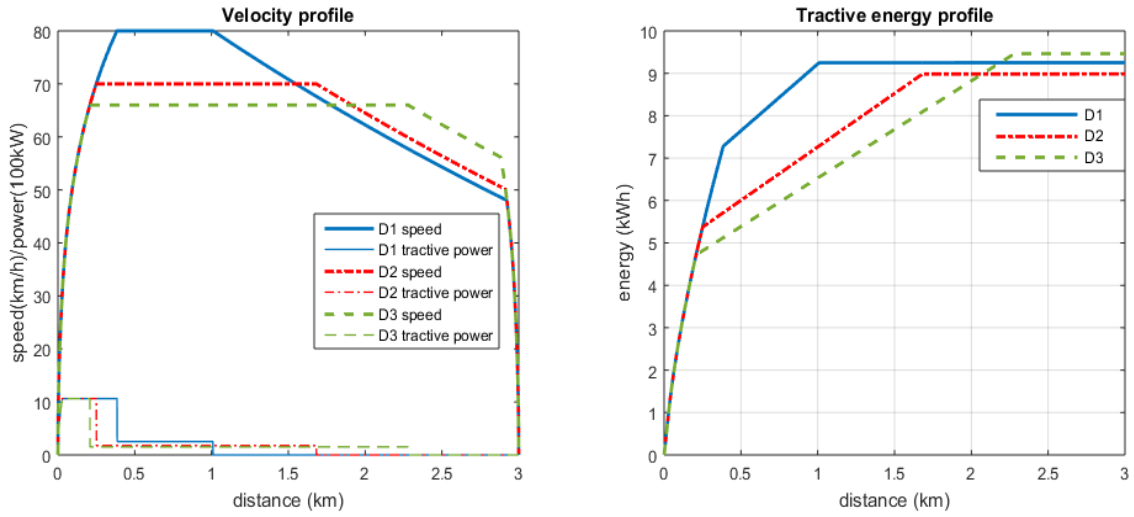

Figure 5.4 Speed and energy diagram of different driving patterns

Table 5.1 Results of different driving patterns

Driving pattern	**D1**	**D2**	**D3**
Distance (km)	3	3	3
Journey time (s)	180	180	180
Cruising speed (km/h)	80	70	66
Coasting speed (km/h)	48	50	56
Traction energy (kWh)	9.25	8.98	9.46
Traction loss (kWh)	1.39	1.35	1.42
Motion loss (kWh)	5.95	5.55	5.45
Kinetic energy (kWh)	1.91	2.08	2.59

5.3 Train Driving Optimisation

5.3.1 Fitness Function

In this thesis, the aim of the train driving optimisation is to search the most appropriate driving controls (cruising speed and coasting speed) to minimise the train energy consumption, given in equation (5.1). The running time is a significant factor in evaluating the performance of energy-efficient driving. The timetable and journey time are regulated by operation companies, based on the passenger demands. The variation of the running time is limited to the regulations. The difference between the actual and scheduled running time is given in equation (5.3). For most of the metro systems, each interstation running time is allowed within 5 seconds.

$$T_{\mathrm{d}} = |T - T_{\mathrm{sh}}| \tag{5.3}$$

Where:

- T_{d} is difference between train running time and scheduled running time;
- T_{sh} is train scheduled running time.

The fitness function with running time constraints of the optimisation is shown in equation (5.4).

$$\begin{cases} min & E_{traction} = f(v_{cr}, v_{co}) \\ s.t. & T_d \leq T_{to} \end{cases} \tag{5.4}$$

Where:

- T_{to} is the tolerance between train running time and scheduled running time.

5.3.2 Brute Force Algorithm

Brute Force (BF) search, also known as exhaustive search, is a straightforward approach to solving problems in the area of computer science by enumerating all the possibilities in the solution domain to find the optimum [138, 139]. As an exact algorithm, BF guarantees to find the optimal solutions if they exist. However, the cost of BF is proportional to the number of candidate solutions, which increases rapidly with the size of the problem. Consequently, it is widely used when the problem size is limited, such as selection sort problems and simple optimisation [140]. In order to minimise this weakness, an enhanced BF searching method was developed to address the complexity problem by constraining the solution domain [34, 141].

In order to limit the possibilities in the solution domain, all the cruising and coasting speeds are assumed as integers. The enhanced BF algorithm used to solve this optimisation is shown in following steps:

- **Step 1: Find the range of the cruising speed within the running time constraints.** The cruising speed range is obtained when coasting mode is not implemented. The shortest running time is achieved by maximum cruising speed. The maximum cruising speed is up to the train maximum speed, as shown in equation (5.5). In order to finish the journey before the running time constraint, the minimum cruising speed can be obtained by equation (5.6).

$$v_{cr\_max} = v_{max} \tag{5.5}$$

$$T_{sh} + T_{to} = g(v_{cr\_min}) \tag{5.6}$$

- **Step 2: Find the range of the coasting speed within the running time constraints.** The maximum cruising speed is up to the train maximum speed, as shown in equation (5.7). The minimum coasting speed occurs when the cruising speed reaches the maximum. The running time fulfils the time constraints as shown in equation (5.8).

$$v_{co\_max} = v_{max} \tag{5.7}$$

$$T_{sh} + T_{to} = g(v_{cr\_max}, v_{co\_min}) \tag{5.8}$$

- **Step 3: Enumerate all possible solutions in the reduced solution domain.** The traction energy consumption and running time can be calculated by each combination of possible cruising and coasting speed, as in equation (5.9).

$$\begin{cases} E_{ij} = f(v_{cr\_i}, v_{co\_j}) \\ T_{ij} = g(v_{cr\_i}, v_{co\_j}) \\ v_{cr\_min} \le v_{cr\_i} \le v_{cr\_max} \\ v_{co\_min} \le v_{cr\_j} \le v_{co\_max} \end{cases} \tag{5.9}$$

- **Step 4: Rank the solutions with constraints and find the result.** The solutions will be discarded if the running time constraints are not achieved. Within the constraints, the solution with the lowest energy consumption will be assumed as the result.

5.3.3 Genetic Algorithm

A Genetic Algorithm (GA) is a metaheuristic optimisation algorithm inspired by the theory of evolution [142, 143]. A GA employs bio-inspired operators to model the natural evaluation process, such as mutation, crossover and selection. From a population of individuals, the next generation of solutions is obtained iteratively according to their quality, until the termination criterion is met [144]. As a heuristic optimisation algorithm, a GA is commonly used to solve problems with a large amount of candidate solutions, where numerical optimisation approaches are not effective. The drawback of heuristic optimisation algorithms is that the final solution cannot be proved as optimal. The local optimal solution could be found if the evolution process of GA is not effective.

The fitness function is important to the quality of the outputs. The best solution may not be selected if the solution possibilities are evaluated improperly. In order to improve the performance of a GA, the objective function to evaluate the solutions is given in equation (5.10). The energy consumption and punctuality penalty are taken into consideration. The weighting coefficients for energy and punctuality are given in equation (5.11). The weighted rate of energy consumption is assumed as a constant with 1. However, the weighted rate for running time difference is a flexible figure, which depends on the amount of punctuality. When the time difference exceeds the running time tolerance, the weighed rate is assumed as 1. It is reduced to 0.5 when the time difference is within the running time tolerance. This objective function with fuzzy logic enables the selection process to occur more intelligently [27].

$$J = \omega_{\mathrm{E}} \times E_{traction} + \omega_T \times T_{\mathrm{d}} \tag{5.10}$$

$$\begin{cases} \omega_E = 1 \\ \omega_T = \begin{cases} 1 & if\ T_{\mathrm{d}} > T_{to} \\ 0.5 & if\ T_{\mathrm{d}} \leq T_{to} \end{cases} \end{cases} \tag{5.11}$$

Where:

- ω_E is the weighted rate for energy consumption;
- ω_T is the weighted rate for running time difference.

The objective function is calculated by the cruising and coasting speed. Therefore, a solution contains (v_{cr}, v_{co}), which are presented as the 'chromosome' of an individual. A GA generates an initial population of individuals randomly. As the population size is suggested to be not less than five times the number of variables [145], the size of the population is set to 40 in this thesis. All the individuals are evaluated and ranked by objective function. The parents for the generation reproducing are chosen by selection operation. The selection is done by 'roulette', which is simulated as a roulette wheel with the area of each segment proportional to its fitness. The next generation are reproduced by elite count, crossover and mutation. By elite count, a number of top individuals are guaranteed to survive to the next generation. The others in the next generation are generated by crossover and mutation of the selected parents. The operation of mutation improves the performance of optimisation by reducing the possibility of local optimisation. The proportions of the next generation produced by elite count, crossover and mutation are 5%, 80% and 15%, respectively. The procedure of the GA for traction energy optimisation is shown in Figure 5.5.

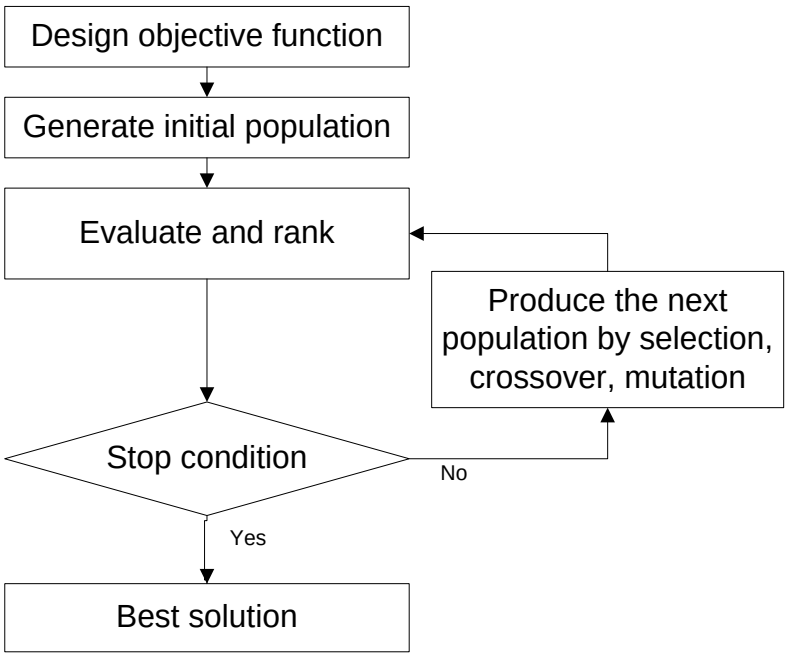

Figure 5.5 Procedure of a GA

5.3.4 Energy-efficient Driving Application

The Driver Advisory System (DAS) is used to deliver optimal driving controls for reducing operating costs, improving energy efficiency and train regulation [146]. DAS is among the latest methods in railway smart operation, which links theoretical optimisation techniques with practical operation [147]. In order to assist human drivers to apply energy-efficient driving strategies in the field test, a stand-alone DAS is designed [148]. The stand-alone DAS is calculated predominately based on static route data and the timetable, which will instruct drivers to achieve different driving controls on time. An example of an optimal speed trajectory in the time-domain is shown in Figure 5.6, converted from the profile in the distance-domain in Figure 5.2.

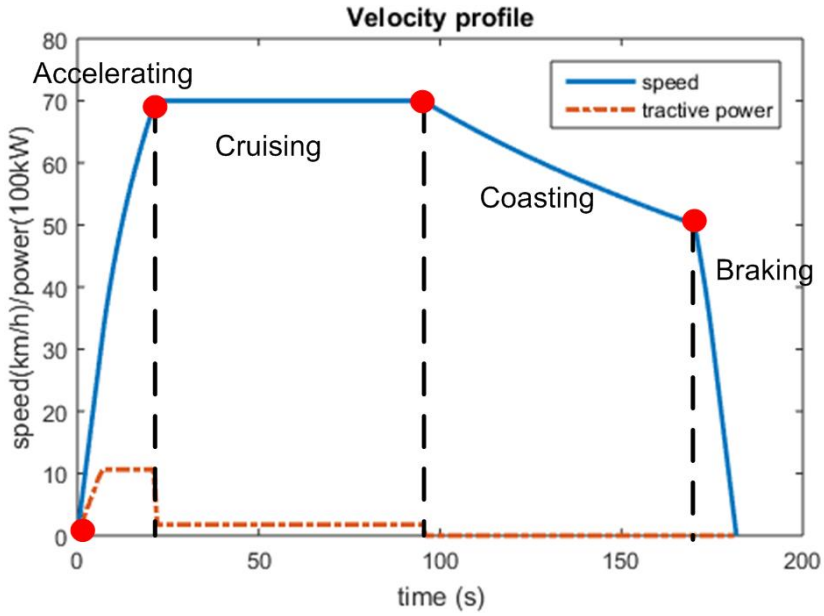

Figure 5.6 A sample of time-domain velocity profile

Based on the location and time information, the driving mode changing instructions are collected as shown in Figure 5.7. The DAS normally contains four stages, including the information for acceleration, cruising, coasting and braking. The first slide shows that the current driving mode is acceleration. From the first slide, the driver can also find that the next driving mode is cruising. In order to instruct the driver to apply the next control, the target speed and target distance are shown, which are 70 km/h and 250 m, respectively. Also, a timer is set up, which informs drivers to switch to the next driving mode after 22 seconds. Similarly, the following slides can instruct drivers to achieve efficient driving controls.

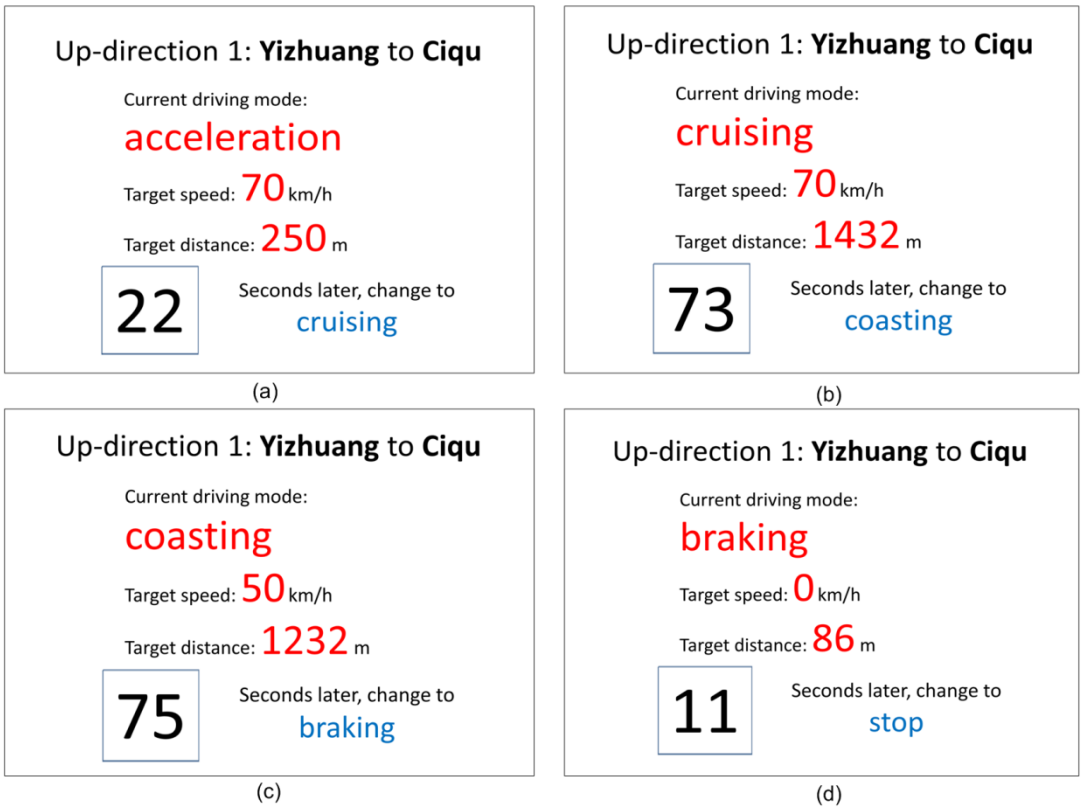

Figure 5.7 DAS instruction for the sample driving

5.4 Case Study

5.4.1 Modelling Formulation

The mathematical model is developed based on the data of Beijing Yizhuang Subway Line. Brute Force algorithm and a GA are used to optimise the train speed trajectory for traction energy saving. To meet the requirement of passenger comfort, the maximum acceleration is set at 1 m/s^2, and the maximum deceleration is 0.55 m/s^2. In order to minimise the impact of the timetable rescheduling, the tolerance of the train running time and scheduled running time is set to 1 second in this case.

5.4.2 Traction Energy Optimisation

The traction energy optimisation approach is used for each interstation journey. The first interstation journey from Yizhuang to Ciqu is presented as an example to illustrate the performance of algorithms.

5.4.2.1 BF

The scheduled running time for this interstation is 105 s. The range of the running time constraints for the BF algorithm is from 104 to 106 s. The cruising speed ranges from 60 to 80 km/h while the coasting speed ranges from 52 to 80 km/h. There are 609 possibilities in the solution domain. It takes 10.3 seconds to evaluate all the possibilities by a computer with 3.4 GHz CPU and 8 GB RAM. The 10 best results of driving are shown in Table 5.2. The top ranking one is selected as the best driving profile.

Table 5.2 Top 10 results by BF algorithm

Rank	Cruising speed (km/h)	Coasting speed (km/h)	Running time (s)	Electrical tractive energy (kWh)	Electrical braking energy (kWh)
1	69	54	104.71	10.10	5.64
2	70	55	104.09	10.35	5.83
3	67	52	105.77	11.16	6.41
4	66	52	105.97	11.23	6.46
5	68	53	105.07	11.34	6.54
6	67	53	105.24	11.43	6.60
7	66	53	105.50	11.51	6.65
8	65	53	105.84	11.57	6.71
9	68	54	104.56	11.62	6.73
10	67	54	104.79	11.70	6.78

5.4.2.2 GA

Table 5.3 presents the final result from the GA. The running time meets the criteria of the scheduled journey time, while the energy consumption is close to the result found using the BF algorithm. Figure 5.8 demonstrates the fitness evaluation of the GA. The population size is set to 40. The fitness converges with the generation and stops at the 50th generation. It takes 34.3 seconds using a computer with 3.4 GHz CPU and 8 GB RAM, where 2000 possibilities are evaluated.

Table 5.3 Best result from the GA

Cruising speed (km/h)	**Coasting speed (km/h)**	**Running time (s)**	**Electrical tractive energy (kWh)**	**Fitness value**
69.06	54.32	104.53	10.14	10.35

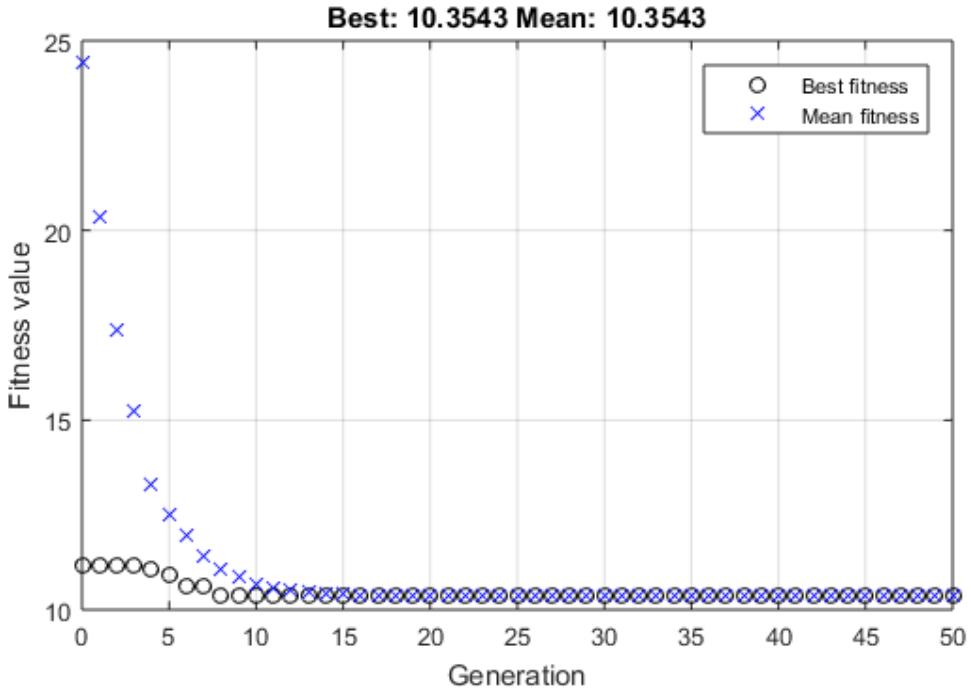

Figure 5.8 Mean and best outputs at each generation

5.4.2.3 Optimisation Results

Both algorithms can achieve good results. Using GA takes a longer computing time since more possibilities are evaluated. There are two variables for the optimisation of one single interstation. The number of possibilities is limited, which makes BF more efficient. Therefore, the BF algorithm is used for searching energy-efficient driving controls for the rest of the single journeys. The optimal driving speed trajectory is shown in Figure 5.9 and Figure 5.10. Coasting driving control is used a lot, which can be verified from the mechanical power curves where the power is zero. The running time and energy consumption results for each interstation are detailed in Table 5.4 and Table 5.5.

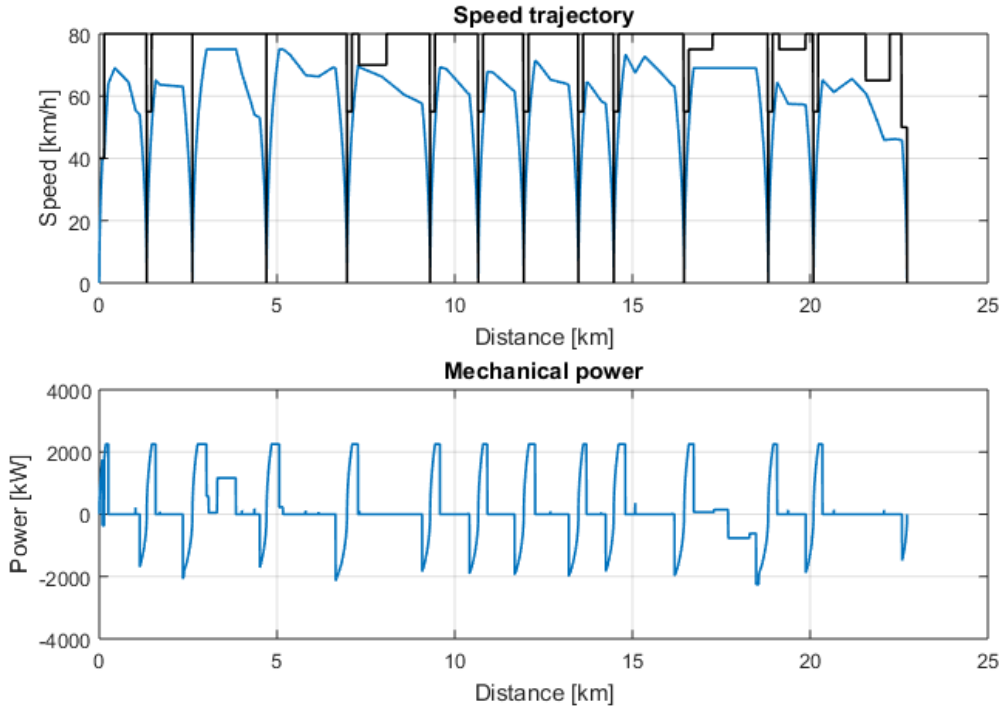

Figure 5.9 Optimal driving profiles by simulation for up-direction

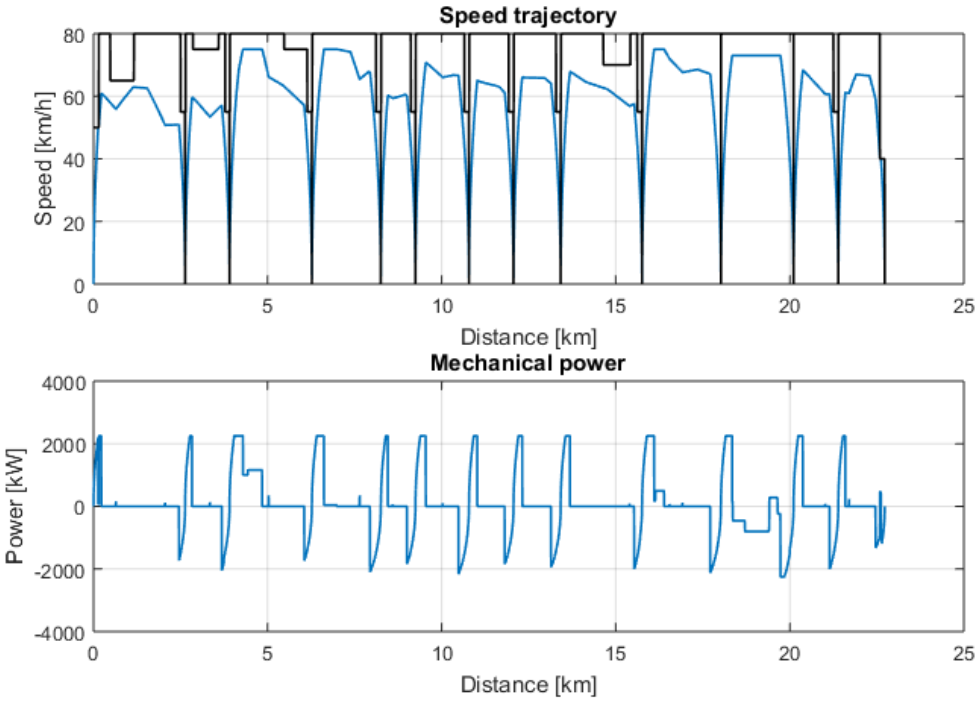

Figure 5.10 Optimal driving profiles by simulation for down-direction

Table 5.4 Journey time and energy for up-direction

	Station	Scheduled running time (s)	Running time (s)	Electrical tractive energy (kWh)	Electrical braking energy (kWh)
1	Yizhuang	-	-	-	-
2	Ciqu	105	104.71	10.10	5.64
3	Ciqunan	101	100.99	12.32	7.24
4	Jinghailu	140	139.61	28.35	5.24
5	Tongjinanlu	148	147.98	16.62	8.83
6	Rongchang	160	159.95	14.73	6.18
7	Rongjing	103	102.85	13.21	6.83
8	Wanyuan	99	98.69	12.38	7.01
9	Wenhuayuan	113	112.84	14.96	7.54
10	Yizhuangqiao	85	84.92	11.24	6.18
11	Jiugong	134	133.61	15.11	7.43
12	Xiaohongmen	155	153.01	14.47	16.37
13	Xiaocun	104	103.84	12.29	6.19
14	Songjiazhuang	193	192.72	12.38	3.90
	total	1640	1635.71	188.17	94.59

Table 5.5 Journey time and energy for down-direction

	Station	**Scheduled running time (s)**	**running time (s)**	**Electrical tractive energy (kWh)**	**Electrical braking energy (kWh)**
1	Songjiazhuang	-	-	-	-
2	Xiaocun	190	189.97	10.46	5.08
3	Xiaohongmen	106	105.99	10.02	6.47
4	Jiugong	156	155.92	26.93	5.76
5	Yizhuangqiao	131	130.81	16.12	8.51
6	Wenhuayuan	86	85.68	10.09	6.52
7	Wanyuan	112	111.64	14.06	8.64
8	Rongjing	100	99.72	11.72	6.64
9	Rongchang	103	102.82	12.23	7.48
10	Tongjinanlu	163	162.22	12.87	6.67
11	Jinghailu	147	146.85	17.92	8.58
12	Ciqunan	135	134.87	16.09	19.81
13	Ciqu	100	99.92	12.84	7.20
14	Yizhuang	103	102.98	10.55	5.32
	total	1632	1629.40	181.90	102.69

5.4.3 Field Test

In order to compare the energy consumption of normal driving and energy-efficient driving, a field test was carried out on the Beijing Yizhuang Subway Line in September 2014. The field test started at midnight when service trains returned back to the depot. Several cycles of no-load driving were recorded, including normal driving by ATO and human driver, as well as energy-efficient driving with the DAS. Figure 5.11 shows the case when a human driver drove the train following the instruction from the DAS. The DAS is implemented by the laptop, which is placed on the left-hand side of the cab desk.

Figure 5.11 Photograph of efficient driving field test with DAS

The actual driving operation data was obtained from the on-board Train Information Measurement System (TIMS), including time, speed, power, and energy consumption. The driving results by the current ATO are illustrated in Section 4.4.2. Figure 5.12 and Figure 5.13 present the train speed and power profiles by a human driver with instruction from the DAS. It can be observed that the coasting control has been used by the driver. However, sometimes the driver used motoring and braking controls during the journey to maintain the speed, which may consume more energy. This is supposed to be improved by practice. The running time and energy consumption results for each interstation are detailed in Table 5.6 and Table 5.7.

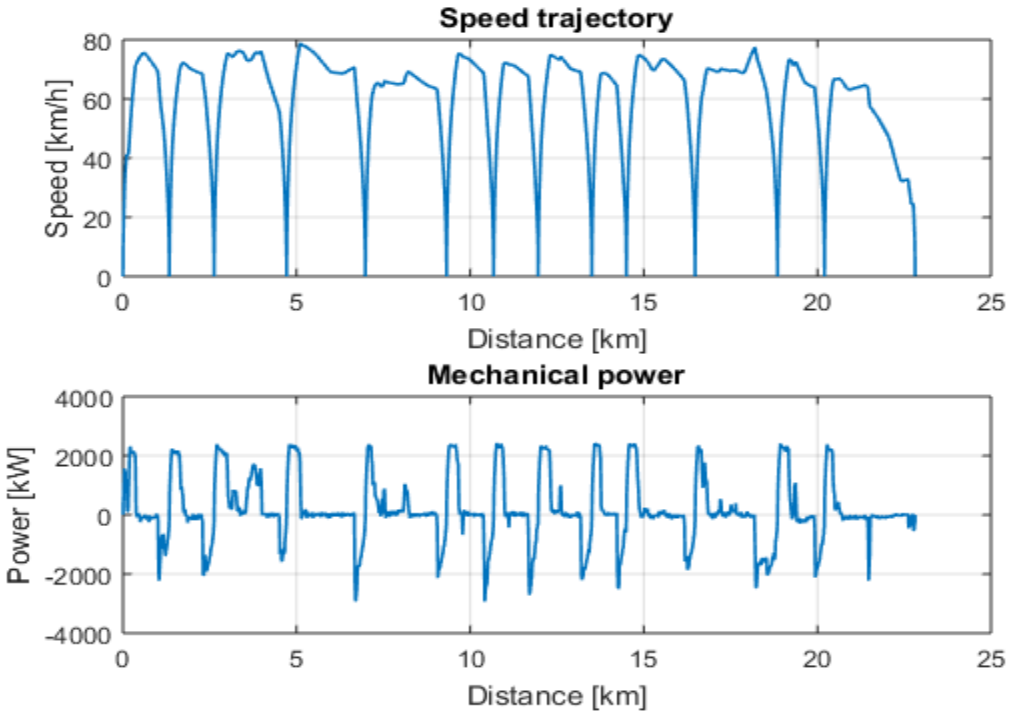

Figure 5.12 Energy-efficient driving profiles by human for up-direction

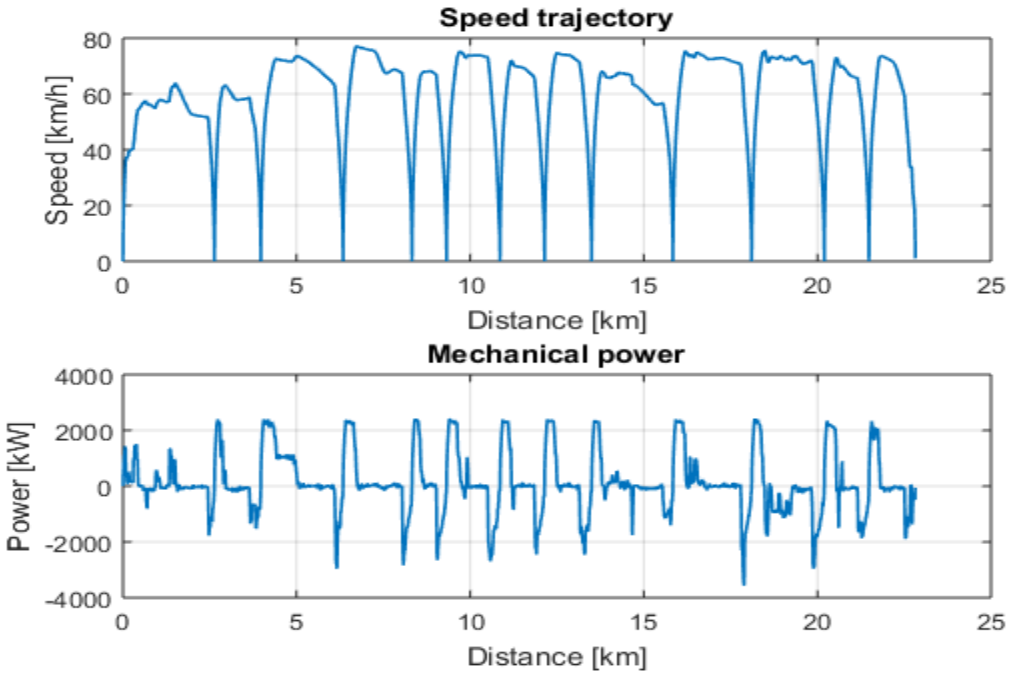

Figure 5.13 Energy-efficient driving profiles by human for down-direction

Table 5.6 Journey time and energy for up-direction

	Station	Scheduled running time (s)	Real journey time (s)	Electrical tractive energy (kWh)	Electrical braking energy (kWh)
1	Yizhuang	-	-	-	-
2	Ciqu	105	103	14	8
3	Ciqunan	101	95	17	10
4	Jinghailu	140	138	29	6
5	Tongjinanlu	148	144	19	9
6	Rongchang	160	156	17	8
7	Rongjing	103	99	16	9
8	Wanyuan	99	96	15	9
9	Wenhuayuan	113	110	18	9
10	Yizhuangqiao	85	82	13	9
11	Jiugong	134	131	17	8
12	Xiaohongmen	155	153	15	18
13	Xiaocun	104	103	17	8
14	Songjiazhuang	193	215	15	4
	total	1640	1625	222	115

Table 5.7 Journey time and energy for down-direction

	Station	Scheduled running time (s)	Real journey time (s)	Electrical tractive energy (kWh)	Electrical braking energy (kWh)
1	Songjiazhuang	-	-	-	-
2	Xiaocun	190	203	15	5
3	Xiaohongmen	106	106	12	7
4	Jiugong	156	206	30	7
5	Yizhuangqiao	131	135	17	9
6	Wenhuayuan	86	71	12	9
7	Wanyuan	112	113	17	11
8	Rongjing	100	100	15	9
9	Rongchang	103	101	15	11
10	Tongjinanlu	163	162	16	7
11	Jinghailu	147	145	20	10
12	Ciqunan	135	135	14	18
13	Ciqu	100	103	15	8
14	Yizhuang	103	105	15	8
	total	1632	1625	213	119

5.4.4 Result Analysis

The speed and power profiles using different driving styles from Yizhuang to Ciqu are presented in Figure 5.14, while the energy consumption results are shown in Table 5.8.

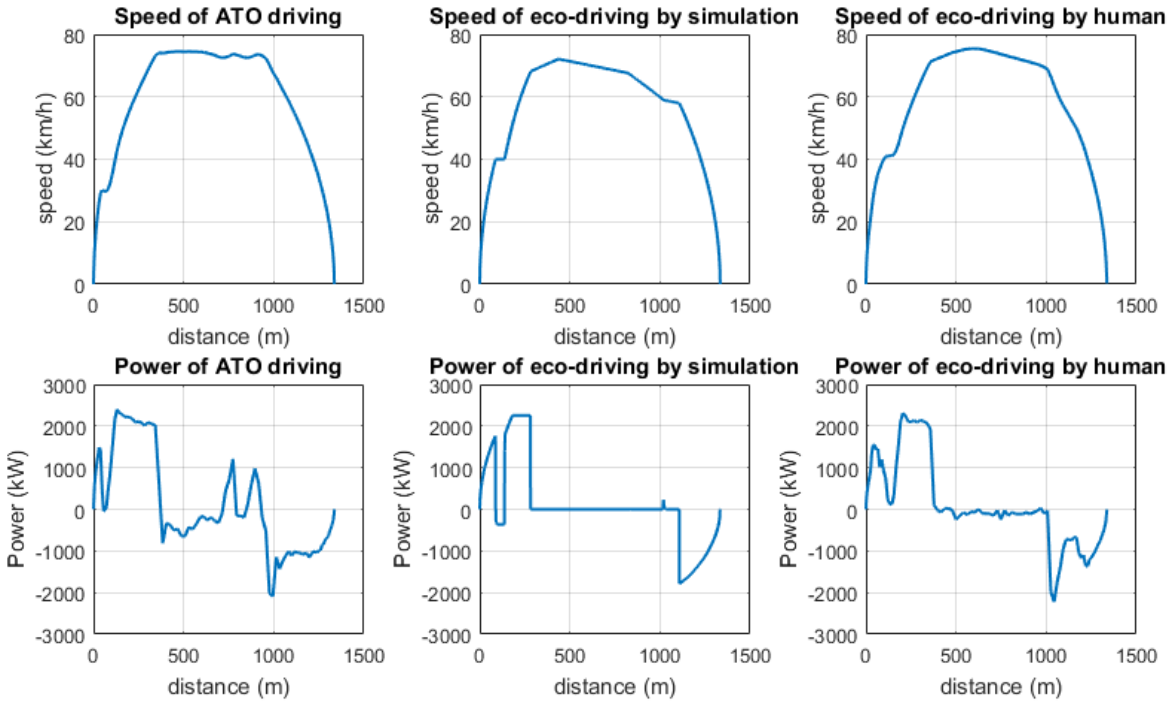

Figure 5.14 Comparison of different driving styles

Table 5.8 Energy results of different driving styles

	Current ATO driving	Efficient driving by simulation	Efficient driving by human
Running time [s]	101	103	103
Electrical tractive energy [kWh]	16	10.9 (-32%)	14 (-13%)
Electrical braking energy [kWh]	9	6.2	8

From the curve of current ATO driving, it can be seen that there is no coasting operation during the journey. When the train reaches 75 km/h, ATO tries to maintain this speed by switching between partial braking and motoring. Finally, the ATO applied braking in order to stop the train at the platforms.

As for the optimal driving by simulation, the train accelerates to 40 km/h and cruises at this speed due to the speed limit. Then the train accelerates to 70 km/h until coasting. When the train is coasting, no tractive power is required. The speed depends on the route gradient and motion resistance only. During coasting, the train speed increases for a while and then decreases. Finally, the train starts braking at 57 km/h. The traction energy consumption is reduced by 32%, compared with current ATO driving, whereas the running time is increased by 2 seconds (around 2% increase).

From the curve of human driving, it is obvious that the human driver applied the coasting control during the journey. But the driver started coasting a little later than the optimal driving and braking a little earlier. Due to the early braking, he had to reduce the braking rate in order to stop at the platform correctly. Because of the slight difference between human driving and simulation optimal driving, the energy consumption was increased. However, compared with current ATO driving, 13% of the final traction energy consumption was still saved.

The energy consumption for each interstation journey is compared in Figure 5.15. It is obvious that the ATO driving costs the highest energy for each interstation, followed by human driving using energy-efficient strategies. The rate of energy saving between ATO driving and human driving for each interstation is not the same, which is determined by a number of factors including route gradients, speed limits, scheduled running time and so

forth. The energy consumption of the driving by simulation is lower than human driving. The difference is caused by the fact that optimal controls can only be achieved by the simulator. The same pattern can be found in the down direction.

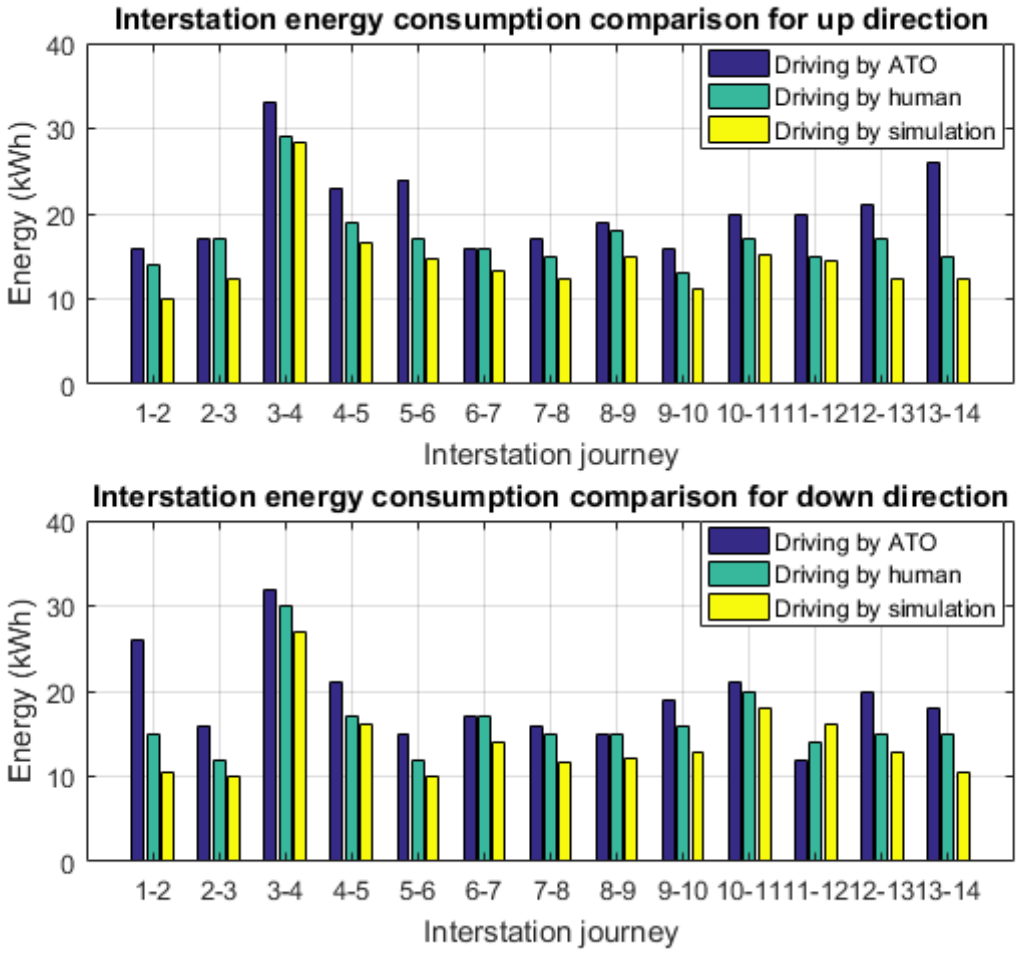

Figure 5.15 Interstation energy comparison

Figure 5.16 reports the comparison of accumulative energy consumption. With the increase in the number of stations, the difference between accumulative energy consumption of driving by ATO and a human driver increases. The difference between the accumulative energy consumption of driving by ATO and simulation increases more significantly with the number of stations. This evidence further supports that a significant amount of energy

consumption can be saved by the simulation. The same pattern can be found in the down direction.

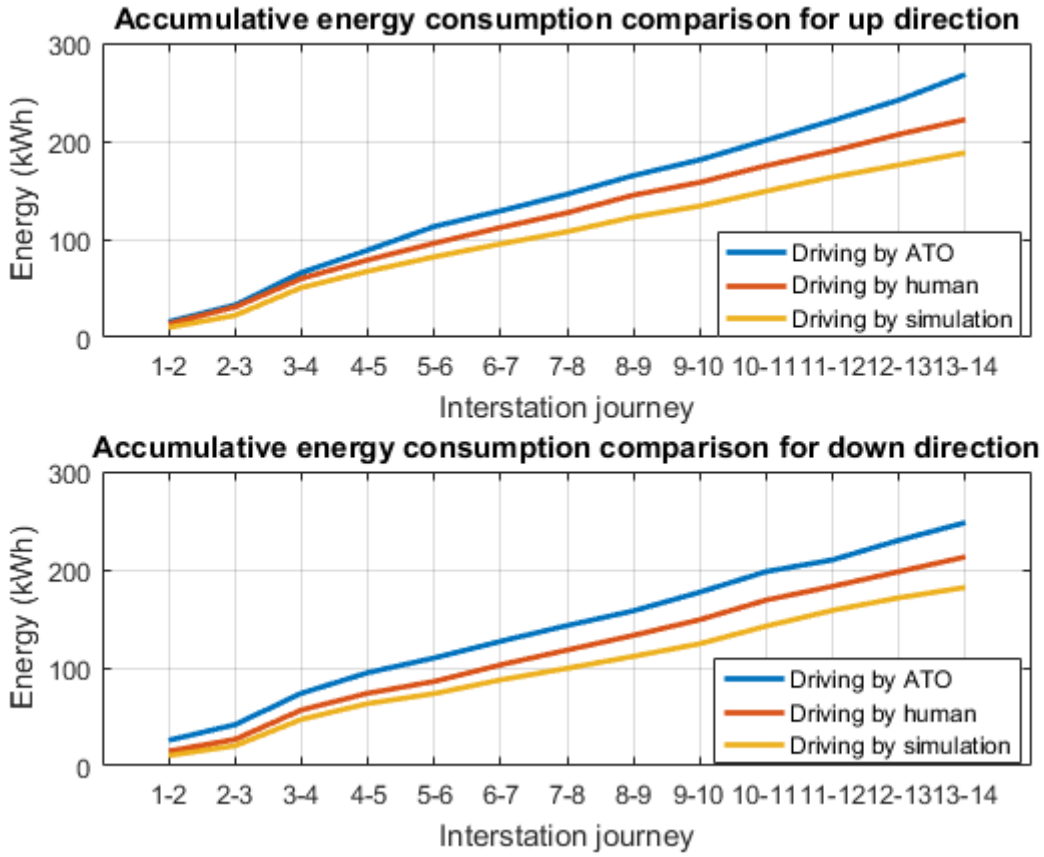

Figure 5.16 Accumulative energy comparison

In Table 5.9, the total energy consumption and running time for a full cycle are compared. The running time of the current ATO driving is shortest, which is 26 seconds shorter than human driving and 41 seconds shorter than simulation driving. The running time of simulation driving meets the requirement of the scheduled journey time which is 3272 seconds. With the slight running time sacrifice, the performance in terms of energy saving is significant. Compared with the energy consumed by ATO driving, 16% of energy can be saved by human driving with optimisation strategies, while 28% can be saved by

simulation driving. The driver utilised energy-efficient driving strategies, which were obtained from the simulation. The simulated energy consumption is about 12% lower than the human driving. This is mainly because this field test was the first time that the driver had utilised energy-efficient driving strategies. The driver tried to follow the suggested controls but differences between human driving and the suggested controls still exist. With practice, human driving skills could be improved and energy consumption could be reduced.

Table 5.9 Total energy consumption and running time results

	Current ATO driving	Efficient driving by human	Efficient driving by simulation
Running time [s]	3224	3250 (+26)	3265 (+41)
Electrical tractive energy [kWh]	516	435 (-16%)	370 (-28%)
Electrical braking energy [kWh]	288	234	197

Based on the results of the field test, human driving using energy-efficient strategies could reduce 81 kWh of traction energy per cycle. Trains run 121 cycles each day on the Beijing Yizhuang Subway Line. The annual energy saving could be up to 3577 MWh. If the electricity price is assumed as 10 pence/kWh, the annual traction energy cost could be reduced by £358 k. Therefore, the approach illustrated in this chapter is proved as an applicable and effective solution to reduce traction energy consumption in railway systems.

5.5 Summary

This chapter presents a methodology to optimise traction energy by searching efficient driving strategies. The modelling of train driving controls with cruising and coasting controls is illustrated in Section 5.2. The energy consumption with respect to the driving operation can be calculated. Section 5.3 demonstrates two optimisation algorithms including Brute Force and a Genetic Algorithm for searching optimal controls. Both algorithms could find the optimal driving controls within journey time constraints. However, Brute Force is more effective as there are limited variables in the single train driving study. In Section 5.4, a field test is presented to validate the performance of energy saving in the Beijing Yizhuang Subway Line. A Driver Advisory System (DAS) has been designed to instruct the train driver to apply optimal driving strategies. The energy consumption of current driving without efficient strategies and eco-driving with the DAS were measured. Theoretically, the ratio of energy savings is 28% based on the results from simulation. In practice, the human driving with the instruction from DAS reduced the traction energy by 16%, which is still an outstanding result. The energy-saving performance could be improved further when the driver is familiar with the controls. Based on the result of the field test, the annual energy saving could be 3577 MWh, which is equivalent to saving £358 k per year.

The approach to reducing traction energy consumption is illustrated in this chapter. In order to reduce the system energy consumption, timetable optimisation should be considered. The next chapter will addresses the driving strategy and timetable optimisation jointly to achieve system energy saving.

Chapter 6

System Energy Optimisation

6.1 Introduction

For metro transit systems with frequently motoring and braking trains, the effective use of regenerated braking energy is a significant way to reduce the net energy consumption. In the previous studies of energy-efficient operation in rails, traction energy reduction and regenerative energy maximisation were separated as two topics [38, 75]. The speed trajectory of the acceleration and braking phase has been studied. Timetable optimisation has been studied for energy saving [41, 79, 99]. However, most of the researches only considered the time synchronisation of adjacent trains without understanding the impact of the power traction network and the energy flow of regenerative energy.

System energy consumption is the energy consumed in substations, which is the net energy consumption of the whole railway system considering the energy used by electricity transmission and traction as well as the payback of regenerative energy. As the number of variables in optimising the system energy consumption increases, it becomes more difficult to find a solution with conventional optimisation algorithms. Monte Carlo simulation is a computerised mathematical technique which is used to determine the properties of complex systems by random samplings [149]. This method has been widely utilised to

understand the impact of risk and uncertainty in financial, physical sciences, artificial intelligence and probabilistic engineering models [150].

This chapter proposes an approach to optimising substation energy consumption by modifying interstation speed profiles and timetables. The system energy consumption statistic characteristics are studied. An 'energy factor' is defined to simplify the optimisation, based on the Monte Carlo simulation. A case study based on the Beijing Yizhuang Subway Line is used to illustrate the performance of the system energy optimisation algorithms.

This chapter is an expanded version of the studies that resulted in a conference paper 'System energy optimisation of metro-transit system using Monte Carlo Algorithm' and a journal paper 'System energy optimisation strategies for metros with regeneration', which were published in *2016 IEEE International Conference on Intelligent Rail Transportation (ICIRT)* and *Transportation Research Part C: Emerging Technologies* [151, 152]. The author of this thesis is the first author of the conference and journal paper and made the major contribution to the papers. This chapter is reproduced by permission of the Institute of Electrical and Electronics Engineers (IEEE) and Elsevier.

6.2 Overview of Substation Energy

Most of the recent studies of energy saving in railways have focused on traction energy consumption optimisation [31, 38, 40, 41]. The train driving speed trajectory was optimised to reduce the traction energy consumption. Different algorithms including a Genetic Algorithm, Brute Force, an Ant Colony Algorithm and Dynamic Programming

were utilised, which were proved to achieve good performance. With the application of the regenerative braking system in modern vehicles, the electro-braking energy was increased by optimising the braking speed trajectory [75]. However, the global energy consumption for railway systems is the energy consumed from substations. The effect on substation energy consumption by traction energy and braking energy optimisation has not been fully understood.

The substation energy consumption is computed based on the modelling of the whole power network with multiple trains. The transmission loss and train power load and regeneration are considered in the power flow analysis. Based on the simulation tools explained in Chapter 3 and Chapter 4, the relationship between substation energy consumption, traction energy consumption, and braking energy consumption is studied. Based on the data of the Beijing Yizhuang Subway Line, 10,000 driving control strategies were randomly selected and evaluated.

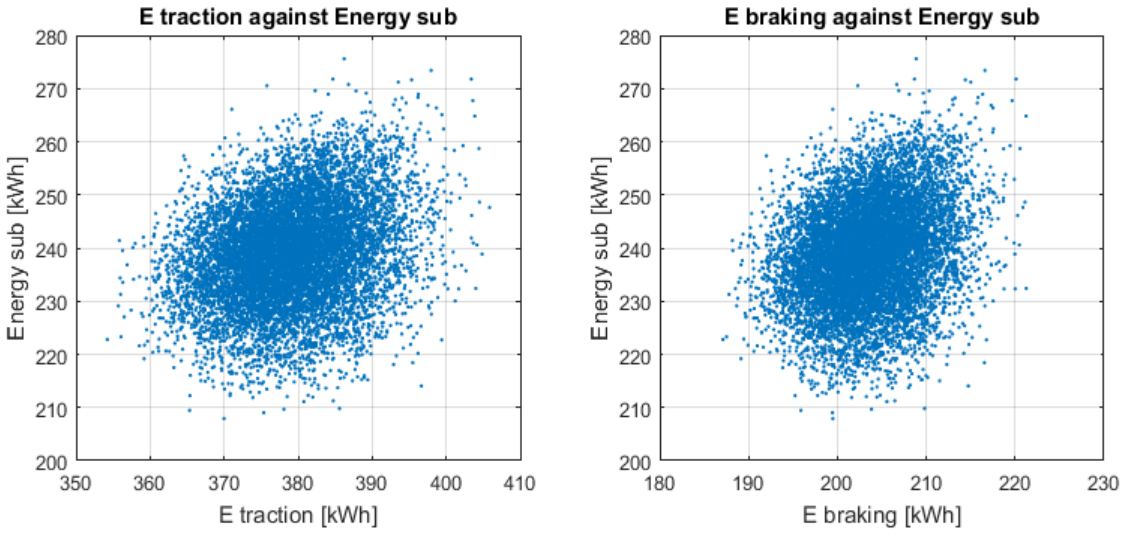

Figure 6.1 Substation energy compared with traction energy and braking energy

The energy results are shown in Figure 6.1. Each point in the left figure presents the traction against substation energy consumption for each driving control, while the right figure presents the relationship of braking against substation energy consumption. From the left figure, there is no linear relation between traction energy and substation energy. For driving styles with the same traction energy consumption, the substation energy varies by around 30%. For example, the substation energy consumption ranges from 208 kWh to 266 kWh for the driving styles with traction energy consumption of 370 kWh. The right figure shows similar results, which indicate that the driving style with high braking energy consumption does not lead to low substation energy consumption. Therefore, minimising traction energy or braking energy does not generally minimise the substation energy.

As a result, the results of traction energy optimisation or braking energy optimisation cannot be assumed as the best results to reduce substation energy consumption. The objective of metro system energy optimisation is to minimise the substation energy consumption, which is given in equation (6.1). The substation energy is the sum of train traction energy, transmission loss and substation loss subtracted by the train regenerative braking energy. The study of substation energy optimisation should be carried out based on the results from equation (6.1) by simulation evaluation.

$$E_{sub} = E_{train} - E_{regen} + E_{trans\_loss} + E_{sub\_loss} \tag{6.1}$$

Trains in a metro system run repetitively and periodically when the headway is constant. During the headway period, each train of a multi-train system finishes one part of the cycle running, and the sum of each train running is the whole cycle journey. Therefore, the sum of each train's traction energy during the headway period is actually the single train traction energy consumption of one cycle. The system energy evaluation for this study is

always the energy consumption during the headway period rather than that of the whole day's operation.

6.3 Methodology

The frequent motoring and braking operations of a metro system make the effective use of regenerative braking energy one of the most significant factors in energy saving methods. Timetable scheduling affecting the use of regenerative braking energy has significant potential for energy-efficiency techniques in metro systems. Rather than traction energy or regenerative braking energy, the substation energy consumption becomes the target of energy minimisation. With an increasing number of variables, solving the optimisation problem becomes increasingly difficult. A statistical approach is introduced to solve system energy optimisation with a number of variables.

6.3.1 Train Driving Strategies

Energy-efficient driving has been studied for a long time, and coasting control has been proved as an energy-efficient operation by the Pontryagin maximum principle [35, 38, 40] Train movement operation in this thesis includes motoring, cruising, coasting and braking. In the motoring mode, the maximal tractive effort is utilised which is always active at the beginning of the journey. The cruising mode is invoked when the train reaches the speed limit. During coasting, only auxiliary power is needed by the train and the speed only depends on the gradient and resistance to motion. The braking mode is applied when the train is approaching a stop or a lower speed limit. In this thesis, it is assumed that only

electric braking is employed in the braking mode and the maximal electric braking effort is utilised for energy-efficiency [42].

Although multiple coasting points control achieves a better energy-efficiency in a long interstation journey, there is not enough room to accommodate multi-coasting commands for the metro system where the interstation distance is short [29]. In this thesis, only one coasting point is utilised in the energy-efficient speed trajectory formulation. The travelling time between the successive stations is determined by the duration of cruising and coasting. For a given journey time there is a unique speed profile that can easily be identified. An example of possible driving speed profiles is shown in Figure 6.2. For each journey time, a speed trajectory can be generated by adjusting the cruising and coasting periods. If a shorter journey time is required, for example, 129 s, the speed profile includes a long cruising and short coasting path. By contrast, if a longer journey time is required, for example, 137 s, the speed profile includes only a coasting path but no cruising path. For each journey with a distinct journey time, there is a unique final coasting speed. Therefore, the final coasting speed can be used as a variable to formulate the speed profile.

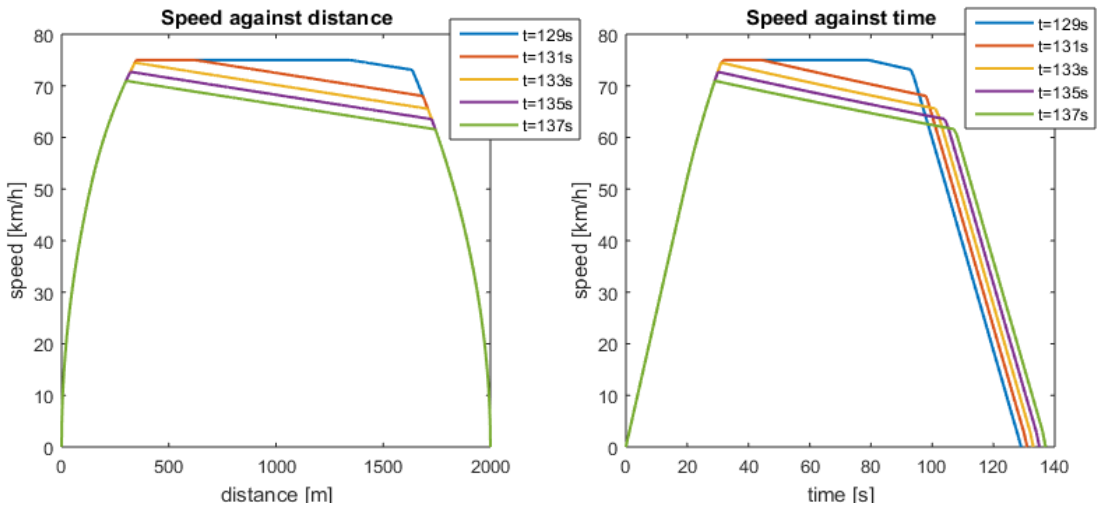

Figure 6.2 Acceptable energy-efficient speed profile

The permitted change of interstation journey time and dwell time from the nominal timetable is limited to 5 s, which is a reasonable range. The journey time and dwell times are assumed to be integers. The total running cycle time is the sum of each interstation travelling time and dwell time, as well as the turnaround time. The permitted difference of cycle journey time between the current operation and optimal operation is limited to 40 s. Turnaround time from up direction to down direction is assumed to be constant.

The combination of each interstation driving which meets the constraints is treated as one possibility. Given the headway period, the substation energy consumption for the multi-train system can be calculated by the power network simulation. The coasting ending speed and each dwell time are used as variables in this optimisation. The substation energy can be expressed in equation (6.2), where f represents the simulation process to calculate substation energy consumption by power network modelling.

$$E_{sub} = f(v_{c1_{up}}, t_{d1_{up}}, v_{c2_{up}} \cdots v_{cn_{up}}, v_{c1_{down}}, t_{d1_{down}}, v_{c2_{down}} \cdots v_{cn_{down}}) \quad (6.2)$$

Where:

- v_c is train coasting speed for each interstation;
- t_d is the dwell time at each station.

The objective of the optimisation becomes searching the best driving control set (D_{set}) within the interstation and whole journey time constraints. The fitness function is given in equation (6.3).

$$\begin{cases} min & E_{sub} = f(D_{set}) \\ s.t. & T_d \leq T_{to} \end{cases} \quad (6.3)$$

Where:

- D_{set} is driving control set including driving information of each interstation;
- T_{d} is difference between train running time and scheduled running time;
- T_{to} is the tolerance between train running time and scheduled running time.

6.3.2 Substation Energy Estimation

The calculation of substation energy consumption requires complex procedures by the power network simulator. It takes a significant amount of time to solve the power flow analysis problem of given operation controls. Therefore, searching for the optimal control set with the lowest substation energy from all possible controls is practically impossible. If it is possible to find a correlation between quantities that can be found quickly and the substation energy consumption, an 'energy factor', then this energy factor can replace the substation energy consumption to become the minimisation objective. In this way, the system energy optimisation problem can be solved by doing a full power flow analysis only on a limited number of candidate solutions that have been pre-selected according to some other easily computed quantity. It is, in effect, a heuristic.

The concept of the overlap of traction power and braking power is proposed to solve the system energy optimisation problem. Overlap power is the minimum value of the sum of all tractive train power and sum of all braking train power at each time step, as shown in equation (6.4).When there is a higher tractive power requirement, the voltage level does not exceed the overvoltage protection limit. Most of the electrical braking power can be transferred into the overhead line. One example of the traction power, braking power and regenerative power relation for all trains at different times is shown in Figure 6.3. The

overlap power is never more than the actual externally regenerated power. The overlap energy is the integral of overlap power over the time, as shown in equation (6.5). The overlap energy can be used to predict the actual regenerative energy by multiplying a regenerative energy coefficient (C_r) shown in equation (6.6). The 'C_r' can be obtained by the linear regression of overlap energy and actual regenerative energy under the whole system energy evaluation using Monte Carlo Simulation.

$$P_{overlap}(t) = min\left\{\sum_{n=1}^{N} P_{elec\_trac\_n}(t), \sum_{n=1}^{N} P_{elec\_brake\_n}(t)\right\} \tag{6.4}$$

$$E_{overlap} = \int_0^T P_{overlap}(t)\, dt \tag{6.5}$$

$$E_{regen} = C_r \times E_{overlap} \tag{6.6}$$

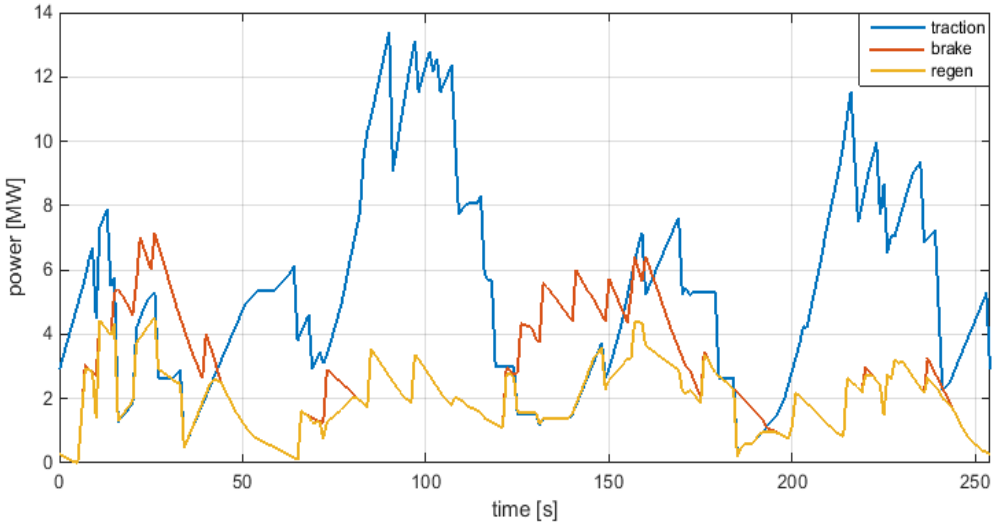

Figure 6.3 Tractive, braking and regenerative power relation

The sum of transmission loss and substation loss is the total power network energy loss shown in equation (6.7). The network loss coefficient (C_n) is used to characterise the

relation between the substation energy and network energy loss in equation (6.8). The 'C_n' can be obtained by the linear regression of substation energy supply and network energy loss under the whole system energy evaluation using Monte Carlo Simulation.

$$E_{network\_loss} = E_{trans\_loss} + E_{sub\_loss} \tag{6.7}$$

$$E_{network\_loss} = C_n \times E_{sub} \tag{6.8}$$

After the initial system energy evaluation using Monte Carlo Simulation, two coefficients 'C_r' and 'C_n' can be obtained based on the current route. These values are specific for a particular metro route and different values will be obtained if the headway, gradients, or distances between platforms are varied. The estimated substation energy can be expressed in equation (6.9) by using equation (6.1), (6.6), (6.7), and (6.8). And finally, the estimated substation energy consumption can be calculated by equation (6.10). Only traction energy consumption and overlap energy are required, which can be obtained without power flow analysis.

$$E_{sub\_est} = E_{elec\_trac} - C_r \times E_{overlap} + C_n \times E_{sub\_est} \tag{6.9}$$

$$E_{sub\_est} = \frac{1}{1 - C_n} \times (E_{elec\_trac} - C_r \times E_{overlap}) \tag{6.10}$$

6.3.3 System Energy Optimisation

The estimated substation energy consumption can be calculated using equation (6.10). The traction energy and overlapping energy can be obtained using the train motion simulation. In equation (6.11), the estimated substation energy is assumed as the objective, where g

represents the simulation process to calculate the estimated substation energy by train motion modelling. The journey times are constrained.

$$\begin{cases} min & E_{sub\_est} = g(D_{set}) \\ s.t. & T_d \leq T_{to} \end{cases} \tag{6.11}$$

As the objective of the optimisation problem, the estimated substation energy is determined by each coasting velocity and dwell time, treated as variables. A Monte Carlo algorithm is used to choose variable combinations. All the possibilities are evaluated quickly by computing the estimated substation energy. After a large number of random choices have been evaluated, the best 100 possibilities are stored and fully evaluated using the power network simulation. Finally, the possibility with the lowest substation energy consumption is identified. Naturally, being a statistical process, there is no guarantee that the best solution will be found, but because of the good correlation between estimated and actual substation energy, there is a good chance that a good solution will be found.

6.4 Case Study

6.4.1 Modelling Formulation

The Beijing Yizhuang Subway Line is used as a case study to illustrate the performance of the system energy minimisation algorithm. The metro line covers a length of 22.73 km and contains 14 stations with both underground and over ground segments. There are 12 rectifier substations with nominal 750 V to power the network. For the power network simulation, the substation is modelled as an 850 V source in series with a 0.02 Ω resistance.

A train driving strategies field test was conducted in September 2014 with no passengers. In order to compare with the field test results, the no-load train parameters are utilised in the simulation. Based on the field test measurement, the maximum service acceleration is measured as 0.8 m/s^2, and the maximum service braking rate is measured as 0.55 m/s^2. As a simplification, the auxiliary power is set to 0 kW. All the parameters under the actual train driving constraints are shown in Table 6.1. In this case study, the energy consumption during the peak hours is studied, where the headway is assumed as a constant with 254 s.

Table 6.1 Infrastructure and vehicle parameters

Item	Quantity	Units
Route length	22.73	km
Number of stations	14	
Number of substations	12	
Substation no-load voltage	850	V
Substation source resistance	0.02	Ω
Overvoltage limitation	950	V
Vehicle mass	199	tonnes
Passenger mass	0	tonnes
Max. tractive effort	160	kN
Max. tractive power	2650	kW
Auxiliary power	0	kW
Max. service acceleration	0.8	m/s^2
Max. service deceleration	0.55	m/s^2

6.4.2 Energy Consumption by Current ATO

Trains in Beijing Yizhuang Subway Line are normally operated by an ATO system. Table 6.2 shows the current timetable and the energy consumption as measured by the ATO system during field tests. Each train travels from Yizhuang station to Songjiazhuang and back again, which is taken as one running cycle. It is usual that braking energy is lower than traction energy. However, in the ‘up’ direction, there is a steep uphill gradient

between Ciqunan and Jinghailu, and a steep downhill gradient between Jiugong and Xiaohongmen. Thus, the electrical braking energy regenerated is lower than normal from Ciqunan to Jinghailu, and the electrical braking energy is even higher than the traction energy from Jiugong to Xiaohongmen. There is a similar pattern for the 'down' direction.

Table 6.2 Current ATO timetable and energy consumption in [kWh]

Index	1	2	3	4	5	6
Station	Yizhuang	Ciqu	Ciqunan	Jinghailu	Tongjinanlu	Rongchang
t_{run} [s]	-	105	101	140	148	160
t_{dwell} [s]	-	45	35	30	30	30
E_{elec_trac}	-	17	15	34	21	23
E_{elec_brake}	-	6	11	9	12	13
Index	7	8	9	10	11	12
Station	Rongjing	Wanyuan	Wenhuayuan	Yizhuangqiao	Jiugong	Xiaohongmen
t_{run} [s]	103	99	113	85	134	155
t_{dwell} [s]	30	30	30	35	30	30
E_{elec_trac}	18	17	20	17	21	18
E_{elec_brake}	10	9	12	10	12	20
Index	13	14	13	12	11	10
Station	Xiaocun	Songjiazhuang	Xiaocun	Xiaohongmen	Jiugong	Yizhuangqiao
t_{run} [s]	104	193	190	106	156	131
t_{dwell} [s]	30	240(turnaround)	30	30	30	35
E_{elec_trac}	21	25	25	14	32	22
E_{elec_brake}	10	11	12	8	10	11
Index	9	8	7	6	5	4
Station	Wenhuayuan	Wanyuan	Rongjing	Rongchang	Tongjinanlu	Jinghailu
t_{run} [s]	86	112	100	103	163	147
t_{dwell} [s]	30	30	30	30	30	30
E_{elec_trac}	16	15	16	15	19	21
E_{elec_brake}	11	11	9	10	10	11
Index	3	2	1			
Station	Ciqunan	Ciqu	Yizhuang	**total**		
t_{run} [s]	135	100	103	**3271**		
t_{dwell} [s]	35	45	-	**1010**		
E_{elec_trac}	14	18	19	**516**		
E_{elec_brake}	18	10	10	**286**		

6.4.3 System Energy Estimation

Using the current timetable, all possible speed profiles that fulfil the interstation journey time constraint (including -5 to 5 s variants) are collected from the motion simulator. The power network simulator evaluates 10,000 combinations of randomly chosen single train inter-station journeys and dwell times (with up to 5 s random variation). The amount of overlap and regenerated energy for each combination is shown in Figure 6.4. A least-square linear fit (forced through the origin) gives a regenerative coefficient 'C_r' (the gradient) equal to 0.944. The Pearson correlation coefficient is 0.917, which denotes a highly linear relationship.

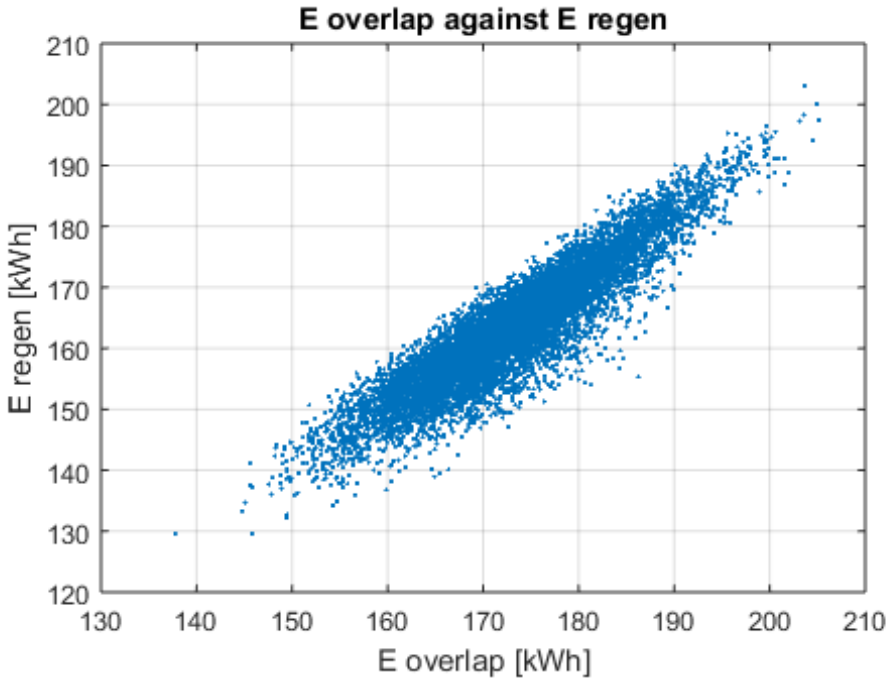

Figure 6.4 Regenerative braking energy compared with overlap energy

The substation energy and network loss results are shown in Figure 6.5. The Pearson correlation coefficient is 0.6447, which is smaller than the correlation between the overlap

energy and regenerative energy. But, as the amount of network loss only accounts for about 10% of the substation energy, it is still a good estimation of network loss using network loss coefficient 'C_n', which is 0.0986.

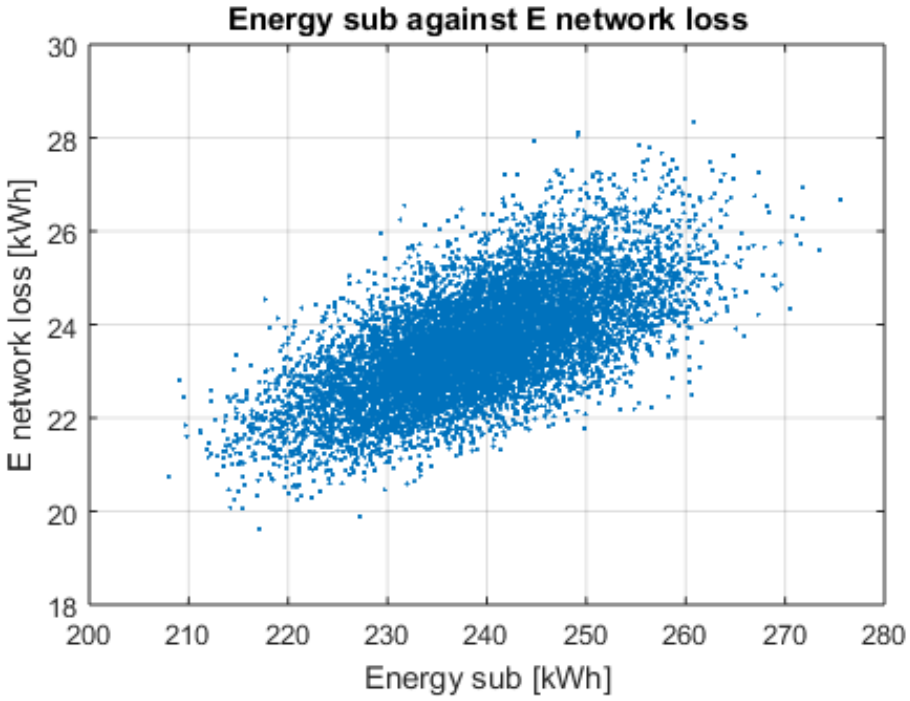

Figure 6.5 Network loss compared with substation energy

According to the regenerative and network loss coefficients, the estimated substation energy can be calculated using equation (6.10). Figure 6.6 shows the relationship between the estimated substation energy and the actual substation energy. The correlation is 0.8615, which proves a significant linear relationship. In order to test the likelihood of the estimation, the cumulative distribution function of the absolute errors of substation energy estimation is shown in Figure 6.7. The probability that the absolute error is lower than 5 kWh is about 70%, becoming 95% when the absolute error is less than 10 kWh. Therefore, estimated substation energy consumption is found to be very close to the actual value, which can then be used for optimising the system energy.

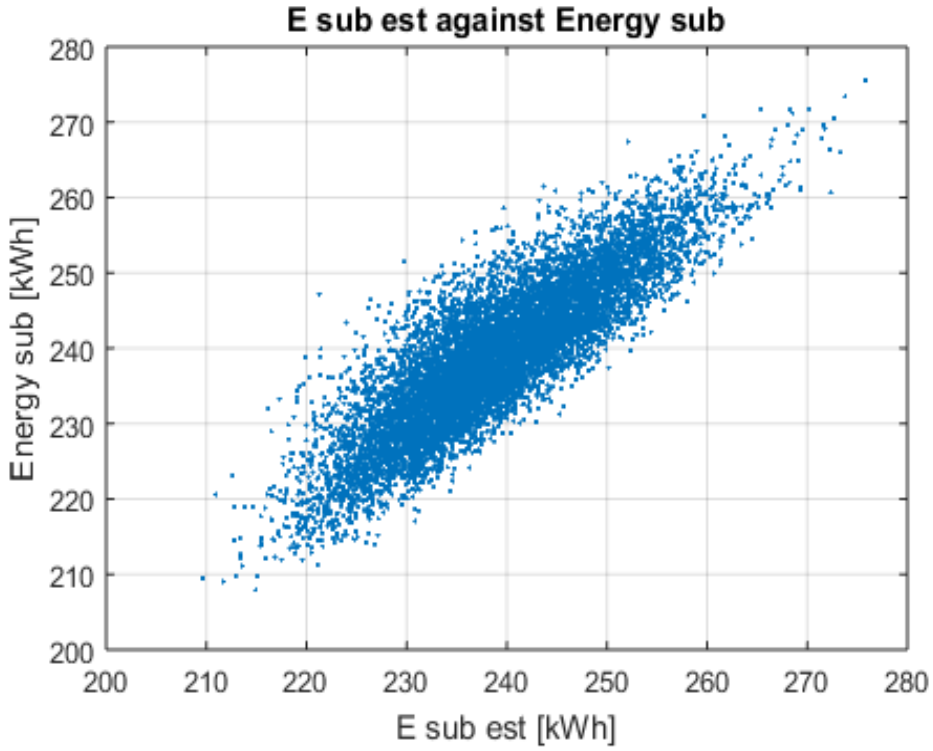

Figure 6.6 Estimated substation energy compared with actual substation energy

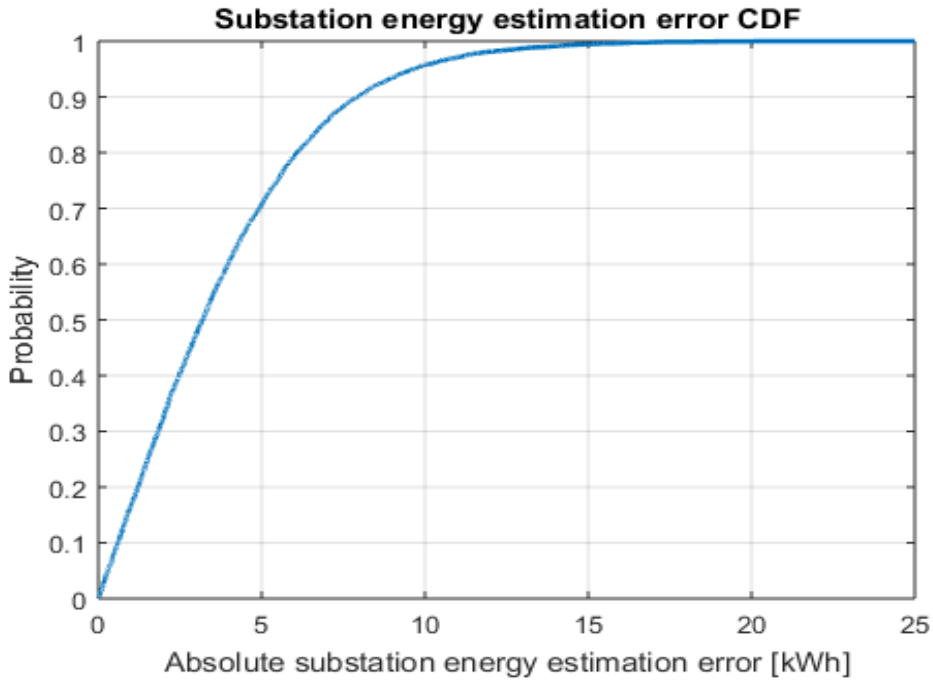

Figure 6.7 Substation energy estimation error cumulative distribution

6.4.4 System Energy Optimisation

Using the two coefficients obtained by Monte Carlo Simulation, the estimated substation energy of 500,000 random driving operation inputs has been evaluated. It takes 3 minutes to calculate the estimated substation energy by a computer with 3.4 GHz CPU and 8 GB RAM. The algorithm stores the 100 cases with the minimum estimated substation energy consumption. Figure 6.8 shows the lowest estimated substation energy is just below 205 kWh, and the decreasing rate of average energy of the best 100 is very slow at 500,000 examples. A downward step occurs whenever better estimated substation energy consumption is found among the random samples. The mean estimated substation energy line is the average of the current best 100. This moves down a smoother path because sometimes one of the best 100 is replaced with a better one and one drops out giving a lower mean.

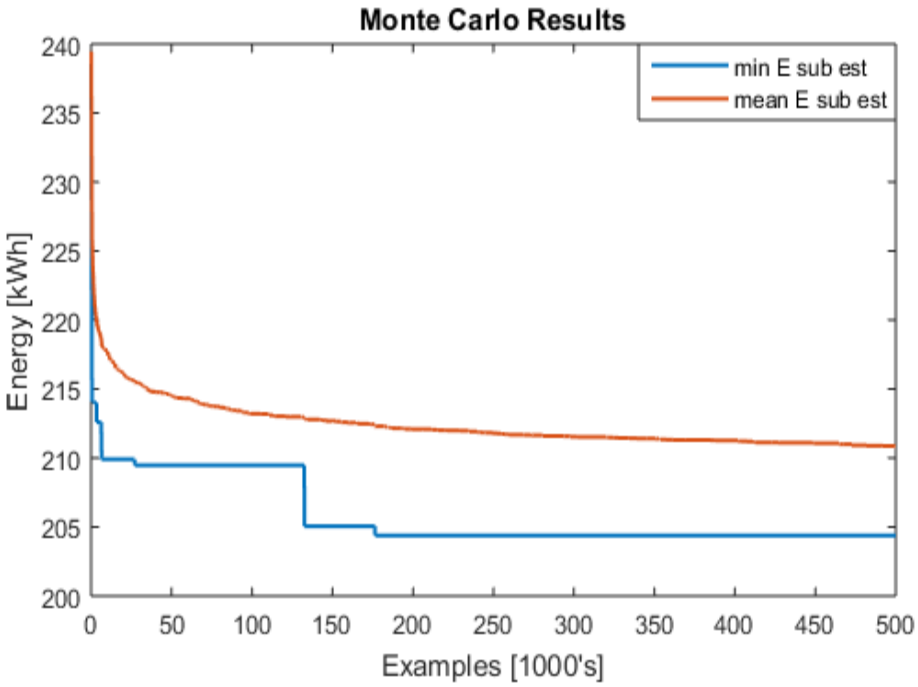

Figure 6.8 Monte Carlo estimated substation energy results

Finally, the best 100 examples are evaluated by the power network simulator. It takes around 3 seconds to calculate the multi-train power flow for the headway period, so about 5 minutes to evaluate all 100 examples. All the 100 inputs show good substation energy consumption and the 8 results with the lowest substation energy consumption are shown in Table 6.3. If all the 500,000 driving operation inputs are evaluated by power network simulation, it will take 17 days to find the best result. The cycle journey time ranges from 4248 s to 4292 s, which results in slightly different traction energy. The regenerative efficiency which equals regenerative energy divided by electrical braking energy is defined by equation (4.26). Due to the short peak-hour headway, the regenerative efficiency of the top 8 results is quite high, more than 90%. The traction energy, regenerative energy and energy loss affect the substation energy consumption together, but all of the top 8 examples show great energy-efficiency.

Table 6.3 Top 8 system energy optimisation results in [kWh]

	1	**2**	**3**	**4**	**5**	**6**	**7**	**8**
T_{cycle} [s]	4248	4248	4289	4292	4291	4292	4290	4267
E_{sub}	203.37	203.95	204.72	204.88	205.50	205.73	205.75	206.35
$E_{sub\ loss}$	4.55	4.72	4.69	5.14	5.06	4.92	4.80	5.08
$E_{trans\ loss}$	16.18	15.44	15.90	16.44	16.42	16.50	16.41	15.67
$E_{traction}$	375.12	369.90	365.16	366.94	364.89	371.28	365.48	369.27
E_{elec_brake}	201.57	198.63	196.34	195.28	194.33	198.50	194.82	195.74
E_{regen}	192.48	186.12	181.04	183.64	180.88	186.96	180.94	183.66
η_{regen}	95.5%	93.7%	92.2%	94.0%	93.1%	94.2%	92.9%	93.8%

Table 6.4 illustrates the timetable and interstation energy consumption of the best solution found. All the optimised interstation journey times and dwell times as well as the single-train traction and braking energy are given. Compared with the current ATO driving results in Table 6.2, the total journey time is reduced by 33 s, while the running time and dwell time are reduced by 6 and 27 s, respectively. At the same time, the traction energy

consumption and electric braking energy are reduced by 27.5% and 29.7%, respectively. The resulting driving pattern is composed of acceleration, cruising, coasting and braking phases that could be implemented using ATO.

Table 6.4 Optimal driving timetable and energy consumption in [kWh]

Index	1	2	3	4	5	6
Station	Yizhuang	Ciqu	Ciqunan	Jinghailu	Tongjinanlu	Rongchang
t_{run} [s]	-	106	100	144	143	162
t_{dwell} [s]	-	44	38	25	33	33
E_{elec_trac}	-	9	13	27	19	14
E_{elec_brake}	-	6	8	4	10	6
Index	7	8	9	10	11	12
Station	Rongjing	Wanyuan	Wenhuayuan	Yizhuangqiao	Jiugong	Xiaohongmen
t_{run} [s]	108	102	114	90	131	154
t_{dwell} [s]	28	26	26	32	29	27
E_{elec_trac}	11	11	14	9	18	14
E_{elec_brake}	5	6	7	5	10	16
Index	13	14	13	12	11	10
Station	Xiaocun	Songjiazhuang	Xiaocun	Xiaohongmen	Jiugong	Yizhuangqiao
t_{run} [s]	106	188	185	103	152	127
t_{dwell} [s]	27	240(turnaround)	30	33	25	32
E_{elec_trac}	11	13	12	11	28	19
E_{elec_brake}	6	4	5	7	7	10
Index	9	8	7	6	5	4
Station	Wenhuayuan	Wanyuan	Rongjing	Rongchang	Tongjinanlu	Jinghailu
t_{run} [s]	87	108	104	99	161	144
t_{dwell} [s]	29	28	35	27	30	26
E_{elec_trac}	9	16	10	15	13	19
E_{elec_brake}	6	10	6	10	7	9
Index	3	2	1			
Station	Ciqunan	Ciqu	Yizhuang	**total**		
t_{run} [s]	135	104	108	**3265**		
t_{dwell} [s]	36	44	-	**983**		
E_{elec_trac}	16	11	9	**374**		
E_{elec_brake}	20	6	4	**201**		

According to the speed profile collected by the ATO system, the system energy consumption can be computed by the power network simulation. Table 6.5 presents the system energy consumption for three different operating regimes: the current ATO

operation, the best identified by minimising the traction energy, and the best found by minimising the substation energy. The current ATO system energy consumption is calculated using a power network simulator using the speed profiles measured by the ATO system. It is found that the simulated traction energy and braking energy are slightly higher than the measured energy consumption shown in Table 6.2 by about 1%, which is acceptable. The traction optimisation column in Table 6.5 presents the energy consumption of the system under traction optimisation but remaining with the original timetable. The interstation journey times and dwell times are fixed and only one coasting point is used in each interstation journey. The results denote that traction energy and substation energy are reduced by 29.2% and 29.9%, respectively. With traction optimisation alone, the regenerative efficiency (regenerative energy divided by braking energy) is almost the same as with ATO, at 80.6% and 82.1%, respectively. With substation energy optimisation, the traction energy consumption and braking energy are almost the same as the traction energy optimisation results, but the substation energy is reduced by 38.6%. This is mainly caused by the higher regenerative efficiency which reaches 95.5%.

Table 6.5 Optimisation results comparison

	Current ATO operation	**Traction optimisation**	**System optimisation**
Cycle running time [s]	4281	4281	4248
Substation energy per headway [kWh]	331.28	232.21 (-29.9%)	203.37 (-38.6%)
Substation loss per headway [kWh]	12.38	6.41	4.55
Transmission loss per headway [kWh]	26.26	16.60	16.18
Traction energy per headway [kWh]	525.94	372.52 (-29.2%)	375.12 (-28.7%)
Braking energy per headway [kWh]	289.51	199.04	201.57
Regenerative energy per headway [kWh]	233.30	163.32	192.48
Efficiency of using regenerative energy	80.6%	82.1%	95.5%

6.5 Summary

Because of the short interstation distance characteristic of a metro system, the trains accelerate and brake frequently. As a result, the regenerative braking energy efficiency becomes an important factor in the metro system energy minimisation problem. This chapter proposes an integrated energy optimisation approach to obtaining an energy-efficient driving profile and timetable results for a DC metro system with regenerating trains. To solve a complex optimisation problem with a great number of variables, the concept of estimation of substation energy consumption is defined. This estimated energy is used to simplify the progress of power flow analysis and reduce optimisation computing time. A Monte Carlo algorithm is employed to identify the initial candidate solutions, acting as a heuristic to guide the optimisation. Finally, the solutions that have been selected for further evaluation are simulated in a full power network simulation to identify the best energy-efficient operation.

The results in this chapter denote that the traction energy optimisation is not necessarily the best solution with the lowest system energy consumption at the substations. The case study based on the Beijing Yizhuang Subway Line illustrates the performance of this integrated optimisation approach. Compared with the current ATO operation, the optimised operation within the time constraints can reduce the substation energy consumption by 38.6%, combining low traction energy consumption and high regenerative braking usage. The usage of regenerated energy accounts for 95.5% of the total electricity produced by electrical braking, which benefits from modifying the interstation travel time and dwell time.

Chapter 7

Conclusions and Future Work

7.1 Conclusions

This thesis reviews previous energy-saving technologies in railway systems. After investigating and comparing the previous literature in Chapter 2, the detailed objectives for improving the energy efficiency of urban rail transit systems are presented.

Chapter 3 demonstrates the development of a railway system simulator. This simulator integrates the modelling of train movement and the traction power network. Energy evaluation studies are carried out based on this simulator in Chapter 4. A case study of the Beijing Yizhuang Subway Line is proposed and the energy loss in the whole railway network is analysed. The results denote that traction energy can be effectively reduced by optimising driving controls. The amount of regenerated braking energy that can be used effectively in a non-reversible substation power system is highly variable. The system energy consumption with regeneration turned on can benefit from timetable optimisation, by increasing the efficiency of regenerative energy utilisation. There is a 35% difference in substation energy consumption between the best and worst headways.

The method to optimise the traction energy consumption is illustrated in Chapter 5. Brute Force and a Genetic Algorithm are used to search for the most efficient driving controls. Compared to the existing normal daily operation, simulation results show that using the most efficient driving controls reduces the traction energy consumption by 28%. A simple DAS system based on these result is designed and applied to the Beijing Yizhuang Subway Line in a field test. A driver guided by the DAS reduced the traction energy consumption by 16%. This would lead to an annual energy saving of 3577 MWh, which is equivalent to a saving of £358 k per year.

In Chapter 6, the integrated approach to optimising the system energy consumption is proposed. A Monte Carlo algorithm is employed in solving the complicated optimisation problem with a large number of variables. The driving controls and timetables are considered jointly in this optimisation. A case study is carried out based on the Beijing Yizhuang Subway Line. Compared with the current operation, the system optimised operation reduces the substation energy consumption by 38.6%. The efficiency of using regenerative braking is improved from 80.6 to 95.5%. The system-optimised operation improves energy-saving performance by 10%, compared with the traction-optimised operation.

From the energy optimisation results illustrated in Chapter 5 and Chapter 6, the hypothesis proposed at the beginning of this thesis is validated. The system energy consumption can be optimised using the integrated approach, based on the global understanding of railway energy systems.

7.2 Main Contributions

7.2.1 Railway System Energy Simulator

A railway system energy simulator is developed in this thesis. This system energy simulator is capable of assessing the energy performance of train movement and traction power networks. This simulator can be used to evaluate the energy consumption for existing routes according to the driving and timetable operations. Also, the railway infrastructure and operation can be designed for energy savings based on this simulator. This simulator has been applied to several research projects in the UK, Singapore and China.

7.2.2 Energy Evaluation Study

Through the study of energy evaluation of railway systems based on system energy simulation, the main factors which influence energy consumption in railway systems are identified. The benefit of using regeneration braking energy is fully studied. The potential energy-saving performance by optimising driving controls and timetables has been explained based on a real case study. The energy evaluation results of current operation could be used to verify the energy efficiency of each sector and assess the potential energy saving performance of existing routes. In addition, this study could be used as a proof for future research on energy-efficient operations. Further research on energy savings can be explored based on the study of energy evaluation.

7.2.3 Energy-efficient Driving Study

A method to optimise driving controls for traction energy savings is proposed. The theoretical optimal driving strategies have been produced by simulation. More importantly, a simple feasible DAS system is designed to advise human drivers to achieve energy-efficient driving controls. A field test on Beijing Yizhuang Subway Line is presented in this thesis. By using the proposed DAS system, the human driver is able to reduce the traction energy consumption significantly. This technology is cheap and effective, and could be widely developed and applied in various metro routes.

7.2.4 System Energy Optimisation Study

The contribution of this study is to propose an integrated energy optimisation approach to obtaining an energy-efficient driving profile and timetable results for railway system energy reduction. Most previous literature on this topic has simplified the decision variables and neglected the impact of the power flow in transmission networks, which leads to uncertainty about the optimal results. However, in this thesis, a Monte Carlo algorithm is used to evaluate the characteristics of energy flow in the power network, which overcomes the drawbacks of previous methods. The driving controls and timetables are optimised jointly by considering the power network modelling. The computing time to solve this problem is reasonable. The performance of energy savings has been presented based on the simulation of a real route.

7.3 Recommendations for Further Research

7.3.1 Application of Energy-efficient Driving Strategies

The driving strategies for traction energy savings have been validated in the field test on the Beijing Yizhuang Subway Line. The future work could focus on the practical application of the energy-efficient driving strategies. In order to use the strategies in daily operation, the DAS explained in this thesis needs to be improved. The user interface could be improved, which is easier and clearer to use. The cruising, coasting and braking posts could be implemented along the route to instruct drivers. More work is required to achieve this objective.

7.3.2 Validation of System Energy Optimisation

The study of system energy optimisation is based on railway system simulation. The results present the performance of substation energy reduction theoretically. A field test should be conducted to validate the results provided by this study. The optimal operations obtained from the simulation study could be applied in a multi-train network with regenerative trains. The energy consumption could be measured from substations.

7.3.3 Further Research Topics

Based on the studies in this thesis, it is worth considering and investigating the following research topics.

- The headway is assumed as a constant in the study of system energy optimisation in this thesis. The relationship between system energy consumption and various

headways could be studied. The headway could be assumed as a decision variable in further optimisation studies.

- With increasing passenger demand, a more powerful electricity supply is required. An approach to upgrading the power supply infrastructure based on passenger flow demand could be studied in the future.
- The robustness of optimal operation strategies could be examined by comparing different energy-efficient operations. The relationship between energy-saving performance and the disturbance (for example, delay or accident) could be further studied.

Appendix A

Publications

Journal papers published during PhD study are listed as follows.

[1] Z. Tian, P. Weston, N. Zhao, S. Hillmansen, C. Roberts, and L. Chen, "System energy optimisation strategies for metros with regeneration," *Transportation Research Part C: Emerging Technologies,* vol. 75, pp. 120-135, 2017.

[2] Z. Tian, S. Hillmansen, C. Roberts, P. Weston, N. Zhao, L. Chen, *et al.*, "Energy evaluation of the power network of a DC railway system with regenerating trains," *IET Electrical Systems in Transportation,* vol. 6, pp. 41-49, 2016.

[3] N. Zhao, L. Chen, Z. Tian, C. Roberts, S. Hillmansen, and J. Lv, "Field test of train trajectory optimisation on a metro line," *IET Intelligent Transport Systems,* vol. 11, pp. 273-281, 2017.

[4] N. Zhao, C. Roberts, S. Hillmansen, Z. Tian, P. Weston, and L. Chen, "An integrated metro operation optimization to minimize energy consumption," *Transportation Research Part C: Emerging Technologies,* vol. 75, pp. 168-182, 2017.

Conference papers published during PhD study are listed as follows.

[5] Z. Tian, P. Weston, S. Hillmansen, C. Roberts, and N. Zhao, "System energy optimisation of metro-transit system using Monte Carlo Algorithm," in *2016 IEEE International Conference on Intelligent Rail Transportation (ICIRT)*, 2016, pp. 453-459.

[6] Z. Tian, S. Hillmansen, C. Roberts, P. Weston, L. Chen, N. Zhao, *et al.*, "Modeling and simulation of DC rail traction systems for energy saving," in *17th International IEEE Conference on Intelligent Transportation Systems (ITSC)*, 2014, pp. 2354-2359.

[7] N. Zhao, Z. Tian, S. Hillmansen, C. Roberts, M. Yuan, J. Li, H. Shi, *et al.*, "Metro Traction and Power System Energy Optimisation," *The Stephenson Conference Research for Railways*, London, UK, 2015.

[8] N. Zhao, C. Roberts, S. Hillmansen, P. Weston, L. Chen, Z. Tian, *et al.*, "Train trajectory optimisation of ATO systems for metro lines," in *17th International IEEE Conference on Intelligent Transportation Systems (ITSC)*, 2014, pp. 1796-1801.

[9] T. Xin, C. Roberts, J. He, S. Hillmansen, N. Zhao, L. Chen, Z. Tian, *et al.*, "Railway vertical alignment optimisation at stations to minimise energy," in *17th International IEEE Conference on Intelligent Transportation Systems (ITSC)*, 2014, pp. 2119-2124.

References

[1] R. Sims, R. Schaeffer, and F. Creutzig, "Climate Change 2014: Mitigation of Climate Change," IPCC-Intergovernmental Panel on Climate Change, Cambridge University Press 2014.

[2] UIC and CER, "Rail Transport and Environment: Facts & Figures," UIC-ETF (Railway Technical Publications) 2015.

[3] P. Fouracre, C. Dunkerley, and G. Gardner, "Mass rapid transit systems for cities in the developing world," *Transport Reviews*, vol. 23, pp. 299-310, 2003.

[4] UIC and CER, "Moving towards sustainable mobility: A strategy for 2030 and beyond for the european railway sector," UIC Communications Department2012.

[5] *Railenergy Project*. Available: http://www.railenergy.org/

[6] *OSIRIS Project*. Available: http://www.osirisrail.eu

[7] *MERLIN Project*. Available: http://www.merlin-rail.eu/

[8] RSSB, "A guide to RSSB research into Energy (T928)," 2014.

[9] A. González-Gil, R. Palacin, and P. Batty, "Optimal energy management of urban rail systems: Key performance indicators," *Energy Conversion and Management*, vol. 90, pp. 282-291, 2015.

[10] A. González-Gil, R. Palacin, P. Batty, and J. P. Powell, "A systems approach to reduce urban rail energy consumption," *Energy Conversion and Management*, vol. 80, pp. 509-524, 2014.

[11] S. Hillmansen and C. Roberts, "Energy storage devices in hybrid railway vehicles: A kinematic analysis," *Proceedings of the Institution of Mechanical Engineers, Part F: Journal of Rail and Rapid Transit,* vol. 221, pp. 135-143, 2007.

[12] B. Mellitt, C. J. Goodman, and R. I. M. Arthurton, "Simulation studies of energy saving with chopper control on the Jubilee line," *Electrical Engineers, Proceedings of the Institution of,* vol. 125, pp. 304-310, 1978.

[13] R. D. White, "DC electrification supply system design," in *Railway Electrification Infrastructure and Systems, 2009. REIS 2009. 4th IET professional Development Course on*, 2009, pp. 44-69.

[14] F. Schmid and C. J. Goodman, "Electric railway systems in common use," in *Railway Electrification Infrastructure and Systems, 2009. REIS 2009. 4th IET professional Development Course on*, 2009, pp. 6-20.

[15] R. J. Hill, "Electric railway traction. Part 3. Traction power supplies," *Power Engineering Journal,* vol. 8, pp. 275-286, 1994.

[16] S. Hillmansen, "Sustainable traction drives," in *2009 4th IET professional Development Course on Railway Electrification Infrastructure and Systems*, 2009, pp. 255-265.

[17] R. J. Hill, "Electric railway traction. I. Electric traction and DC traction motor drives," *Power Engineering Journal,* vol. 8, pp. 47-56, 1994.

[18] R. J. Hill, "Electric railway traction. II. Traction drives with three-phase induction motors," *Power Engineering Journal*, vol. 8, pp. 143-152, 1994.

[19] S. Lu, "Optimising power management strategies for railway traction systems," PhD, University of Birmingham, 2011.

[20] C. J. Goodman, "Overview of electric railway systems and the calculation of train performance," in *Electric Traction Systems, 2010 IET Professional Development Course on*, 2010, pp. 1-24.

[21] K. Ichikawa, "Application of Optimization Theory for Bounded State Variable Problems to the Operation of Train," *Bulletin of JSME,* vol. 11, pp. 857-865, 1968.

[22] H. Douglas, C. Roberts, S. Hillmansen, and F. Schmid, "An assessment of available measures to reduce traction energy use in railway networks," *Energy Conversion and Management,* vol. 106, pp. 1149-1165, 2015.

[23] G. M. Scheepmaker, R. M. P. Goverde, and L. G. Kroon, "Review of energy-efficient train control and timetabling," *European Journal of Operational Research,* vol. 257, pp. 355-376, 2017.

[24] Q. Gu, T. Tang, and Y.-D. Song, "A Survey on Energy-Saving Operation of Railway Transportation Systems," *Measurement and Control,* vol. 43, pp. 209-211, 2010.

[25] B. Mellitt, S. Sujitjorn, C. J. Goodman, and N. B. Rambukwella, "Energy Minimisation Using an Expert System for Dynamic Coast Control in Rapid Transit Trains," presented at the Conference on Railway Engineering, Perth, 1978.

[26] C. S. Chang and S. S. Sim, "Optimising train movements through coast control using genetic algorithms," *Electric Power Applications, IEE Proceedings* -, vol. 144, pp. 65-73, 1997.

[27] Y. V. Bocharnikov, A. M. Tobias, C. Roberts, S. Hillmansen, and C. J. Goodman, "Optimal driving strategy for traction energy saving on DC suburban railways," *Electric Power Applications, IET,* vol. 1, pp. 675-682, 2007.

[28] Y. Fu, Z. Gao, and K. Li, "Optimization Method of Energy Saving Train Operation for Railway Network," *Journal of Transportation Systems Engineering and Information Technology*, vol. 9, pp. 90-96, 2009.

[29] K. K. Wong and T. K. Ho, "Coast control for mass rapid transit railways with searching methods," *Electric Power Applications, IEE Proceedings* -, vol. 151, pp. 365-376, 2004.

[30] K. K. Wong and T. K. Ho, "Coast control of train movement with genetic algorithm," in *Evolutionary Computation, 2003. CEC '03. The 2003 Congress on*, 2003, pp. 1280-1287 Vol.2.

[31] S. Lu, S. Hillmansen, T. K. Ho, and C. Roberts, "Single-Train Trajectory Optimization," *IEEE Transactions on Intelligent Transportation Systems*, vol. 14, pp. 743-750, 2013.

[32] C. S. Chang, A. Khambadkone, and X. Zhao, "Modeling and simulation of DC transit system with VSI-fed induction motor driven train using PSB/MATLAB," in *2001 4th IEEE International Conference on Power Electronics and Drive Systems*, 2001, pp. 881-885

[33] N. Zhao, C. Roberts, S. Hillmansen, and G. Nicholson, "A Multiple Train Trajectory Optimization to Minimize Energy Consumption and Delay," *IEEE Transactions on Intelligent Transportation Systems*, vol. PP, pp. 1-10, 2015.

[34] N. Zhao, C. Roberts, and S. Hillmansen, "The application of an enhanced Brute Force Algorithm to minimise energy costs and train delays for differing railway train control systems," *Proceedings of the Institution of Mechanical Engineers, Part F: Journal of Rail and Rapid Transit*, vol. 228, pp. 158-168, 2014.

[35] P. G. Howlett, I. P. Milroy, and P. J. Pudney, "Energy-efficient train control," *Control Engineering Practice,* vol. 2, pp. 193-200, 1994.

[36] P. Howlett, "Optimal strategies for the control of a train," *Automatica,* vol. 32, pp. 519-532, 1996.

[37] P. Howlett and J. Cheng, "Optimal driving strategies for a train on a track with continuously varying gradient," *ANZIAM Journal (formerly J of the Australian Math Soc Series B),* vol. 38, pp. 388-410, 1997.

[38] P. G. Howlett, "The Optimal Control of a Train," *Annals of Operations Research,* vol. 98, pp. 65-87, 2000.

[39] P. G. Howlett, P. J. Pudney, and X. Vu, "Local energy minimization in optimal train control," *Automatica,* vol. 45, pp. 2692-2698, 2009.

[40] R. Liu and I. M. Golovitcher, "Energy-efficient operation of rail vehicles," *Transportation Research Part A: Policy and Practice,* vol. 37, pp. 917-932, 2003.

[41] S. Su, T. Tang, X. Li, and Z. Gao, "A Subway Train Timetable Optimization Approach Based on Energy-Efficient Operation Strategy," *IEEE Transactions on Intelligent Transportation Systems,* vol. 14, pp. 883-893, 2013.

[42] S. Su, T. Tang, X. Li, and Z. Gao, "Optimization of Multitrain Operations in a Subway System," *IEEE Transactions on Intelligent Transportation Systems,* vol. 15, pp. 673-684, 2014.

[43] S. Su, T. Tang, and Y. Wang, "Evaluation of Strategies to Reducing Traction Energy Consumption of Metro Systems Using an Optimal Train Control Simulation Model," *Energies,* vol. 9, p. 105, 2016.

[44] B. R. Ke and N. Chen, "Signalling block layout and strategy of train operation for saving energy in mass rapid transit systems," *IEE Proceedings - Electric Power Applications*, vol. 152, pp. 129-140, 2005.

[45] B. R. Ke, C. L. Lin, and C. C. Yang, "Optimisation of train energy-efficient operation for mass rapid transit systems," *IET Intelligent Transport Systems*, vol. 6, pp. 58-66, 2012.

[46] B. R. Ke, M. C. Chen, and C. L. Lin, "Block-Layout Design Using MAX-MIN Ant System for Saving Energy on Mass Rapid Transit Systems," *IEEE Transactions on Intelligent Transportation Systems*, vol. 10, pp. 226-235, 2009.

[47] P. Johnson and S. Brown, "A simple in-cab schedule advisory system to save energy and improve on-time performance," in *IET Conference on Railway Traction Systems (RTS 2010)*, 2010, pp. 1-5.

[48] C. S. Chang and D. Y. Xu, "Differential evolution based tuning of fuzzy automatic train operation for mass rapid transit system," *IEE Proceedings - Electric Power Applications*, vol. 147, pp. 206-212, 2000.

[49] N. Zhao, C. Roberts, S. Hillmansen, P. Weston, L. Chen, Z. Tian, *et al.*, "Train trajectory optimisation of ATO systems for metro lines," in *17th International IEEE Conference on Intelligent Transportation Systems (ITSC)*, 2014, pp. 1796-1801.

[50] M. Domínguez, A. Fernández, A. P. Cucala, and P. Lukaszewicz, "Optimal design of metro automatic train operation speed profiles for reducing energy consumption," *Proceedings of the Institution of Mechanical Engineers, Part F: Journal of Rail and Rapid Transit* vol. 225, pp. 463-474, 2011.

[51] A. Fernández-Rodríguez, A. Fernández-Cardador, A. P. Cucala, M. Domínguez, and T. Gonsalves, "Design of Robust and Energy-Efficient ATO Speed Profiles of Metropolitan Lines Considering Train Load Variations and Delays," *IEEE Transactions on Intelligent Transportation Systems,* vol. 16, pp. 2061-2071, 2015.

[52] W. Carvajal-Carreño, A. P. Cucala, and A. Fernández-Cardador, "Optimal design of energy-efficient ATO CBTC driving for metro lines based on NSGA-II with fuzzy parameters," *Engineering Applications of Artificial Intelligence,* vol. 36, pp. 164-177, 2014.

[53] W. Carvajal-Carreño, A. P. Cucala, and A. Fernández-Cardador, "Fuzzy train tracking algorithm for the energy efficient operation of CBTC equipped metro lines," *Engineering Applications of Artificial Intelligence,* vol. 53, pp. 19-31, 2016.

[54] S. Su, T. Tao, L. chen, and B. Liu, "Energy-efficient train control in urban rail transit systems," *Proceedings of the Institution of Mechanical Engineers, Part F: Journal of Rail and Rapid Transit,* 2014.

[55] R. Ellis, P. Weston, E. Stewart, S. Hillmansen, P. Tricoli, C. Roberts, *et al.*, "Observations of train control performance on a camshaft-operated DC electrical multiple unit," *Proceedings of the Institution of Mechanical Engineers, Part F: Journal of Rail and Rapid Transit,* vol. 230, pp. 1184-1201, 2015.

[56] R. S. Luijt, M. P. F. van den Berge, H. Y. Willeboordse, and J. H. Hoogenraad, "5 years of Dutch eco-driving: Managing behavioural change," *Transportation Research Part A: Policy and Practice,* vol. 98, pp. 46-63, 2017.

[57] X. Feng, H. Zhang, Y. Ding, Z. Liu, H. Peng, and B. Xu, "A Review Study on Traction Energy Saving of Rail Transport," *Discrete Dynamics in Nature and Society,* vol. 2013, p. 9, 2013.

[58] H. Liu, B. Mao, Y. Ding, W. Jia, and S. Lai, "Train Energy-saving Scheme with Evaluation in Urban Mass Transit Systems," *Journal of Transportation Systems Engineering and Information Technology,* vol. 7, pp. 68-73, 2007.

[59] K. Kim and S. Chien, "Optimal Train Operation for Minimum Energy Consumption Considering Track Alignment, Speed Limit, and Schedule Adherence," *Journal of Transportation Engineering,* vol. 137, pp. 665-674, 2011.

[60] K. Kim and S. Chien, "Simulation-based analysis of train controls under various track alignment," *J. Transp. Eng.*, vol. 136, p. 937, 2010.

[61] X. Hu and J. Zhang, "Research on Optimal Scheme for Energy - saving Slope of Urban Rail Transit," *Journal of Railway Engineering Society,* vol. 30, pp. 27-30, 2013-05-15 2013.

[62] T. Xin, C. Roberts, J. He, S. Hillmansen, N. Zhao, L. Chen, *et al.*, "Railway vertical alignment optimisation at stations to minimise energy," in *17th International IEEE Conference on Intelligent Transportation Systems (ITSC)*, 2014, pp. 2119-2124.

[63] K. Matsuoka and M. Kondo, "Energy Saving Technologies for Railway Traction Motors," *IEEJ Transactions on Electrical and Electronic Engineering,* vol. 5, pp. 278-284, 2010.

[64] M. Kondo, M. Miyabe, and S. Manabe, "Development of a high efficiency induction motor and the estimation of energy conservation effect," *Quarterly Report of RTRI,* vol. 55, pp. 138-143, 2014.

[65] H. Douglas, F. Schmid, C. Roberts, and S. Hillmansen, "Evaluation of Permanent Magnet Motor energy saving technology for different types of railways," in *2016 IEEE International Conference on Intelligent Rail Transportation (ICIRT)*, 2016, pp. 123-129.

[66] A. Hoffrichter, A. R. Miller, S. Hillmansen, and C. Roberts, "Well-to-wheel analysis for electric, diesel and hydrogen traction for railways," *Transportation Research Part D: Transport and Environment,* vol. 17, pp. 28-34, 2012.

[67] A. Hoffrichter, S. Hillmansen, and C. Roberts, "Conceptual propulsion system design for a hydrogen-powered regional train," *IET Electrical Systems in Transportation,* vol. 6, pp. 56-66, 2016.

[68] A. Hoffrichter, "Hydrogen as an Energy Carrier for Railway Traction," PhD, University of Birmingham, 2013.

[69] S. Lu, S. Hillmansen, and C. Roberts, "A Power-Management Strategy for Multiple-Unit Railroad Vehicles," *IEEE Transactions on Vehicular Technology,* vol. 60, pp. 406-420, 2011.

[70] C. Köbel, "Bombardier energy saving technologies and their applications," in *AusRAIL PLUS 2008, 1-2 December 2008, Melbourne, Victoria, Australia*, 2008.

[71] R. S. Raghunathan, H.-D. Kim, and T. Setoguchi, "Aerodynamics of high-speed railway train," *Progress in Aerospace sciences*, vol. 38, pp. 469-514, 2002.

[72] Z. Tian, S. Hillmansen, C. Roberts, P. Weston, N. Zhao, L. Chen, *et al.*, "Energy evaluation of the power network of a DC railway system with regenerating trains," *IET Electrical Systems in Transportation*, vol. 6, pp. 41-49, 2016.

[73] B. Chang-han, J. Dong-uk, K. Yong-gi, C. Se-ky, and M. Jai-kyun, "Calculation of regenerative energy in DC 1500V electric railway substations," in *2007 7th Internatonal Conference on Power Electronics*, 2007, pp. 801-805.

[74] A. González-Gil, R. Palacin, and P. Batty, "Sustainable urban rail systems: Strategies and technologies for optimal management of regenerative braking energy," *Energy Conversion and Management,* vol. 75, pp. 374-388, 2013.

[75] S. Lu, P. Weston, S. Hillmansen, H. B. Gooi, and C. Roberts, "Increasing the Regenerative Braking Energy for Railway Vehicles," *IEEE Transactions on Intelligent Transportation Systems*, vol. 15, pp. 2506-2515, 2014.

[76] A. Nasri, M. F. Moghadam, and H. Mokhtari, "Timetable optimization for maximum usage of regenerative energy of braking in electrical railway systems," in *SPEEDAM 2010*, 2010, pp. 1218-1221.

[77] A. Ramos, M. T. Pena, A. Fernández, and P. Cucala, "Mathematical programming approach to underground timetabling problem for maximizing time synchronization," in *XI Congreso de Ingeniería de Organización*, 2007, pp. 1395-1405.

[78] M. Peña-Alcaraz, A. Fernández, A. Cucala, Paloma., A. Ramos, and R. Pecharromán, R. , "Optimal underground timetable design based on power flow for maximizing the use of regenerative-braking energy," *Proceedings of the Institution of Mechanical Engineers, Part F: Journal of Rail and Rapid Transit*, vol. 226, pp. 397-408, 2012.

[79] X. Yang, X. Li, Z. Gao, H. Wang, and T. Tang, "A Cooperative Scheduling Model for Timetable Optimization in Subway Systems," *IEEE Transactions on Intelligent Transportation Systems*, vol. 14, pp. 438-447, 2013.

[80] X. Yang, A. Chen, X. Li, B. Ning, and T. Tang, "An energy-efficient scheduling approach to improve the utilization of regenerative energy for metro systems," *Transportation Research Part C: Emerging Technologies*, vol. 57, pp. 13-29, 2015.

[81] X. Yang, B. Ning, X. Li, and T. Tang, "A Two-Objective Timetable Optimization Model in Subway Systems," *IEEE Transactions on Intelligent Transportation Systems*, vol. PP, pp. 1-9, 2014.

[82] X. Yang, B. Ning, X. Li, T. Tang, and X. Song, "A Subway Timetable Optimization Model for Maximizing the Utilization of Recovery Energy," presented at the Joint Rail Conference, USA, 2013.

[83] A. B. Turner, "A Study of Wayside Energy Storage Systems (WESS) for Railway Electrification," *IEEE Transactions on Industry Applications,* vol. IA-20, pp. 484-492, 1984.

[84] T. Ratniyomchai, S. Hillmansen, and P. Tricoli, "Recent developments and applications of energy storage devices in electrified railways," *Electrical Systems in Transportation, IET,* vol. 4, pp. 9-20, 2014.

[85] T. Ratniyomchai, S. Hillmansen, and P. Tricoli, "Energy loss minimisation by optimal design of stationary supercapacitors for light railways," in *Clean Electrical Power (ICCEP), 2015 International Conference on*, 2015, pp. 511-517.

[86] T. Ratniyomchai, S. Hillmansen, and P. Tricoli, "Optimal capacity and positioning of stationary supercapacitors for light rail vehicle systems," in *Power Electronics, Electrical Drives, Automation and Motion (SPEEDAM), 2014 International Symposium on*, 2014, pp. 807-812.

[87] R. Takagi and T. Amano, "Evaluating on-board energy storage systems using multi-train simulator RTSS," in *IET Conference on Railway Traction Systems (RTS 2010)*, 2010, pp. 1-3.

[88] R. Takagi and T. Amano, "Optimisation of reference state-of-charge curves for the feed-forward charge/discharge control of energy storage systems on-board DC electric railway vehicles," *Electrical Systems in Transportation, IET,* vol. 5, pp. 33-42, 2015.

[89] M. Z. Chymera, A. C. Renfrew, M. Barnes, and J. Holden, "Modeling Electrified Transit Systems," *IEEE Transactions on Vehicular Technology,* vol. 59, pp. 2748-2756, 2010.

[90] M. Chymera, A. C. Renfrew, and M. Barnes, "Measuring the performance of a centenary class tram on the Blackpool Tramway," in *Power Electronics, Machines and Drives, 2008. PEMD 2008. 4th IET Conference on*, 2008, pp. 645-649.

[91] M. Chymera, A. C. Renfrew, and M. Barnes, "Analysis of power quality in a DC tram system," in *Power Electronics, Machines and Drives, 2006. PEMD 2006. The 3rd IET International Conference on*, 2006, pp. 96-100.

[92] T. Suzuki, "DC power-supply system with inverting substations for traction systems using regenerative brakes," *Electric Power Applications, IEE Proceedings B,* vol. 129, pp. 18-26, 1982.

[93] B. Mellitt, Z. S. Mouneimne, and C. J. Goodman, "Simulation study of DC transit systems with inverting substations," *Electric Power Applications, IEE Proceedings B,* vol. 131, pp. 38-50, 1984.

[94] T. Yii Shen, W. Ruay-Nan, and C. Nanming, "Electric network solutions of DC transit systems with inverting substations," *IEEE Transactions on Vehicular Technology*, vol. 47, pp. 1405-1412, 1998.

[95] H. Douglas, C. Roberts, and S. Hillmansen, "Method to evaluate solutions for complex systems: rail energy," *Proceedings of the Institution of Civil Engineers - Transport,* vol. 169, pp. 283-297, 2016.

[96] X. Li and X. Yang, "A stochastic timetable optimization model in subway systems," *International Journal of Uncertainty, Fuzziness and Knowledge-Based Systems,* vol. 21, pp. 1-15, 2013.

[97] X. Li and H. K. Lo, "An energy-efficient scheduling and speed control approach for metro rail operations," *Transportation Research Part B: Methodological,* vol. 64, pp. 73-89, 2014.

[98] X. Li and H. K. Lo, "Energy minimization in dynamic train scheduling and control for metro rail operations," *Transportation Research Part B: Methodological,* vol. 70, pp. 269-284, 2014.

[99] N. Zhao, C. Roberts, S. Hillmansen, Z. Tian, P. Weston, and L. Chen, "An integrated metro operation optimization to minimize energy consumption," *Transportation Research Part C: Emerging Technologies,* vol. 75, pp. 168-182, 2017.

[100] J. Liu, H. Guo, and Y. Yu, "Research on the Cooperative Train Control Strategy to Reduce Energy Consumption," *IEEE Transactions on Intelligent Transportation Systems,* vol. 18, pp. 1134-1142, 2017.

[101] S. Su, T. Tang, and C. Roberts, "A Cooperative Train Control Model for Energy Saving," *IEEE Transactions on Intelligent Transportation Systems,* vol. PP, pp. 1-10, 2014.

[102] S. Su, T. Tang, C. Roberts, and L. Huang, "Cooperative train control for energy-saving," in *IEEE International Conference on Intelligent Rail Transportation Proceedings*, 2013, pp. 7-12.

[103] M. Miyatake and H. Ko, "Numerical analyses of minimum energy operation of multiple trains under DC power feeding circuit," in *Power Electronics and Applications, 2007 European Conference on*, 2007, pp. 1-10.

[104] H. Ko and M. Miyatake, "A numerical algorithm for run-curve optimization of trains considering a DC feeding circuit," *WIT Transactions on The Built Environment*, vol. 88, 2006.

[105] Á. J. López-López, R. R. Pecharromán, A. Fernández-Cardador, and A. P. Cucala, "Assessment of energy-saving techniques in direct-current-electrified mass transit systems," *Transportation Research Part C: Emerging Technologies*, vol. 38, pp. 85-100, 2014.

[106] A. J. López-López, R. R. Pecharromán, A. Fernández-Cardador, and A. P. Cucala, "Smart traffic-scenario compressor for the efficient electrical simulation of mass transit systems," *International Journal of Electrical Power & Energy Systems*, vol. 88, pp. 150-163, 2017.

[107] A. L. López, R. Pecharromán, E. Pilo, A. Cucala, and A. Fernández-Cardador, "Analysis of energy-saving strategies in railway power supply systems," in *9th World Congress on Railway Research-WCRR*, 2011, pp. 22-26.

[108] M. Domínguez, A. Fernández-Cardador, A. P. Cucala, and R. Pecharromán, R., "Energy Savings in Metropolitan Railway Substations Through Regenerative Energy Recovery and Optimal Design of ATO Speed Profiles," *IEEE Transactions on Automation Science and Engineering*, vol. 9, pp. 496-504, 2012.

[109] M. Domínguez, A. Fernández-Cardador, A. P. Cucala, T. Gonsalves, and A. Fernández, "Multi objective particle swarm optimization algorithm for the design of efficient ATO speed profiles in metro lines," *Engineering Applications of Artificial Intelligence*, vol. 29, pp. 43-53, 2014.

[110] B. Mellitt, C. J. Goodman, and R. I. M. Arthurton, "Simulator for studying operational and power-supply conditions in rapid-transit railways," *Electrical Engineers, Proceedings of the Institution of,* vol. 125, pp. 298-303, 1978.

[111] C. J. Goodman and L. K. Siu, "DC railway power network solutions by diakoptics," in *Proceedings of the 1994 ASME/IEEE Joint (in Conjunction with Area 1994 Annual Technical Conference)*, 1994, pp. 103-110.

[112] Y. Cai, M. R. Irving, and S. H. Case, "Modelling and numerical solution of multibranched DC rail traction power systems," *Electric Power Applications, IEE Proceedings -*, vol. 142, pp. 323-328, 1995.

[113] Y. Cai, M. R. Irving, and S. H. Case, "Iterative techniques for the solution of complex DC-rail-traction systems including regenerative braking," *Generation, Transmission and Distribution, IEE Proceedings-*, vol. 142, pp. 445-452, 1995.

[114] C. L. Pires, S. I. Nabeta, and J. R. Cardoso, "ICCG method applied to solve DC traction load flow including earthing models," *IET Electric Power Applications,* vol. 1, pp. 193-198, 2007.

[115] Z. Tian, S. Hillmansen, C. Roberts, P. Weston, L. Chen, N. Zhao, *et al.*, "Modeling and simulation of DC rail traction systems for energy saving," in *17th International IEEE Conference on Intelligent Transportation Systems (ITSC)*, 2014, pp. 2354-2359.

[116] C. Goodman, "Modelling and Simulation," in *Railway Electrification Infrastructure and Systems, 2007 3rd IET Professional Development Course on*, 2007, pp. 217-230.

[117] Y. Cai, M. R. Irving, and S. H. Case, "Compound matrix partitioning and modification for the solution of branched autotransformer traction feeds," *Electric Power Applications, IEE Proceedings* -, vol. 143, pp. 251-257, 1996.

[118] R. Murata, M. Miyatake, T. Akiba, and M. Tajima, "Study on a feeding circuit model formulated to use multipurpose solvers for multi-train simulators," in *2016 International Conference on Electrical Systems for Aircraft, Railway, Ship Propulsion and Road Vehicles & International Transportation Electrification Conference (ESARS-ITEC)*, 2016, pp. 1-9.

[119] B. Mao, W. Jia, S. Chen, and J. Liu, "A computer-aided multi-train simulator for rail traffic," in *2007 IEEE International Conference on Vehicular Electronics and Safety*, 2007, pp. 1-5.

[120] R. Takagi, "Preliminary evaluation of the energy-saving effects of the introduction of superconducting cables in the power feeding network for dc electric railways using the multi-train power network simulator," *Electrical Systems in Transportation, IET*, vol. 2, pp. 103-109, 2012.

[121] BS-EN50641, "Railway applications - Fixed installations - Requirements for the validation of simulation tools used for the design of traction power supply systems," *BSI*, 2014.

[122] S. Hillmansen, "Electric railway traction systems and techniques for energy saving," in *IET Professional Development Course on Electric Traction Systems (2012)*, 2012, pp. 19-23.

[123] B. P. Rochard and F. Schmid, "A review of methods to measure and calculate train resistances," *Proceedings of the Institution of Mechanical Engineers, Part F: Journal of Rail and Rapid Transit*, vol. 214, pp. 185-199, 2000.

[124] M. Chymera and C. J. Goodman, "Overview of electric railway systems and the calculation of train performance," in *Electric Traction Systems (2012), IET Professional Development Course on*, 2012, pp. 1-18.

[125] H. Douglas, P. Weston, D. Kirkwood, S. Hillmansen, and C. Roberts, "Method for validating the train motion equations used for passenger rail vehicle simulation," *Proceedings of the Institution of Mechanical Engineers, Part F: Journal of Rail and Rapid Transit*, vol. 231, pp. 455-469, 2017.

[126] P. Pozzobon, "Transient and steady-state short-circuit currents in rectifiers for DC traction supply," *IEEE Transactions on Vehicular Technology*, vol. 47, pp. 1390-1404, 1998.

[127] C. J. Goodman, L. K. Siu, and T. K. Ho, "A review of simulation models for railway systems," in *Developments in Mass Transit Systems, 1998. International Conference on (Conf. Publ. No. 453)*, 1998, pp. 80-85.

[128] BS-EN50388, "Railway applications - Power supply and rolling stock - Technical criteria," *BSI*, 2012.

[129] BS-EN50163, "Railway applications - Supply voltages of traction systems," *BSI*, 2007.

[130] A. Finlayson, C. J. Goodman, and R. D. White, "Investigation into the computational techniques of power system modelling for a DC railway," *Computers in Railways X: Computer System Design and Operation in the Railway and Other Transit Systems* 2006.

[131] W. Mingli, C. Roberts, and S. Hillmansen, "Modelling of AC feeding systems of electric railways based on a uniform multi-conductor chain circuit topology," in *Railway Traction Systems (RTS 2010), IET Conference on*, 2010, pp. 1-5.

[132] M. N. O. S. Charkes K. Alexander, *Fundamentals of Electric Circuits- 5th Edition*, 2013.

[133] TINA. Available: https://www.tina.com/

[134] R. R. Pecharroman, A. Lopez-Lopez, A. P. Cucala, and A. Fernandez-Cardador, "Riding the Rails to DC Power Efficiency: Energy efficiency in dc-electrified metropolitan railways," *Electrification Magazine, IEEE*, vol. 2, pp. 32-38, 2014.

[135] R. Takagi, "Energy Saving Techniques for the Power Feeding Network of Electric Railways," *IEEJ Transactions on Electrical and Electronic Engineering*, vol. 5, pp. 312-316, 2010.

[136] N. Zhao, L. Chen, Z. Tian, C. Roberts, S. Hillmansen, and J. Lv, "Field test of train trajectory optimisation on a metro line," *IET Intelligent Transport Systems*, vol. 11, pp. 273-281, 2017.

[137] P. G. Howlett, P. J. Pudney, and V. Xuan, "Brief paper: Local energy minimization in optimal train control," *Automatica*, vol. 45, pp. 2692-2698, 2009.

[138] A. Levitin and S. Mukherjee, *Introduction to the design & analysis of algorithms*: Addison-Wesley Reading, 2003.

[139] C. Paar and J. Pelzl, *Understanding cryptography: a textbook for students and practitioners*: Springer Science & Business Media, 2009.

[140] D. E. Knuth, *The art of computer programming: sorting and searching* vol. 3: Pearson Education, 1998.

[141] H. M. Faheem, "Accelerating motif finding problem using grid computing with enhanced Brute Force," in *2010 The 12th International Conference on Advanced Communication Technology (ICACT)*, 2010, pp. 197-202.

[142] D. E. Goldberg and J. H. Holland, "Genetic algorithms and machine learning," *Machine learning*, vol. 3, pp. 95-99, 1988.

[143] M. Gen and R. Cheng, *Genetic algorithms and engineering optimization* vol. 7: John Wiley & Sons, 2000.

[144] T. Jones, "Evolutionary algorithms, fitness landscapes and search," PhD, The University of New Mexico, 1995.

[145] E. Cox, *Fuzzy modeling and genetic algorithms for data mining and exploration*: Elsevier, 2005.

[146] RSSB, "GB Operational Concept Standalone Driver Advisory System (S-DAS)," *The Rail Safety and Standard Board*, 2012.

[147] Z. Hainan, S. Xubin, C. Lei, G. Shigen, and D. Hairong, "Analysis and design of Driver Advisory System (DAS) for energy-efficient train operation with real-time information," in *2016 IEEE International Conference on Intelligent Rail Transportation (ICIRT)*, 2016, pp. 99-104.

[148] L. Yang, T. Lidén, and P. Leander, "Achieving energy-efficiency and on-time performance with Driver Advisory Systems," in *2013 IEEE International Conference on Intelligent Rail Transportation Proceedings*, 2013, pp. 13-18.

[149] M. H. Kalos and P. A. Whitlock, *Monte Carlo Methods*: Wiley-VCH, 2008.

[150] S. Chun-Lien, "Probabilistic load-flow computation using point estimate method," *IEEE Transactions on Power Systems*, vol. 20, pp. 1843-1851, 2005.

[151] Z. Tian, P. Weston, N. Zhao, S. Hillmansen, C. Roberts, and L. Chen, "System energy optimisation strategies for metros with regeneration," *Transportation Research Part C: Emerging Technologies*, vol. 75, pp. 120-135, 2017.

[152] Z. Tian, P. Weston, S. Hillmansen, C. Roberts, and N. Zhao, "System energy optimisation of metro-transit system using Monte Carlo Algorithm," in *2016 IEEE International Conference on Intelligent Rail Transportation (ICIRT)*, 2016, pp. 453-459.